Uncovering novel suppressors of endogenous nucleic acid ligands

Julian Robert Smith

A dissertation

submitted in partial fulfillment of the

requirements for the degree of

Doctor of Philosophy

University of Washington

2023

Reading Committee:

Ram Savan, Chair

Adam Lacy-Hulbert

Jennifer Hyde

Program Authorized to Offer Degree:

Immunology

University of Washington

Abstract

Uncovering novel suppressors of endogenous nucleic acid ligands

Julian Robert Smith

Chair of the Supervisory Committee:
Ram Savan
Department of Immunology

Type I interferons (IFNs) are important for controlling viral infections, but aberrant IFN expression can result in tissue damage. IFNs are induced following activation of pattern recognition receptors that sense pathogen associated DNA and RNA. RIG-I-like receptors (RLRs), RIG-I and MDA5, sense viral RNA and signal through the adaptor protein MAVS, while cGAS and DDX41 sense viral DNA signal though the adaptor protein STING. Activation of MAVS or STING leads to the phosphorylation and nuclear translocation of the transcription factor IRF3, in turn inducing IFNs. While activation of these pathways is often driven by viral nucleic acids, both pathways can be activated by host endogenous nucleic acids. Therefore, several mechanisms exist to prevent recognition of host nucleic acids by these receptors in order to prevent aberrant expression of IFN and IFN-mediated disease. Identifying factors important

for suppressing endogenous DNA and RNA ligands is critical for preventing IFN-induced autoimmunity. In this dissertation, we identify two novel regulators that suppresses endogenous nucleic acids that activate the RLR pathway or the cGAS/DDX41/STING pathway. We discovered that the transcription factor MEF2A is required to suppresses the accumulation of RNA:DNA hybrids and DNA-damage which leads to the unscheduled activation of STING and production of IFN. Interestingly, STING activation required cGAS and DDX41 demonstrating a previously undescribed role for DDX41 driven activation of STING through genomic RNA:DNA hybrids. We also uncovered a novel role for the splicing factor CELF2 as a suppressor of endogenous RNA ligands. Depletion of CELF2 in monocytes leads to a spontaneous IFN and IFN-stimulated gene signature, dependent on the RIG-I-MAVS pathway. These data are the first to demonstrate a role for MEF2A and CELF2 in suppressing endogenous nucleic acid ligands, which can activate host pattern recognition receptors to induce an IFN signature. Overall, these findings suggest that MEF2A and CELF2 are important for preventing IFN-induced inflammation.

TABLE OF CONTENTS

LIST OF FIGURES

LIST OF TABLES

ACKNOWLEDGEMENTS

I have been very fortunate enough to have amassed a large support network from the beginning of my academic career unto this day. A network that consists of mentors, family and friends. First, I would like to thank my graduate advisor, Dr. Ram Savan. Savan brings in wonderful and talented people into his lab which make the day-to-day time spent in the lab a pleasure. He often says that his favorite part of training people is seeing the delta from where they started to where they end up and that is quite evident as the support and patience, he has for his trainees is one of a kind. When you go to him with a problem as small as needing a reagent urgently or as large as an existential crisis about your future in science, he is there to offer whatever support he can to ensure you have the necessary tools to carry on. Thank you for you unwavering support and patience with me through the good and the bad that come with graduate school. I would also like to thank Dr. Adriana Forero, who second to Savan, played a large part in my ultimate decision to join the Ram lab. I had the pleasure of working closely with her throughout the entirety of my graduate experience and the knowledge and skills I learned from her are immeasurable. Thank you, Adriana, for not only being a second mentor to me but also one of my best friends. As I mentioned the people in the Ram lab have made the seemingly never-ending day-to-day lab life so much better. Thank you, Drs. Johannes Schwerk, Nandan Gokhale, Mathew Hendricks, Yo Okamura, and Kim Somfleth, as well as my fellow graduate students Dr. Frank Soveg and Rachel van Gelder and the undergraduates especially Noa Etzyon whom I had the pleasure of mentoring. Thank you to my committee for your support and guidance throughout the years. I would also like to thank Dr. Dritan Agalliu for the 4 years I worked in his lab and the training that prepared me for graduate school.

Graduate school is made that much better by fellow students to learn and grow with. I had the pleasure of getting to known some of the most talented people that attended the UW Immunology graduate program with me. I have had some of the best times of my life from skate sessions with Jared and Jack, to after work hangouts at MOHAI. While I would like to recognize you all by name, to save space I will just have to say thank you all for your companionship over the last 6 years. I do however want to give a special shout out to my entering class of 2017 and my former roommate, Frank Soveg. Tyler, Miranda, Brittany, Sigal, Jessica and Ragan, you will always hold a special place in my heart, I couldn't imagine a better group of people to call my cohort. Best class ever. Frank was not only my lab mate, but my roommate during the pandemic and one of my best friends. Thank you for keeping me sane during the pandemic and pushing me out of my shell on numerous occasions. Graduate school would not have been the same without you.

It goes without saying that my family and friends are the most important people in my life, and I thank you all for your support and words of encouragement during graduate school. I love you Mom, Dad, Ashley, and Jennifer. Hearing your voices on the phone and seeing your faces on trips home made all the stress and pressure of graduate school melt away. Thank you to my two best friends, Bradyen Ward and Wesley Baxter for your steadfast friendship since we were literal children. It is so rare to retain friends from childhood but the fact that we've stuck together for almost two decades is incredible and you two mean the world to me. Thank you, Emmanuelle Genoyer, meeting you was the highlight of my time in graduate school. I am extremely lucky to have a partner as thoughtful, loving and intelligent as you. I love you.

Finally, thank you to the pets in my life, Stinkerbell (RIP), Bruce, and Sylvie for always being a there when I needed a friend most.

DEDICATION

I dedicate this dissertation to my family. To my mom for always giving me the love, freedom, and confidence to explore the world. To my dad for always believing in me. To my stepmom for showing me how to approach the world with optimism. To my sister for giving me a reason to be someone to look up to.

Chapter 1. Introduction

Parts of this chapter were adapted with permission from the following publication:

Gokhale, N.S., Smith, J.R., Van Gelder, R.D., Savan, R., 2021. RNA regulatory mechanisms that control antiviral innate immunity. *Immunol. Rev*. 304, 77–96.

DOI:https://doi.org/10.1111/imr.13019

The immune system at its basic function is to protect a host organism from foreign pathogens by discerning non-self from self. The adaptive immune system, consisting of lymphocytes, T and B cells, is critical in clearing pathogens and generating memory to combat subsequent insult through somatic mutation and recombination. However, this arm of the immune system is mobilized days after infection which leaves a pathogen with ample time to replicate and wreak havoc. Therefore, rapid initial recognition of a pathogen's presence is key to kickstarting the immune response and is orchestrated by germline encoded pattern recognition receptors (PRRs)[1]. PRRs, first hypothesized by Charles Janeway in 1989[2], recognize pathogen associated molecular patterns (PAMPs) of which a pathogen may have difficulty drifting away from evolutionarily and thus remain relatively constant to allow immediate recognition of non-self-entities by non-adaptable PRRs[3]. This response is termed the "innate immune response" and is key to; recognize and initiate a program of intracellular defense against pathogens, notify neighboring cells of danger through production of inflammatory signaling molecules known as cytokines, recruit innate and adaptive immune cells to sites of infection through use of chemoattractant signaling molecules known as chemokines and awaken the adaptive immune system to begin responding to infection[1,3,4]. PRRs are excellent sentinels to quickly respond to

PAMPs, but this comes with a tradeoff as many of these conserved patterns can be found within host cells and recognition of self in the absence of an infection can lead to autoinflammation and damaging tissue pathology[5].

Several basic cellular processes can generate intermediates or products that the innate immune system can see as "foreign" in a loss of self vs non-self-discernment. This is especially true in the case of PRRs that recognize nucleic acids. Nucleic acids are the building blocks of life, as DNA encodes tools necessary for cells to survive and function, and RNA performs a multitude of functions such as containing the code read to make proteins, scaffolding massive molecular machines such as ribosomes and the spliceosome and fine-tuning gene expression through RNA-based degradation mechanisms. Due to the importance of nucleic acids in life and biology, pathogens like viruses and bacteria cannot alter the overall structure of their DNA and RNA and still reproduce, making DNA and RNA constant targets by the innate immune system[1]. Dozens of PRRs that recognize nucleic acids have evolved over time to sense invaders. Some recognize DNA, such as cyclic GMP-AMP synthase (cGAS) and Toll-like receptor 9 (TLR9), and others recognize RNA such as the retinoic acid-inducible gene I (RIG-I)-like receptors and TLR3/7[3]. All of these sensors trigger innate immune responses that initiate a program of defense against an invading pathogen but have also been implicated in autoinflammatory diseases through sensing of self-nucleic acids[6].

Given that self-nucleic acids have the potential to activate host PRRs, expanding our knowledge of what self-nucleic acids can act as ligands and the mechanisms that suppress their generation or recognition by PRRs is of great importance. This understanding can not only help prevent unwanted activation of host innate immune responses but also provide valuable targets to generate new antiviral therapeutics, vaccine adjuvants, and anti-tumor therapeutics. This

dissertation describes two novel factors; the transcription factor myocyte enhancing factor 2A (MEF2A) and the splicing factor CUGBP elav-like family protein 2 (CELF2), that suppress the generation of nucleic acid self-ligands. Specifically, this work describes ways by which transcriptional stress and RNA splicing disruptions can generate RNA or RNA:DNA ligands that activate host PRRs and drive autoinflammation.

1.1 Innate immune pattern recognition receptors

Several PRR nucleic acid-sensors exist to defend the host against viral infection. For the sake of this work, this introduction will focus on three classes of innate immune sensors; the RNA sensing RIG-I like receptors (RLRs) (consisting of RIG-I and melanoma differentiation-associated protein 5 [MDA5]), the DNA sensor cGAS, and the DEAD-box helicase protein, DEAD-box helicase 41 (DDX41). While toll-like receptors (TLRs) play a critical role in nucleic acid sensing within endosomes, this dissertation will not focus on them as they are not relevant to this study.

1.1.1 RNA sensing by RIG-I-like receptors

The RLRs are considered DEAD-box helicase RNA binding proteins (RBPs). When the RLRs RIG-I or MDA5 interact with viral "non-self" or endogenous "self" RNA motifs, they undergo conformational changes, oligomerize through their caspase activation and recruitment domains (CARDs) and translocate to the vicinity of the adaptor protein MAVS[7]. MAVS is anchored to both mitochondria and contact sites between mitochondria and ER, as well as to peroxisomes. MAVS itself encodes a CARD, and as such, activated RIG-I or MDA5 oligomers trigger the aggregation of MAVS through CARD-CARD interactions, building a platform for downstream signaling. While a diverse array of proteins are involved in MAVS signalosome

function, the kinases, inhibitor of nuclear factor kappa-B kinase (IKK)ε and tank-binding kinase (TBK)1, which phosphorylates the transcription factor interferon regulatory factor 3 (IRF3), are especially critical[7,8]. Phosphorylated homodimers of IRF3 translocate into the nucleus and induce type I and III interferons (IFNs) (**Figure 1.1**). IFNs are cytokines that act in both autocrine and paracrine fashions to induce hundreds of interferon-stimulated genes (ISGs), which are potent cellular defense factors that establish an antiviral state and counteract infection[9]. Interferons are indispensable for a robust antiviral response. Type I IFNs, comprised of the fourteen subtypes of IFNα plus the singular IFN-β, are arguably the most critical molecules that drive antiviral immunity. Once secreted from infected cells, type I IFNs bind a heterodimeric receptor composed of IFNAR1 and IFNAR2 (referred to as IFNAR) on the surface of the same, neighboring, or distal cells. Signaling downstream of IFNAR proceeds through the JAK and STAT families of signal transducers[10]. The four subtypes of type III IFNs act in a similar fashion at epithelial surfaces, albeit through IFNLR1/IL10R2 receptor complex. Through these receptors, both type I and III IFNs activate a common transcription factor complex of composed of STAT1, STAT2, and IRF9 which induces hundreds of ISGs[10,11]. Many ISGs code for direct antiviral effectors, as well as proteins involved in feedback loops that amplify or inhibit antiviral pathways[9,12]. RLRs and the MAVS signalosome also activate NF-κB, augmenting robust IFN induction. This subsection will discuss self and non-self RNA sensing by RLRs.

The composition and structure of "non-self" viral RNA determine how it is sensed by RLRs. Both RIG-I and MDA5 can recognize double-stranded RNA (dsRNA). MDA5 senses long dsRNA intermediates of viral replication during infection by enteroviruses and coronaviruses[13–17]. On the other hand, RIG-I is activated by short dsRNA containing either a 5′ triphosphate (5′-ppp) or diphosphate (5′-pp), but lacking an m7G cap[18–21]. RIG-I (and potentially

MDA5) can also recognize RNA lacking 2′O-methylation at its 5′ end[22–24]. Both the m7G cap and terminal 2′O-methylation, found on "self" mRNAs, prevent RIG-I from recognizing endogenous mRNAs and aberrantly activating an IFN response. The antiviral effector IFIT1, an ISG upregulated downstream of RIG-I and MDA5 signaling, senses the lack of 2′O-methylation on viral transcripts and acts to limit the translation of viral RNA[25]. Emulating the 5′ cap structure is an efficient strategy for viruses to avoid detection by RIG-I and to engage cap-dependent translation machinery. NS5, the RNA-dependent RNA polymerase of flaviviruses, which are positive-sense, single-stranded RNA viruses, encodes both m7G- and 2′O-methyltransferase activity[26–28]. Mutation of NS5 2′O-methyltransferase activity in yellow fever virus and West Nile virus (WNV) results in increased IFN production, demonstrating that flaviviruses use this strategy to evade recognition by RIG-I[22,29]. Similarly, the NSP16 protein of coronaviruses has cap 2′O-methyltransferase activity[24,30,31]. Ablation of NSP16 cap 2′O-methyltransferase activity attenuates the diverse coronavirus species in a sensing- and IFN-dependent manner. In addition to the 5′ cap structure, several families of viruses contain m6A and other RNA modifications within their transcripts[32]. In vitro transcribed RNAs containing modified nucleobases like m6A can suppress detection by RLRs and TLRs[33,34]. Inhibition of RLR activation through m6A modifications has been demonstrated to occur during hepatitis C virus (HCV), hepatitis B virus, and human metapneumovirus infection[35,36]. Thus, viruses may co-opt cellular RNA modification processes to appear more like endogenous transcripts, thereby shielding their genomes from detection by PRRs.

RIG-I-like receptors can also sense "self" RNAs which become unmasked during infection or accumulate due to loss of proper RNA metabolism. Sensing of such transcripts may enhance antiviral signaling. During infection by the DNA viruses herpes simplex virus (HSV)-1

and Epstein-Barr virus (EBV), as well as by the negative-stranded RNA virus influenza A virus (IAV), RIG-I is activated by the mis-localized host 5S ribosomal RNA pseudogene transcript RNA5SP141, which accumulates aberrantly in the cytosol. RNA5SP141 contains dsRNA elements plus a 5′-ppp moiety and is therefore a potent RIG-I substrate. Recognition of RNA5SP141 by RIG-I has been shown to be critical for the induction of IFN and restriction of viral replication during HSV-1 infection[37]. Similarly, the reactivation of the DNA virus Kaposi's sarcoma herpes virus (KSHV) leads to the accumulation of 5′-ppp containing vault RNAs, a class of poorly understood small RNAs, which act as RIG-I agonists. At homeostasis, 5′-ppp on vault RNA is reduced by the cellular triphosphatase DUSP11; however, KSHV reactivation inhibits the transcription of DUSP11, increasing the immunostimulatory potential of these small RNA species[38]. During viral infection, the activation of the OAS-RNase L antiviral system also generates “self” ligands that trigger RLR activation. The 2′-5′ oligoadenylate synthetase (OAS) family of ISGs sense viral dsRNA and catalyze the production of the second messenger 2′-5′ adenylate (2′-5′A). 2′-5′A then activates the latent endoribonucleolytic activity of RNase L, which cleaves both viral and host single-stranded RNA[39,40]. Although RNase L-mediated RNA cleavage primarily denies a permissive cellular environment for viral replication, RNase L cleavage products can also form small duplex RNA ligands that activate both RIG-I and MDA5 to amplify the antiviral response[40].

“Self” RLR activation can promote antiviral immunity through counteracting viral mechanisms that hide viral RNA from cellular pathogen sensors. However, RLR signaling in the absence of infection is detrimental and may lead to inflammatory and autoimmune diseases[6,5]. As such, the host employs multiple strategies to restrict sterile activation of RLR pathways during homeostasis. As mentioned, the triphosphatase DUSP11 restricts RIG-I-activating 5′-ppp

moieties in certain "self" non-coding RNAs[38,41]. Keeping aberrant MDA5 activation in check, however, involves the suppression of endogenous dsRNA. For example, an RNA degradome comprised of the helicase SUV3 and the polynucleotide phosphorylase PNPT1 is responsible for rapid turnover of dsRNA intermediates that result from mitochondrial transcription. Inhibition of SUV3 and PNPT1 leads to accumulation of mitochondrial dsRNA, which enters the cytoplasm and engages MDA5[42]. Pairs of Alu elements, ~300 nt long retrotransposons abundantly dispersed throughout primate genomes, can form long dsRNA regions in cellular RNAs and also act as a potent substrate for MDA5 activation[43,44]. However, adenosine deaminase acting on RNA (ADAR) edits structured Alu elements, changing adenosine bases to inosine, thereby reducing base-pairing potential and inhibiting MDA5 filament assembly plus downstream signaling[45,46]. Gain-of-function mutations in MDA5 that promote MDA5-RNA binding and loss-of-function mutations in ADAR1 that inhibit RNA editing both cause autoimmune interferonopathies such as Aicardi-Goutières syndrome[45,47–49].

Differential splicing (splicing discussed in section 1.2) of cellular RNAs may alter RLR signaling. This facet of RNA regulation is best exemplified in tumor cell suppression of IFN activation. Transcriptomic analyses of tumor samples reveal dramatic alterations to RNA splicing[50]. The splicing factor hnRNPC, upregulated in many cancers, suppresses the retention of Alu element-containing introns during mRNA processing[51–53]. Depletion of hnRNPC in breast cancer cell lines causes tumor suppression through heightened sensing of Alu elements in endogenous dsRNA ligands, which subsequently induces type I IFN[54]. Furthermore, spliceosome-targeted therapies (STTs) which aim to repress key splicing factors, have shown efficacy in cancer models. In a recent report, STTs resulted in the production of dsRNA species via intron retention, thus activating the RLR pathway[55]. In murine breast cancer models, STTs

that activated the RLR pathway resulted in increased antiviral immune signaling, tumor cell death, and increased adaptive immune responses. Similarly, breast cancer patients with increased intron retention exhibited improved disease-free survival compared to those with lower intron retention.

Sensing of immunostimulatory RNA danger-associated molecular patterns (DAMPs) in cancer cells may also lead to increased resistance to radiotherapy or chemotherapy. In breast cancer models, stromal fibroblasts co-cultured with tumor cells produce RNA containing exosomes, which activate STAT1 in a RIG-I-dependent manner. Activation of STAT1 and ISG induction via exosome RNA (exoRNA) and NOTCH3 signaling in breast cancer cells cooperatively render these cancer cells refractory to therapy, likely by promoting DNA damage resistance[56]. Interestingly, these exoRNAs consist mainly of 7SL RNA transcripts such as RN7SL1, which normally nucleate the signal recognition particle (SRP), a highly conserved RNP essential for protein membrane localization and secretion[57,58]. RN7SL1 contains a terminal triphosphate moiety within its 5′ Alu-like RNA sequence. In the cytoplasm of homeostatic cells, the heterodimeric SRP proteins SRP9 and SRP14 interact with the Alu domain of RN7SL1 to shield the 5′-ppp from RIG-I. However, reduced SRP9/14 incorporation into exosomes exposes the 5′-ppp of RN7SL1, which can then be sensed by RIG-I in tumor cells[57]. Taken together, these findings reveal that both “self” and “non-self” RNAs are important in regulating IFN production through the RLR pathway. While RLR recognition of “non-self” RNA is largely understood, future studies, including the work described in this dissertation, will undoubtedly reveal further cellular factors and mechanisms that either promote or prevent the detection of “self” RNA motifs to control IFN activation.

1.1.2 DNA sensing by the cGAS-STING Pathway

The cGAS-STING pathway is responsible for the recognition of non-self and self-cytoplasmic DNA. Prior to the discovery of cGAS or STING it was known that similar to RNA sensing, DNA derived from viruses or bacteria could initiate a similar signaling cascade leading to TBK1 and IRF3 activation and production of IFN[59]. It was then discovered that the ER-resident protein stimulator of IFN genes (STING: former gene name *TMEM173*, now *STING1*) was required for the innate immune response to intracellular DNA but it was thought that STING directly interacted with cytoplasmic DNA[60,61]. It was not until a few years later that STING was discovered to be the receptor for a unique set of cyclic di-nucleotides with a 2'-3' phosphodiester linkage[62]. Subsequent studies determined that cGAS was in fact the sensor of cytoplasmic DNA and cyclic di-nucleotide synthase that converted GTP and ATP into 2'-3' cyclic GMP-AMP (cGAMP)[63–66]. cGAMP then interacts with STING to induce activation of IRF3 and transcription of IFN (**Figure 1.1**). In the years since, the cGAS-STING pathway has been studied extensively and investigations of this pathway have provided the bases for therapeutics including vaccine design, autoimmunity and cancer.

cGAS is responsible for sensing non-self and self-DNA in a sequence-independent manner and can recognize long dsDNA with high affinity, but also single-stranded (ss)DNA and RNA:DNA hybrids known as R-loops with lower affinity[67–69]. Upon encountering DNA ligands, cGAS undergoes a confirmational change and dimerization reveling the catalytic domain required to synthesize cGAMP[70,71]. While dimerization of cGAS is required for they synthesis of cGAMP is has been shown that short DNA substrates less than 20 base pairs are weak activators of cGAS and that long DNA substrates can induce larger cGAS oligomers and liquid-liquid

phase separation (LLPS) suggesting that cGAS forms large complex phase separated hubs for cGAMP synthesis[72]. Indeed the protein G3BP1, a major component of the LLPS structures known as stress granules, has been shown to enhance cGAS interactions with dsDNA supporting the idea that LLPS is crucial to cGAS function[73]. Numerous other molecules play a role in cGAS sensing of DNA. The RBP PQBP1 can act as a cosensor and binding partner to cGAS to coordinate sensing and immune activation of retroviral cDNA[74]. However, the role for PQBP1 has been contested in subsequent reports suggesting that PQBP1 may act as a negative regulator of cGAS signaling activated by non-retroviral DNA[75]. Therefore, future studies are required to determine the context dependent role of PQBP1 in DNA-driven innate immune activation. The long-noncoding RNA *NEAT1* also plays a role in enhancing cGAS driven immune responses through scaffolding cGAS interactions with PQBP1 and the RBP HEXIM1 into a ribonucleoprotein (RNP) complex required to recruit STING[76]. The full extent of cGAS interacting proteins is still under investigation.

Originally it was thought that cGAS resided within the cytoplasm and away from host DNA in the nucleus as a way of limiting recognition of self-nucleic acids. However, recent studies have provided evidence that a majority of cGAS resides within the nucleus, suggesting a more nuanced mechanism of cGAS regulation. Supporting this idea of nuclear cGAS localization, cGAS sensing of HIV-2 DNA happens in the nucleus and requires the nuclear protein NONO to aid in DNA sensing[77]. At steady state cGAS is sequestered away from genomic DNA by anchoring to chromatin and centromeres to keep cGAS quiescent while residing in the nucleus[78–80]. During mitosis, cGAS function is restricted by a series of N-terminal phosphorylation events driven by cell-cycle kinases to prevent sensing of DNA and immune activation again through chromatin tethering, suggesting that cGAS is permitted to associate with

chromatin in an effort by the cell to limit self-reactivity[81]. In addition to the sequestration of cGAS, mechanisms to limit the accumulation of self-DNA accessible to cGAS are required to prevent autoreactivity. Mutations in the DNA exonuclease TREX1 are associated with autoinflammation and the interferonopathy disease known as Aicardi-Goutières syndrome[82,83]. Indeed, cGAS is required for the sensing of immunostimulatory self-DNA following the loss of TREX1[84,85]. Together these findings suggest multiple mechanisms of cGAS regulation, but suppression of the cGAS-STING pathway also happens downstream of cGAS activation.

cGAMP produced by cGAS upon sensing of DNA is differentially regulated to both enhance and limit its function in a context dependent manner. Once synthesized, cGAMP can be transmitted into adjacent cells via gap junctions or be taken up and hide away in viral particles like a trojan horse to enter newly infected cells and amplify antiviral sigaling[86,87]. To limit activation of the DNA sensing pathway, cGAMP is degraded by hydrolase ecto-nucleotide pyrophosphatase/ phosphodiesterase 1 (ENPP1)[88,89]. However, ENPP1 exists on the extracellular surface of cells, a conundrum which remained elusive until it was discovered that cGAMP is rapidly exported following its synthesis by ATP-binding cassette transporter 1 (ABCC1)[90]. This regulation of cGAMP is necessary to fine tune DNA sensing and regulate cGAMP interaction with the cyclic di-nucleotide sensor STING.

STING is an ER-resident transmembrane protein that upon binding cGAMP goes on to trigger activation of IRF3 and IFN. At steady state, STING exists as a dimer at with its C-terminal tail (CTT) and (ligand binding domain) facing the cytoplasm. cGAMP binding to the LBD induces confirmational change allowing the CTT to interact with TBK1[91–93]. STING undergoes oligomerization with multiple copies of itself and TBK1 and exits from the ER towards the Golgi apparatus[94]. Self-phosphorylation by TBK1 and phosphorylation of the

STING CTT by TBK1 is a critical step in STING signaling as CTT phosphorylation at S366 acts as a docking site for IRF3[92]. Signaling of STING-TBK1 and activation of IRF3 occurs prior to STING reaching the Golgi, at the ER-Golgi intermediate complex (ERGIC) and prevention of STING exit from the ER completely ablates IRF3 phosphorylation and subsequent IFN production[94]. These findings suggest that STING migration is critical for its function and immune signaling. STING activation can also occur through cGAMP-independent mechanisms as ER stress can drive STING-IRF3 interactions and activation in the absence of cGAMP accumulation [95].

The cGAS-STING pathway is critical for sensing of pathogenic derived DNA, but cellular sources of DNA can activate the cGAS-STING pathway and in some cases, such as described with TREX1 mutations, can result in damaging tissue pathology. A major source of cellular DNA that activates cGAS and STING is DNA damage. Indeed DNA damage caused by ionizing radiation activates the cGAS-STING pathway[96]. Increased IFN and accumulation of ISGs follows DNA damage by ionizing radiation but is ablated by deletion of either cGAS or STING. Loss of genomic integrity can result in the formation of extra nuclear DNA positive structures within the cell known as micronuclei[97]. In Harding et al., they demonstrated that cGAS enters the micronuclei structures to sense DNA and initiate an immune response. Similarly, cGAS enters micronuclei following cell-intrinsic DNA damage via loss of *Rnaseh2b* following breakdown of the micronuclei membrane, a process known as chromothripsis[98,99]. However, cGAS can also senses DNA damage within chromosome bridges, structures formed when lagging chromosomes improperly segregate and lead to micronuclei formation, rather than the micronuclei themselves[100]. Regardless of the mode of entry, these data provide evidence that cGAS senses DNA damage within cells to activate a sterile form of IFN production. Mutations in

RNASEH2B, like *TREX1*, are associated with Aicardi-Goutières syndrome (AGS) by inducing DNA damage because of unresolved R-loop formation. DNA damage resulting from loss of RNASEH2B induces IFN production via cGAS-STING implicating a role for DNA damage sensing in AGS disease progression[101].

DNA damage is constantly occurring within cells via both cell-intrinsic and -extrinsic processes, but regardless of the cause, cells respond by activation of the DNA-damage response kinases (DDRs). The three DDRs consist of DNA protein kinase catalytic subunit (DNA-PKcs), Ataxia-Telangiectasia mutated (ATM) or ATM and Rad3-related (ATR)[102]. These DNA damage response kinases play specific roles in the DNA damage response and cell cycle checkpoints. DNA-PKcs and ATM are typically required to respond to double-stranded breaks in DNA and ATR responds to replicative stress and single-stranded breaks, and respond by inducing phosphorylation of hundreds of cell cycle regulators to prevent DNA-damage accumulation[102]. In addition to these homeostatic roles, these kinases have been implemented in innate immune activation. DNA damage sensed by ATM can lead to a non-canonical form of STING activation which drives NF-κB-driven genes to a greater extent than IRF3-driven genes[103]. Upon DNA damage ATM phosphorylates and activates the tumor suppressor p53, which associates with the nuclear DNA sensor, interferon gamma inducible protein 16 (IFI16), and in cooperation with TRAF6 induces ubiquitination of STING, driving NF-κB activation rather than association with TBK1. Similarly, replicative stress in hair follicle stem cells induces the activation of ATR which in turn drives IFI16-STING mediated inflammation in the inflammatory skin disease, hidradenitis suppurativa[104]. Alternatively, loss of these key DDR kinases leads to autoinflammation. It has been known since the 1970s that ataxia telangiectasia, for which ATM is named and mutations are key in driving disease, exhibit severe autoimmunity[105]. Indeed, cells

derived from ataxia telangiectasia patients exhibit exacerbated response to viral infection as a result of immune priming by STING and DNA-damage accumulation due to the loss of ATM function[106]. ATR appears to play a similar role to ATM in priming immune responses, as ATR inhibition leads to increased cytosolic nucleic-sensing following DNA damage induced by ionizing radiation[107]. cGAS-STING activation following ATR inhibition was utilized in a mouse model of cancer and was found to enhance anti-PD-L1 cytotoxicity in a prostate cancer model[108]. In addition to ATR and ATM mediated immune signaling, DNA-PKcs can act as a sensor of immunostimulatory DNA by binding cytoplasmic DNA and initiating STING-TBK1 driven IRF3 activation[109]. Surprisingly, pathway activation is independent of DNA-PKcs kinase activity, suggesting that DNA-PKcs might aid in scaffolding immunostimulatory DNA with other DNA sensors. Interestingly, DNA-PKcs can play a role in DNA sensing and activation of IRF3 but in a cGAS-STING independent manner, suggesting that cGAS and STING are dispensable in some contexts for DNA-dependent IRF3 activation[110]. In the absence of STING, DNA-PKcs senses the free ends of DNA and induces phosphorylation of IRF3 in the absence of TBK1, suggesting direct phosphorylation of IRF3 by DNA-PKcs. Taken together, these data suggest that the immunostimulatory DNA sensing pathway and the DNA damage response pathway are intertwined. However, the full extent of how DNA damage affects innate immune signaling is still unknown and future studies are needed to further elucidate these mechanisms.

1.1.3 DDX41 and immune regulation by DEAD-box helicases

The DEAD/DAED-box (DDX) helicases are RBPs with diverse functions ranging from RNA metabolism, genome stability and immune regulation[111–113]. DEAD-box helicases belong to the largest family of RNA helicases, super family 2 (SF2), which is defined by a series of conserved motifs within the family[114]. These DEAD/DAED-box helicases are named according

to their conserved amino acid sequence; Asp-Glu-Ala-Asp (DEAD) or Asp-Ala-Glu-Asp (DAED) as described in 1989 and predicted to be involved in ATP-binding and hydrolysis[115]. DEAD-box helicases are thought to exert their function through unwinding nucleic acid base pairs in an ATP dependent manner but many DDX helicases can function without unwinding base pairs and rather recruit other proteins to function[111].

DDX proteins play a pivotal role in both innate and adaptive immune functions. DDX1 for example is important for immunoglobulin heavy-chain class switch recombination by converting G-quadruplex RNA structures into RNA:DNA hybrids (R-loops) at switch regions in the *IgH* locus, thereby promoting the recruitment of activation induced cytidine deaminase (AID) to induce recombination[116]. During innate immune responses, DDX proteins play a more expanded role, with a number of them being ISGs[112]. Indeed, the previously described RLRs; RIG-I and MDA5, are themselves DEAD-box helicases[117]. In addition to the RLRs, other DEAD-box RNA helicases have been shown to play diverse roles in the RLR pathway, primarily through modulating export of host mRNA transcripts central to viral RNA sensing pathways[118]. DDX46 negatively regulates the production of type I IFN during viral infection by retaining MAVS, TRAF3, and TRAF6 mRNAs in the nucleus[119]. These transcripts all contain the RNA modification m6A, which is known to promote nuclear export[120]. However, during viral infection, DDX46 recruits the m^6A "eraser" ALKBH5 to demethylate these transcripts, resulting in nuclear retention and reduced protein expression. The splicing factor DDX39A also inhibits nuclear export of MAVS, TRAF3, and TRAF6 during viral infection[121]. The addition of the small ubiquitin-like modifier protein SUMO to DDX39A inhibits its ability to bind RNA. However, viral infection reduces SUMOylation of DDX39A by downregulating its E3-ligase, RanBP2. In the absence of SUMOylation, DDX39A binds MAVS, TRAF3, and TRAF6 mRNAs

and sequesters them in the nucleus. Whether DDX39A and DDX46 co-operate in nuclear retention of the same set of transcripts is unknown.

DDX helicases outside of the RLR pathway can also act as direct sensors of nucleic acids. The helicases DDX1, DDX21 and DHX36 associate with the adaptor protein TRIF as well as directly with cytosolic dsRNA to induce activation of IRF3/7 and production of type I IFN in a TLR3-independent manner[122]. DDX41 on the other hand plays an interesting role in nucleic acid sensing, as it can sense both DNA and RNA:DNA hybrids. Initial studies describe DDX41 as a sensor of cytosolic DNA[123]. In dendritic cells DDX41 senses synthetic immunostimulatory DNA as well as pathogenic DNA from bacteria and DNA viruses to induce IFN. This was proposed to be through direct interactions with STING, but the exact mechanism is lacking (**Figure 1.1**). DDX41 also senses cyclic-di-nucleotides produced during viral infection to promote STING activation[124]. It was later shown that Bruton's tyrosine kinase (BTK) is required for DDX41 interaction with DNA and STING[125]. BTK phosphorylates DDX41 at tyrosine 364 and 414 and loss of BTK kinase activity prevents not only DDX41 interactions with dsDNA but also DDX41 interaction with STING. BTK also directly interacts with STING but the kinase function of BTK is not required for STING activation, suggesting that BTK serves an adaptor role, perhaps to bridge various components of the STING signalosome. Recently it was shown that DDX41 feeds into the cGAS-STING signaling pathway through annealing ssDNA to form dsDNA which then serves as cGAS lingads[126]. DDX41 possesses ATP-independent annealing activity in addition to the standard DDX ATP-dependent helicase activity. Mutations found in DDX41 that affect its helicase activity but not annealing activity enhance cGAS-STING dependent signals suggesting that in addition to interacting with STING directly, DDX41 acts upstream to regulate dsDNA accessibility.

It has become more appreciated recently that DDX41 in addition to interacting with dsDNA can interact with RNA:DNA hybrids or R-loops. Indeed, DDX41 is essential for sensing retroviral RNA:DNA intermediates generated during murine leukemia virus (MLV) replication (**Figure 1.1**)[127]. DDX41 functions before cGAS during MLV replication as RNA:DNA intermediates are formed before cDNA generation; cDNA can then go on to activate cGAS. Interestingly, much as with the initial discovery of DDX41 as dsDNA sensor, DDX41 functions as a viral-derived R-loops sensor in dendritic cells specifically, suggesting cell type specific roles for DDX41 as an innate immune sensor. In addition, DDX41 is required to sense and respond to genomic R-loops. R-loops are scattered throughout 5-10% of the genome at any given time and serve to control transcription rates, chromosome segregation and as previously mentioned, class switch recombination[128–131]. However, unchecked accumulation of R-loops can serve to promote DNA damage or induce damaging pathology as described previously in the case of AGS[132,133]. As such, expression of nucleases and helicases, including many DDX helicases, are required to limit the abundance of R-loops[113,134,135]. Using a proximity proteomics approach, Mosler et al. demonstrated that that DDX41 localizes to and resolves nuclear R-loops[136]. In the absence of DDX41, R-loops are increased and lead to transcriptional stress and activation of the DNA damage response driven by ATR. Indeed, in zebra fish DDX41 suppresses R-loops and associated DNA damage during hematopoietic stem and progenitor cell development limiting aberrant hematopoietic output[137,138]. DNA damage that follows the loss of DDX41 results in cGAS-STING activation, a phenotype conserved in human cells. Thus, DDX41 can act as a sensor of DNA and R-loops to activate innate immune signaling, but also acts to suppress the accumulation of both nucleic acids to prevent innate immune activation. How DDX41 diversifies these functions and if genomic R-loops can promote DDX41 driven innate immunity is

unknown. Taken together, these findings establish DDX41 as an interesting sensor during the innate immune response whose role is still under investigation.

Together these sets of sensors are all critical for establishing early defense against invading pathogens and recognize a diverse array of nucleic acids. However, under homeostatic conditions these sensors should remain quiescent. Several factors control the spontaneous generation of several ligands but often these mechanisms of suppression are lost. A better understanding of not only what these factors are, but how they function to suppress unwanted inflammation is key to preventing diseases driven by these sensors.

1.2 CUGBP elav-like family member 2 and RNA splicing

Around 95% of human genes undergo a biochemical reaction known as RNA splicing, by which introns, sequences that intersperse protein coding exons, are removed and exons joined together[139]. In addition, around 94% of human genes undergo a process known as alternative splicing (AS) which induces differential exon and intron usage, greatly increasing the diversity of the proteosome[140,141]. Splicing is a key biological process and is required for proper cellular functions including immune response and immune cell function[142,143]. Splicing is conducted by a complex molecular machine composed of dozens of proteins and 5 small nuclear RNAs (snRNAs) known as the spliceosome[144]. The 5 snRNAs, termed U1, U2, U4, U5 and U6, associate with several small proteins known as Sm proteins to form their respective small nuclear ribonuclear proteins (snRNPs, pronounced “snurp”) and function at various stages of the splicing process[139]. In addition to snRNPs, hundreds of other proteins including ATP-dependent helicases and *trans*-acting RNA splicing factors are critical during this process.

On pre-RNA itself, 3 key sequences are important for RNA splicing: the 5’ splice site (SS), the 3’SS and the branch point (BP). The 5’SS sits at the 5’ end of an intron just before the

upstream exon. The 5'SS in lower eukaryotes such as yeast is GUAUGU and is conserved across species. However, this is less conserved in humans but usually consists of a GURAGN, where R is any purine and N is any nucleotide[139]. Similarly, the BP in yeast is conserved, UACUAAC, but in humans is YNYURAY, where Y is any pyrimidine, R is any purine and N is any nucleotide. The 3'SS is conserved between humans and yeast and is YAG, but the human 3'SS is proceeded by a poly-pyrimidine tract[139]. Briefly, splicing is initiated by the U1 and U2 snRNPs recognizing the 5'SS and BP, followed by the recruitment of the U4/U6 and U5 tri-snRNP complex. The removal of introns is carried out by two transesterification reactions orchestrated by the spliceosome and associated proteins. The first transesterification is called "branching" where the 5'SS is cleaved from the 3'end of the upstream exon and attached to the BP adenosine forming a lariat intermediate[145,146]. The next step is "exon ligation" where the 3'SS is cleaved and the 3'nucleotide of the upstream exon and the 5'nucleotide of the downstream exon are combined leaving a mature exon-exon junction and a looped intron known as a lariat[145].

Alternative splicing is regulated at the initial steps of RNA splicing. Specialized RBPs known as splicing factors regulate the interactions of the U1 and U2 snRNPs with pre-RNA and are the major determining factors of splice-cite usage[147]. Splicing factor expression can be developmentally, stimulus and cell type specific and can recognize RNA in a sequence specific manner. Several conserved RNA splicing factors contain sequences known as RNA recognition motifs RRMs and make up the most abundant class of single-stranded RNA binding proteins. One such family of RRM containing splicing factors are the CUGBP elav-like family (CELF) splicing factors. Humans possess 6 CELF proteins (CELF1-6) all of which contain two N-terminal RRMs (RRM1 and RRM2) and one C-terminal RRM3 separated by a divergent domain, which is the driving factor of CELF protein differentiation[148]. CELF proteins play diverse roles

in RNA metabolism with critical functions during development and neuronal function. Many of the CELF proteins have temporal and spatial expression restrictions with CELF1 being the most ubiquitously expressed[149]. CELF1 and CELF2 have the most sequence homology, with >70% total amino acid sequence homology and >90% RRM sequence homology[150]. CELF3-6 are more lowly expressed and exhibit very specific tissue restriction. CELF2 (also called ETR3, CUGBP2, NAPOR and BRUNOL3) is critical for heart and muscle development and global deletion of *Celf2* in mice is embryonic lethal[149,151]. Like the other CELF proteins, CELF2 was originally discovered to bind to octets of CUG repeats in RNA, but this has since been expanded to general G/U rich elements which are predominantly found within introns and the 3' UTR[148,152]. CELF2 not only regulates splicing but also alternative poly-adenylation and mRNA translation in the cytoplasm[153–155].

CELF2 is abundantly expressed in immune cells but most of the studies focus on the role of CELF2 following T cell receptor (TCR) activation. CELF2 is not only induced following TCR activation, but regulates an entire program of alternative splicing and alternative poly-adenylation, including splicing of the *CELF2* 3' UTR itself thus stabilizing its own expresson[153,156–158]. In addition to stabilizing its own expression CELF2 induces splicing of MKK7 which acts upstream of c-Jun[157]. MKK7 splicing induced by CELF2 generates a docking site for JNK on MKK7, which phosphorylates c-Jun and promotes a positive feedback loop of CELF2-induced splicing of MKK7 and JNK/c-Jun activation. CELF2 also regulates non-canonical NF-κB activation following TCR activation by promoting the splicing and removal of exon 8 of TRAF3[159,160]. TRAF3ΔE8 loses the ability to interact with NF-κB-inducing kinase (NIK) allowing NIK to induce the non-canonical activation of NF-κB. For CELF2 to regulate the splicing of TRAF3 it requires co-regulation by another RRM containing splicing factor,

hnRNPC. Interestingly, CELF2 and hnRNPC coregulate each other expression with hnRNPC regulating transcription of CELF2 and CELF2 regulating hnRNPC translation. CELF2 regulation of immune responses in macrophages is understudied with the only known role regulating IL-10 signaling via the RNA processing of miR-155[161]. CELF2 suppresses miR-155 expression following IL-10 signaling in macrophages resulting in decreased inflammatory cytokine production after lipopolysaccharide (LPS) stim. CELF2 has never been associated with regulation of innate immune nucleic acid censors or type I IFN production.

As previously described (Section 1.1.1 RLRs), perturbations in RNA splicing are known to result in the generation of endogenous RNA ligands, including hnRNPC, which is both closely related to and interacts with CELF2. Given the increased expression of CELF2 in immune cells and close relation to other RRM containing splicing factors, chapter 3 of this dissertation aims to investigate the role of CELF2 in immune cells and suppression of endogenous RNA ligands.

1.3 Myocyte enhancing factor 2A and transcription

The regulation of IFN production and signaling can be affected by several different transcription factors (TF), many of which are not yet fully understood. One family of TFs that has been found to play a role in IFN signaling is the myocyte enhancing factor 2 (MEF2) family of TFs. The MEF2 TFs play pleotropic roles in development of a wide variety of cell types including cardiac and skeletal muscle, neuronal tissue and immune cells[162]. Vertebrates have four MEF2 family proteins, MEF2A-D, whereas *D. melanogaster*, *C. elegans* and *S. cerevisiae* have a single gene[163]. All MEF2 proteins share the same structure with an N-terminal Minichromosome Maintenance 1, Agamous, Deficiens and Serum Response Factor (MADS)-box followed by a MEF2 domain, both of which are critical for DNA binding and the later also contributing to protein-protein interactions[164]. MEF2 proteins also have a C-terminal transactivation domain

(TAD) which exhibits great diversity between the MEF2 family TFs due to alternative splicing[164]. MEF2 family TFs usually follow a specific hierarchy of expression where MEF2A is the most highly expressed followed by MEF2D, MEF2C and MEF2B is lowly expressed[165]. MEF2 family TFs play critical roles in development as genetic deletion of these factors in mice results in embryonic or early post-natal lethality[166,167]. While these factors are critical during development, their role at homeostasis and maintenance of immune homeostasis is less understood.

The role for MEF2 proteins in inflammation and IFN regulation is just beginning to emerge with novel *in vivo* studies in mouse brains and macrophages. MEF2C suppresses age related inflammation in murine microglia[168]. Aged mice exhibit increased type I IFN signatures and overexpression of IFNβ in adult mice mimics aged signatures and contributes to defects in learning. Increased IFN in the brain also correlates with decreased expression of MEF2C, altering microglial immune states and making microglia more prone to inflammation. In addition, early loss of MEF2C nuclear function in microglia can be observed in mouse models of Alzheimer's disease and is dependent on type I IFN signaling on microglia[169]. Together, these findings suggest that MEF2C can regulate inflammatory responses in microglia and MEF2C can be functionally altered by type I IFN. MEF2D also plays an immunoregulatory role in microglia, however MEF2D is required for proper type I IFN production[170]. Loss of MEF2D significantly reduces the expression of ISGs in LPS stimulated microglia due to decreased IRF7 expression. The *Irf7* promotor possesses two MEF2 binding sites suggesting that the MEF2 family of TFs can transcriptionally regulate the expression of *Irf7*. In murine macrophages, MEF2A was shown to be important for ISG expression downstream of multiple stimuli, including viral and bacterial infection as well as LPS, synthetic RNA and direct STING stimulation[171]. Peaks in MEF2A

DNA binding sites following LPS stimulation overlap with specific *Ifnb1* enhancer sites including those occupied by IRFs, PU.1 and C/EBPβ. However, MEF2D and to a lesser extent, MEF2C also occupy these sites. MEF2A and MEF2D can function as heterodimers through their MEF2 domains, and it is unclear if both are necessary for the function of *Ifnb1* transcription or if other MEF2 family proteins can provide assitance[172]. Nonetheless, MEF2 TFs play a critical role in regulation of inflammatory responses including IFN responses, but the extent to their regulation is unknown.

MEF2A plays a critical role in cardiac function, much like its family members. Inherited mutations in MEF2A are associated with coronary artery disease and myocardial infarction. A 7 amino acid deletion mutation results in autosomal dominant defects in MEF2A that prevents the nuclear localization of MEF2A[173]. This MEF2A mutation is believed to cause abnormalities in the vascular epithelium potentially allowing for increased monocyte entry and atherosclerotic plaques. Indeed, *Mef2a*$^{-/-}$ mice who die within the first week exhibit dilation of the right ventricle[167]. Monocytes have also been shown to be the cause of severe IFN driven inflammation during myocardial infarction[174]. What role MEF2A plays in cardiac cell immune homeostasis is not known. Chapter 2 of this dissertation aims to uncover the role MEF2A plays in immune homeostasis of cardiomyocytes.

1.4 Concluding remarks

While our understanding of PRRs has evolved since the 1980s, there is still much more to uncover. Understanding the factors that contribute to the suppression of self-nucleic acid ligands could have implications to treat autoinflammatory diseases, cancers, and develop better antiviral RNA or DNA therapies or adjuvants for vaccines. This dissertation investigates and describes

two novel suppressors of self-nucleic acids, CELF2 and MEF2A, that when lost lead to the activation of PRRs and lead to aberrant IFN production.

1.5 Figures

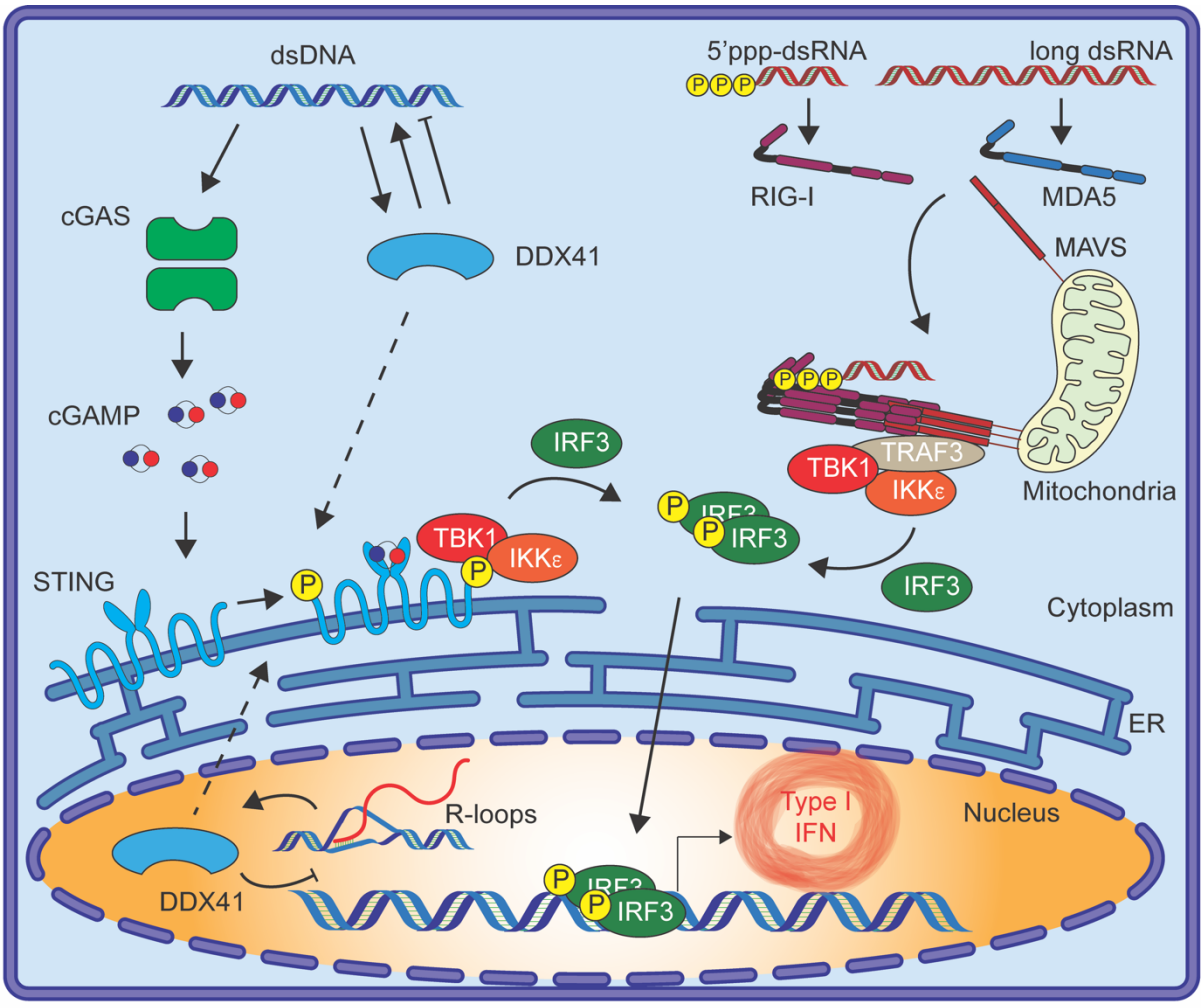

Figure 1.1. Innate immune nucleic acid sensors.

The RLRs, RIG-I and MDA5 sense 5'ppp-dsRNA and long dsRNA respectively. Upon ligand binding they oligomerize with the adaptor protein MAVS via their CARD domains. This forms the MAVS signalosome with recruits several proteins including TRAF3, TBK1 and IKKε to

induce the phosphorylation of IRF3. Similarly, cGAS senses dsDNA and produces the second messenger cGAMP. cGAMP activates STING which recruits TBK1 and IKKε which phosphorylate IRF3. Phosphorylated IRF3 dimerizes and translocates into the nucleus where it can induce the expression of IFNs. DDX41 can also induce the activation of STING through interactions with dsDNA or RNA:DNA hybrids known as R-loops. DDX41 can also wind ssDNA into dsDNA generating dsDNA ligands or unwind dsDNA limiting dsDNA ligands. DDX41 can also unwind R-loops limiting their accumulation in the genome.

Chapter 2. MEF2A suppresses stress responses that trigger DDX41 dependent IFN production

Parts of this chapter were adapted with permission from the following publication:

Smith, J.R., Dowling, J.W., McFadden, M.I., Karp, A., Schwerk, J., Woodward, J., Savan, R., Forero., A.R. (2023). MEF2A suppresses stress responses that trigger DDX41-dependent IFN production. *Cell Rep.*, DOI:https://doi.org/10.1016/j.celrep.2023.112805

2.1 Introduction

The detection of nucleic acids or DNA breaks by pattern recognition receptors (PRR) promotes the formation of signalosomes that recruit Tank-binding kinase 1 (TBK1) to phosphorylate transcription factors such as interferon regulatory factor 3 (IRF3). Phosphorylation of C-terminal serine residues of IRF3 allow for its dimerization and translocation to the nucleus where it transactivates type I interferon (IFNα/β) and type III interferon (IFNλ) gene expression. IFNs activate Signal Transducer And Activator Of Transcription (STAT) to form the transcriptionally active complex, ISGF3, and drive IFN-stimulated gene (ISG) expression[175]. The ISGs are critical effectors of the antiviral immune response and regulate various cellular processes to inhibit cell proliferation and promote inflammation. While the regulation of IFN responses is best characterized in the context of viral infection, accumulation and mis-localization of self-nucleic acids or the loss of nuclear genome integrity can also drive noxious sterile IFN-mediated inflammation. These latter processes are the hallmark of autoinflammatory pathologies known as interferonopathies[176]. Thus, it is critical to define the factors that protect organelle and genomic integrity, thereby preventing the unscheduled or excessive inflammation.

The major nucleic acid sensing pathways induced by the accumulation of mis-localized or damaged DNA converge on the adaptor molecule, Stimulator of Interferon Genes (STING). Three nucleic acid sensors have been characterized as upstream regulators of STING: cyclic GMP-AMP synthase (cGAS), IFN gamma inducible factor 16 (IFI16), and DEAD-box helicase 41 (DDX41). Accumulation of double-stranded DNA (dsDNA) activates cGAS-mediated synthesis of the second messenger, 2′,3′-cyclic GMP-AMP (cGAMP), which induces STING activation[177,178]. Genomic DNA breaks induce IFI16-dependent non-canonical pathway to drive cGAS-independent STING activation[179]. R-loops are RNA:DNA hybrid structures occurring naturally in ~5-10% of the genome[180], but their accumulation is associated with Aicardi-Goutières syndrome (AGS)[132], an autoinflammatory disorder driven by STING-mediated inflammation[181]. DEAD-box RNA helicases recognize these RNA:DNA structures to prevent their accumulation[182,183]. One such helicase, DDX41, activates STING after recognition of dsDNA[184–186] and RNA:DNA transcripts generated by retroviral infection[187]. Recent studies have shown that DDX41 is recruited to R-loops, promoting their resolution to prevent DNA damage[188]. However, a role, if any, for DDX41-dependent processes in the induction of IFN-mediated inflammation upon R-loop enrichment remains to be determined.

The DNA damage response (DDR) kinases Ataxia–telangiectasia mutated (ATM), ATM and RAD3-related (ATR), and DNA-dependent protein kinase catalytic subunit (DNA-PKcs) coordinate cell cycle arrest and repair of DNA damage and host inflammatory responses associated to genotoxic stress[189,190], cytosolic DNA accumulation[191,192], and DNA virus infection[193]. Amongst these kinases, ATR is the central regulator of the replicative stress response (RSR) that occurs under conditions associated with stalled replication fork progression, such as nucleotide pool depletion, and R-loop accumulation. ATR phosphorylates substrates that

mediate cell cycle arrest to prevent chromosomal breaks[194,195], and promotes R-loop resolution and proper chromosome segregation[130,196,197]. While ATM and DNA-PKcs have been linked to IRF3 activation and IFN-driven inflammatory responses, the mechanisms by which ATR contributes to IFN production are less clear.

The myocyte enhancing factor 2 (MEF2) transcription factors, composed of 4 evolutionarily conserved proteins, MEF2A-D, have emerged as potential regulators of inflammation[198–201]. MEF2 proteins have important developmental[202] and homeostatic roles as mice deficient in these factors display embryonic lethality or early post-natal lethality[166,203]. Our study focuses on MEF2A, the least characterized immune regulator in this family. MEF2A loss of function (LOF) mutations associate with an enhanced risk for adverse coronary artery disease outcomes, which could be exacerbated by aberrant IFN induction[204]. We show that acute depletion of MEF2A results in spontaneous IFN antiviral and inflammatory responses. We demonstrate that MEF2A expression prevents the induction of transcriptional stress and the accumulation of R-loops. This increase in RNA:DNA hybrid formation drives DDX41/cGAS/STING-mediated IFN responses and the activation of ATR. Lastly, we show that ATR kinase activity is required to support STING activation in this context. These findings position MEF2A as a positive regulator of genomic stability that protects from unscheduled IFN-driven inflammation.

2.2 Results

2.2.1 Loss of MEF2A leads to spontaneous IFN production and type I IFN-dependent inflammation.

Given the potential connection between MEF2 proteins and inflammation, we examined the impact of one MEF2 family member on the transcriptional program in myocytes, a cellular

target of inflammation caused by viral infections. As such, we used dicer substrate small interfering (dsiRNA) to transiently deplete highly expressed MEF2 genes in the human cardiomyocyte cell line, AC16. Transient depletion of *MEF2A* allowed us capture acute gene expression changes while circumventing possible functional compensation by other MEF2 paralogs, as previously described in knock-out cells[205]. AC16 cells expressed high levels of *MEF2A* and *MEF2D*, moderate levels of *MEF2C*, and low levels of *MEF2B* mRNA (**Figure 2.1A).** This is consistent with the expression of MEF2 transcription factors in left ventricular adult human cardiomyocytes (GTEx database) **(Figure 2.7A**). Thus, we independently targeted MEF2A, MEF2C and MEF2D and measured changes in IFN induction. The depletion of *MEF2A* (**Figure 2.1B, left**) resulted in an increase in *IFNB1* mRNA expression (**Figure 2.1B, right**). Neither the silencing of *MEF2C* or *MEF2D* elicit significant changes in *IFNB1* mRNA expression relative to control transfected cells (**Figure 2.1B and 2.1C**). To validate the reproducibility of *MEF2A*-targeting in driving IFN induction we tested two additional MEF2A-targeting siRNAs. We found that in all cases, *MEF2A* silencing led to the phosphorylation of the IFN responsive transcription factor STAT1 at tyrosine 701 (Y701) relative to control transfected cells **(Figure 2.7B**). Genome-wide transcriptional signatures captured by RNA-sequencing revealed robust differentially expressed (DE) transcripts, in which 519 genes were significantly upregulated and 201 genes were significantly downregulated in *MEF2A*-targeted cells compared to cells transfected with non-targeting control (NC) dsiRNA (**Figure 2.1D**). Gene ontology analysis identified enriched biological functions amongst the upregulated genes following MEF2A depletion. We observed significant enrichment in pathways associated with innate immune inflammation and type I IFN responses amongst the upregulated genes (**Figure 2.1E**). This was consistent with an increase in the expression not only in *IFNB1* expression, but also an

increase in the ISG, *CXCL10,* in MEF2A knockdown (KD) cells (**Figure 2.1F**). We recapitulated this phenotype in immortalized human fibroblasts, which have similar MEF2 gene expression profiles to myocytes (**Figure 2.7C**). Silencing of *MEF2A* was sufficient to induce both *IFNB1* mRNA and that of ISGs such as *CXCL10* (**Figure 2.7D, left**). Finally, we observed similar upregulation of *IFNB1* and *CXCL10* mRNA in human macrophage-like cells, THP-1, induced by the knockdown of *MEF2A* expression (**Figure 2.7D, right**). Together, these results suggest that MEF2A, but not other MEF2 protein family members, is a negative regulator of spurious type I IFN transcription across multiple human cell types.

Having observed an enrichment of genes involved in IFN responses, we addressed whether this was associated with increased resistance to viral infection. *MEF2A* silencing protects cells from the cytolytic effects of vesicular stomatitis virus (VSV) infection compared to control cells (**Figure 2.2A**). Similarly, loss of MEF2A conferred AC16 cells with protection against the cardiotropic enterovirus, Coxsackievirus B3 (CVB3), which exhibited a 75% reduction in viral RNA accumulation relative to control cells (**Figure 2.2B**). Previously, we have demonstrated that such decreases in viral RNA correspond to a significant attenuation in infectious virus production[206]. These data suggest that MEF2A loss leads to the secretion of bioactive IFN that can establish a cellular antiviral state.

Cell intrinsic antiviral responses are coordinated by both type I and III IFNs. Both IFN families can promote the activation of ISGF3 to promote transcriptional induction of ISG expression[207]. As we observed both type I and III IFN gene mRNA induction after MEF2A depletion we asked whether the secretion of IFN drove MEF2A-dependent inflammatory responses. We engineered an Huh7 cell-based luciferase reporter assay to monitor ISGF3-mediated transcriptional activation in response to secreted IFN. Transfer of supernatants from

MEF2A KD muscle cells led to a significant increase in luciferase activity relative to treatment with supernatants derived from control transfected cells (**Figure 2.2C**). Huh7 cells respond to exogenous type I and III IFN stimulation (**Figure 2.8A**). We examined whether human cardiomyocytes could respond to exogenous recombinant type I (IFNβ) and III (IFNλ3) IFN stimulation by measuring the induction of ISG mRNA. Treatment with recombinant IFNβ induced significant expression of *ISG15* and *CXCL10* mRNAs at 9h and 24 h post stimulation (**Figure 2.2D**). In contrast, IFNλ3 stimulation did not induce the expression of either of these two ISGs (**Figure 2.2D**). We then confirmed the predominant inflammatory role for type I IFN by treating AC16 cells with the pan-type I IFN inhibitor, B18R[208]. B18R pre-treatment decreased *ISG15* mRNA induction post *MEF2A* silencing (**Figure 2.2E**). This was concomitant with decreased STAT1 phosphorylation (Y701) in B18R treated cells relative to vehicle treatment (**Figure 2.2F**). IRF3 activation (Serine 386 phosphorylation) was unaffected by B18R blockade of type I IFN signaling (**Figure 2.2G**), suggesting that decreases in MEF2A promote signaling transduction cascades upstream of IRF3 to drive IFN expression. Of note, levels of phosphorylated STAT1 induced by silencing of MEF2A were comparable to those induced by IFNβ stimulation, both of which enhanced IRF3 activation and increased IRF1 protein expression (**Figure 2.8B**). Exogenous expression of dsiRNA-resistant *MEF2A* (**Figure 2.8C**) suppressed IRF3 activation after targeting of endogenous *MEF2A* (**Figure 2.2H and Figure 2.8D**) demonstrating the specificity of MEF2A in preventing spurious IFN responses. Together, these data suggest that IFN is secreted after MEF2A silencing and the establishment of the antiviral state in cardiomyocytes depends solely on type I IFNs.

2.2.2 Inflammatory responses in MEF2A depleted cells are STING-dependent

To further define signaling mechanisms for IFN responses in the wake of MEF2A deficiency, we first confirmed that IRF3 was indispensable for this process. For this purpose, we generated *IRF3*-deficient cardiomyocytes using CRISPR-Cas9 genome editing technologies. Deletion of IRF3 abrogated the activation of STAT1 in response to *MEF2A* silencing (**Figure 2.3A**), suggesting minimal compensation from additional IRFs, such as IRF1 or IRF7, which can transactivate IFN genes[189,209,210] and are induced by MEF2A depletion (**Figure 2.9B**). IRF3 activation is mediated by RNA and DNA sensors, and converge on adaptor molecules such as MAVS (RNA sensing) and STING (DNA sensing)[211]. We confirmed that both RNA and DNA sensing pathways were functional in our cellular model by measuring the induction of IFN (*IFNB1*, *IFNL1*) and ISG (*CXCL10*) mRNAs following the transfection of cells with either a specific RIG-I RNA agonist[212] or calf-thymus DNA[213] (**Figure 2.9A**). In addition, AC16 cells responded to TLR3 activation with poly(I:C) and infection with Sendai virus (SeV) (**Figure 2.9B**), which activate MAVS-dependent responses through RIG-I and MDA5[214].

To discern which of these nucleic acid sensing pathways is engaged in response to *MEF2A* silencing, we depleted either STING (*TMEM173*) or *MAVS* prior to targeting *MEF2A* expression. We found that STING, but not MAVS, was necessary to promote the activation and phosphorylation of TBK1 and IRF3 upstream of type I IFN induction. Similarly, we observed that STAT1 phosphorylation following *MEF2A* depletion (**Figure 2.3B**) was muted only in cells deficient for STING. Silencing of *MAVS* did not abrogate STAT1 phosphorylation relative to that observed in control cells (**Figure 2.3B**). We then generated STING knockout cells by targeting *TMEM173* using CRISPR-Cas9 genome editing (**Figure 2.3C**). In these cells, silencing of *MEF2A* (**Figure 2.9C**), did not promote the accumulation of *IFNB1* mRNA that was observed

in control (H1) cells (**Figure 2.3C**). Consistent with the previous results, *MEF2A* KD was sufficient to promote STING phosphorylation at serine 366, a prerequisite for IRF3 activation[215] (**Figure 2.3E**). Together, these data indicate that MEF2A promotes homeostatic functions that prevent STING activation and inhibit spontaneous IFN-mediated inflammation.

2.2.3 The loss of MEF2A compromises genomic integrity

Both the loss of nuclear DNA integrity and the accumulation of endoplasmic reticulum (ER) stress have been associated with pathogen-independent, STING-mediated inflammation[216]. To determine whether MEF2A is necessary to sustain either DNA integrity or ER function, we silenced MEF2A expression in AC16 cells, and measured DNA damage or ER stress response markers. The loss of MEF2A led to an accumulation of phosphorylated histone 2AX (γH2A.X), a marker of DNA damage (**Figure 2.3F**). Similar γH2A.X increases were observed following treatment with the topoisomerase II inhibitor, etoposide, known to elicit genotoxic stress (**Figure 2.3F**). However, neither the loss of *MEF2A* nor treatment with etoposide led to an accumulation of ATF4 or enhanced splicing of XBP1 (XBP1s), hallmarks of the ER stress response (**Figure 2.9D**). On the other hand, treatment with thapsigargin, a sarco/ER calcium ATPase (SERCA) inhibitor, led to expected increases in both ATF4 protein expression and XBP1 splicing. We conclude that loss of MEF2A results in the accumulation of γH2A.X and DNA damage, which activates STING and type I IFN induction.

The accrual of DNA breaks can result in an accumulation of extranuclear DNA in the form of micronuclei. Experimentally, inhibition of microtubule dynamics by treatment with nocodazole promotes the mis-segregation of chromosomes and accumulation of micronuclei (**Figure 2.3G, right**). We assessed whether the DNA damage response associated with MEF2A KD was accompanied by accumulation of chromosomal aberrations by quantifying the

percentage of cells with noticeable micronuclei (**Figure 2.3G, left**). Compared with non-targeted controls, depletion of MEF2A led to a significant increase in the percentage of cells containing micronuclei. Thus, loss of MEF2A compromises genomic integrity, promoting cellular stress via the STING-IFN axis.

The accumulation of cytosolic nucleic acid or the loss of nuclear DNA compartmentalization is sensed by cGAS, and results in the synthesis of 2′,3′-cGAMP. To assess if cGAS was required for IFN induction upon *MEF2A* silencing, we generated *cGAS* KO cells by CRISPR-Cas9 genome editing. Functional ablation of cGAS was confirmed by measuring 2′,3′-cGAMP synthesis upon calf-thymus DNA transfection. Cells deficient in cGAS were impaired in 2′,3′-cGAMP synthesis, while there was detectable accumulation of cGAMP in WT (H1) non-targeted control cells (**Figure 2.9E**). We depleted MEF2A in either H1 or *cGAS* KO cells and observed that both STING phosphorylation (**Figure 2.3H**) and IRF3 activation were dampened by cGAS deletion (**Figure 2.3I**). Because IFI16 can also mediate non-canonical induction of type I IFN responses in response to DNA breaks, in a STING-dependent manner[179], we generated IFI16 KO cells (**Figure 2.3J**). Unlike data from cGAS-deficient counterparts, IFI16 KO and control cells induced comparable levels of *IFNB1* mRNA upon MEF2A depletion (**Figure 2.3K**). We conclude that MEF2A expression is necessary to prevent accumulation of DNA damage responses at steady-state, which would drive IFN production in a cGAS/STING-dependent, but IFI16-independent pathway.

2.2.4 ATR kinase is pivotal for production of IFN following MEF2A depletion

The accumulation of DNA lesions activates DNA damage responses (DDR) coordinated by the kinases ATM, ATR, and DNA-PKcs to ultimately promote DNA repair[130,196,197,217]. In addition, DDR kinases have been implicated in the regulation of IFN following genotoxic

stress[179,189,191]. Thus, we addressed whether DDR kinase activity was necessary for the induction of inflammation in response to cellular stress elicited by decreased MEF2A expression. We pre-treated human fibroblasts with selective inhibitors of ATR (ATRi, ETP46464), ATM (ATMi, KU-55933) or DNA-PKcs (DNA-PKi, NU7441) kinase activity two hours prior to MEF2A depletion. Inhibition of ATR kinase activity specifically muted the activation of both IRF3 and STAT1 in response to the loss of MEF2A (**Figure 2.4A**). In contrast, robust IRF3 and downstream STAT1 phosphorylation was observed when cells were treated with ATM kinase inhibitors as previously reported[218]. Inhibition of DNA-PK kinase activity led to a minimal increase in basal IRF3 and STAT1 phosphorylation but did not affect STAT1 activation in response to MEF2A KD (**Figure 2.4A**). In addition, we observed that decreased MEF2A expression enhanced serine 33 phosphorylation of the ATR substrate, RPA32[219]. Pre-treatment of cells with a highly specific ATR kinase inhibitor (AZD6738) at non-cytotoxic doses (**Figure 2.10A**) led to a marked decrease in basal RPA32 S33 phosphorylation. ATR kinase inhibition also prevented increases in RPA32 S33 phosphorylation in response to MEF2A depletion (**Figure 2.4C**). Of note, RPA32 phosphorylation at serine 4/8, substrate for ATM and DNA-PK, was not induced by MEF2A depletion. On the other hand, S4/8 phosphorylation was enhanced by ATR kinase inactivation. These data suggest that induction of MEF2A induces stress responses that drive ATR activation. In addition, it is possible that the resulting IFN induction is not induced by DNA damage responses in this model.

We further defined the requirement for ATR kinase activity for IFN production in cardiac muscle cells using a fluorescent cell-based assay (AC16-ISRE-GFP) in which activation of ISRE-mediated transcription drives the expression of green fluorescent protein (GFP)[220]. As a primary control, IFN treatment of AC16-ISRE-GFP cells resulted in GFP increases as did

MEF2A silencing (**Figure 2.4D and Figure 2.10B**). The increase in GFP expression elicited by *MEF2A* KD (**Figure 2.10C, left**), was not due to changes in cellular viability after transfection (**Figure 2.10C, right**). Pre-treatment of reporter cells with ATR kinase inhibitors muted the expression of GFP in response to the loss of MEF2A (**Figure 2.4D**). To test if activation of ATR in a MEF2A-independent context could stimulate IFN production, we treatment with hydroxyurea (HU). HU depletes deoxynucleoside triphosphates (dNTPs) and activates ATR[221]. Low doses of HU induced ATR dependent ISRE activity (**Figure 2.10D**) and STING phosphorylation in AC16 cells (**Figure 2.10E**). These data suggest a potentially conserved mechanism by which ATR kinase activation promotes IFN responses.

In this regard, we next assessed whether ATR kinase inhibition regulated the activation of STING in the context of MEF2A-depletion. Treatment of AC16 cells with AZD6738 prior to siRNA transfection inhibited both STING and IRF3 phosphorylation upon the silencing of *MEF2A* (**Figure 2.4E**). This decrease in STING activation was not due to changes in the expression of DNA sensors (**Figure 2.10G**). As expected, the loss of STING and IRF3 activation was accompanied by a decrease in *IFNB1* mRNA induction (**Figure 2.4F**). This phenotype was recapitulated in fibroblasts. Inhibition of ATR kinase activity led to similarly decreased expression of type I IFN after MEF2A silencing relative to control transfected cells (**Figure 2.10D**). Interestingly, we found that ATR kinase inhibition did not affect the recognition of dsDNA ligands such as polydA:dT (**Figure 2.10H**). Together, these data suggested that ATR kinase activity is necessary to drive the induction of inflammatory responses independent from dsDNA recognition.

2.2.5 MEF2A depletion promotes the accumulation of R-loops

ATR functions as a protector of the genome in the case of aberrant R-loop formation[196]. R-loops are triple-stranded nucleic acid structures that form during transcription as nascent RNA threads back into the template DNA strand and to form an RNA:DNA hybrid[222]. The failure to resolve these structures can further result in replication fork stalling and renders the genome susceptible to DNA breaks[223]. To determine whether MEF2A loss impacted R-loop homeostasis, we probed the formation of RNA:DNA hybrids *in vitro* by assessing the cross reactivity of genomic DNA isolated from *MEF2A*-depleted and control cells with S9.6, an antibody that recognizes RNA:DNA (**Figure 2.5A**). We observed an enhanced level of S9.6 antibody reactivity in nucleic acid MEF2A KD samples relative to control cells. Importantly, treatment with recombinant Rnase H, which specifically degrades RNA:DNA hybrid strands, resulted in the near complete loss of S9.6 staining, further confirming an accumulation of R-loops in muscle cells lacking MEF2A. As an additional control, neither silencing of MEF2A nor treatment with RNAseH affected dsDNA-specific antibody reactivity in any of the samples. Using an orthogonal approach, we conducted immunofluorescence-based assessment of R-loop accumulation in cells after knockdown of MEF2A, using an antibody specific for RNA:DNA hybrids (S9.6) (**Figure 2.5B**). Overall, we observed a significant increase in the intensity of nuclear S9.6 foci in *MEF2A*-depleted cells relative to non-targeted control cells (**Figure 2.5C**). RNASEH1 is a cell endogenous ribonuclease that specifically targets RNA in RNA:DNA hybrids and thus functions to resolve cellular R-loops. We measured IFN production in cells in which we overexpressed RNASEH1 prior to targeting *MEF2A*. The levels of *IFNB1* mRNA induction (**Figure 2.5D**) were decreased in RNASEH1 overexpressing cells relative to vector expressing cells (**Figure 2.5E**). Conversely, we observed synergistically enhanced *IFNB1*

mRNA expression (**Figure 2.5F**) in cells in which we silenced both *RNASEH1* and *MEF2A* (**Figure 2.5G**). Taken together, our data indicate that the loss of MEF2A drives IFN responses due to R-loop accumulation as their resolution restores immune homeostasis.

2.2.6 DDX41 is required for the induction of R-loop mediated IFN responses

The accumulation of R-loops is known to drive inflammatory response due to cGAS/STING pathway activation[184,187]. The DEAD-box helicase, DDX41, is recruited to R-loops to promote their resolution[135,224,225]. However, whether DDX41 promotes or prevents the inflammatory responses associated with R-loop accumulation has yet to be addressed. Accordingly, we generated DDX41-deficient cells by CRISPR-Cas9 genome editing and measured inflammatory responses upon MEF2A depletion. The phosphorylation of IRF3 and STAT1 was attenuated dramatically in DDX41-deficient cells relative to WT controls (**Figure 2.6A**). Consistent with these findings, *DDX41* KO cells showed decreased STING phosphorylation (**Figure 2.6B**) and a decreased induction of *IFNB1* mRNA following *MEF2A* silencing relative to WT controls (**Figure 2.6C**). Interestingly, DDX41 deficiency associated with a noticeable increase in S9.6 positivity, supporting the role of DDX41 in preventing R-loop accumulation (**Figure 2.11A**). This prompted us to examine whether ATR kinase inhibition affected R-loop formation thereby indirectly affecting inflammatory responses. We observed a basal increase in R-loops in ATR kinase inhibitor treated cells and an enhancement in RNA:DNA hybrids after MEF2A depletion (**Figure 2.11B**). These data show that R-loops accumulation and inflammatory responses can be uncoupled by deletion of DDX41.

An array of post-translational DDX41 modifications contribute to its nucleic acid binding capacity, including phosphorylation at tyrosine 414 (Y414) by Bruton's tyrosine kinase (BTK)[186]. Having demonstrated the genetic requirement for DDX41 in STING activation

following MEF2A depletion, we asked whether chemical inhibition of BTK could abrogate this inflammatory response in U937 cells. Differentiation of U937 cells into monocytes by PMA treatment can promote basal BTK activity (**Figure 2.12A**). Like cardiomyocytes, depletion of MEF2A in differentiated U937 cells induces IRF3 and STAT phosphorylation (**Figure 2.12A**) and IFN secretion (**Figure 2.126B**). Inhibition of BTK kinase activity with ibrutinib significantly reduced phosphorylation of IRF3 and STAT1 relative to vehicle-treated cells in which MEF2A was depleted (**Figure 2.12C**). This decrease in IFN responses was not due to changes in the expression of either cGAS or DDX41 (**Figure 2.126C**). These data indicate that both the expression of DDX41 and its activation are required for the induction of STING-mediated inflammation in the context of MEF2A silencing. Importantly, the unscheduled activation of these responses could be targeted using chemical kinase inhibitors.

We conducted genome-wide transcriptional profiling to better understand the mechanisms by which the MEF2A/DDX41 axis promotes inflammatory responses. Overall, the cellular response to MEF2A knockdown was diminished in DDX41 KO cells relative to WT counterparts (**Figure 2.6D**). The number of differentially expressed (DE) genes was also lower in DDX41 KO cells (**Figure 2.6E**). Geneset enrichment analysis (GSEA) revealed DDX41 expression is necessary for the accumulation of genes involved in cytosolic DNA sensing, IFN responses, and antiviral control (**Figure 2.6F**). Indeed, an overview of the overlap of genes induced by MEF2A KD identified 1356 DE genes uniquely induced by *MEF2A* silencing in WT, but not KO cells, that were associated with antiviral and IFN responses (**Figure 2.6H**). We then conducted functional enrichment analysis on the 418 DE genes induced by loss of MEF2A in both WT and KO cells (263 transcripts) and uniquely DE in *DDX41* KO cells (155 transcripts). These genes were associated with GO biological functions such as cellular differentiation and

motility as well as the positive regulation of transcription (**Figure 2.6I**). Similar enrichment of transcriptional regulatory pathways was observed using the REACTOME pathway database (**Figure 2.6J**). Cellular hyperproliferation and increases in transcription can promote the accumulation of R-loops[226]. As R-loop formation occurs during transcription as the nascent RNA binds back to the DNA template[180,226] we asked whether the inhibition of *de novo* transcription could prevent R-loop accumulation after *MEF2A* depletion. Treatment of cells with Actinomycin D treatment resulted in decreased S9.6 reactivity in *MEF2A* depleted cells (**Figure 2.6K**). Together, these data suggest that MEF2A maintains the cellular transcriptional output and its loss promotes unscheduled R-loop accumulation. Moreover, our study shows that these structures likely trigger ATR-dependent, DDX41/cGAS-dependent activation to promote unscheduled inflammatory responses.

2.3 Discussion

In this study, we have identified MEF2A as a regulator of genomic stability that suppresses aberrant STING-dependent IFN activation. The inflammatory response correlated with chromosomal breaks, as evidenced by micronuclei accumulation, increases in γH2A.X, and enhanced phosphorylation of the ATR substrate, RPA32. Importantly, inhibition of ATR kinase activity mitigated the induction of IFN responses upon MEF2A depletion. Downregulation of MEF2A expression resulted in the accumulation of R-loops, triple-stranded structures composed of a ssDNA and an RNA:DNA hybrid. Genetic ablation of *DDX41* or chemical inhibition of the DDX41 regulatory kinase, BTK, prevented the spontaneous production of IFN that follows the loss of MEF2A. These findings position the transcription factor MEF2A as an enforcer of genomic stability that, when compromised, leads to stress-induced, IFN-mediated inflammation. We found that the acute loss of MEF2A results in the induction of an antiviral state across

multiple cell types, including cardiomyocytes, fibroblasts, and monocytes. Importantly, understanding the context in which nucleic acid mis-localization and lesion accumulation drives PRR activation is critical for the design and implementation of STING immunomodulatory therapies to manage autoinflammation and cancer[227].

Depletion of MEF2A expression induced both type I and type III IFN expression. Although these two IFN families promote an antiviral state in target cells, expression of type I and III IFN receptors varies across tissue types. The type I IFN receptor is expressed on all nucleated cells while, the type III IFN receptor expression is restricted primarily to epithelial barriers and a subset of immune cells[228]. We used orthogonal approaches to demonstrate that cardiac muscle cells respond primarily to type I IFNs. Treatment of cells with recombinant type III IFN failed to induce the expression of ISGs, while blockade of secreted type I IFN by treatment with B18R was sufficient to abrogate the induction of antiviral responses induced by the loss of transcriptional homeostasis. The translational potential of our findings is underscored by emerging virus outbreaks, which have refocused the attention on the use of recombinant IFN therapies for the clinical management of viral disease[229]. Our findings suggests that type I IFN targeted therapies may have a greater benefit in the management of cardiotropic virus infections. Conversely, type III IFN induction might contribute less to adverse outcomes after myocardial infarction, compared with type I IFN. In addition, induction of IFN responses during ischemic injury to cardiomyocytes can induce STING/IRF3-dependent inflammation that hinders tissue repair[204,230].

MEF2 proteins are transcriptional factors implicated in the control of inflammatory responses. In primary aged murine microglial cells, a decrease of MEF2C exacerbated IFN-related inflammatory responses[201]. *In vitro*, microglial expression of MEF2D is required to

sustain *Irf7* expression thereby promoting type I IFN responses[198]. In murine macrophages, MEF2A is necessary to promote chromatin accessibility at the *Ifnb1* locus. Deletion of *Mef2a* suppresses the induction of *Ifnb1* following LPS stimulation[199]. Whether MEF2 transcription factors regulate inflammatory responses in human cells is less understood. Our results using immortalized cardiomyocytes, fibroblast, and myeloid cells indicate that MEF2A acts indirectly as a negative regulator of inflammation by preventing cellular transcriptional stress. Silencing of MEF2A led to the induction of DNA damage responses, as well as the accumulation of R-loops. Previous studies have demonstrated that murine MEF2A silencing can alter the expression profile of cell cycle regulatory genes, impacting the DNA content profile[231]. Indeed, we observed a downregulation in mitotic regulatory genes upon transient depletion of these genes in human cardiac muscle cells. Importantly, our study correlates the induction of cellular transcriptional stress and IFN-mediated inflammation. Future studies should address the extent to which disruption of the rate of cell cycle progression and transcriptional homeostasis through the loss of transcription factor expression and function promotes inflammatory responses and how these prevent further genomic instability.

R-loops function to promote mitochondrial DNA replication, control transcriptional rates, coordinate faithful chromosome segregation, and facilitate immunoglobulin class switch recombination[128,130,232]. Pathological R-loop accumulation is the hallmark of inflammatory neurodegenerative diseases such as amyotrophic lateral sclerosis (ALS), Fragile X syndrome, and AGS[132,133]. Excessive R-loop formation is also observed in several proliferative malignancies. Cellular nucleases and helicases metabolize RNA:DNA hybrids to mitigate the cytotoxicity of their aberrant accumulation. The expression of Senataxin (SETX) and the related DEAxQ-like domain containing helicase Aquarius (AQR)[134,135] are necessary to curb R-loop

accumulation. DEAD/DEAH-box helicases, such as DDX5, DDX19, and DDX41 amongst others, are also recruited to R-loops and metabolize RNA:DNA hybrids[182]. On the other hand, DExD/H-box helicases, such as DHX9, both promote physiological R-loop formation at centromeres and drive their pathogenic accumulation during defective splicing[233]. Given the physiological importance of these helicases in the formation and resolution of R-loops, understanding the factors that control their recruitment, activation, and downstream effector functions of these helicases should be further explored across cell and tissue types.

DDX41 can bind both viral dsDNA and viral RNA:DNA hybrids to drive STING-mediated IFN production. In addition, proximity ligation studies show DDX41 occupancy at R-loops is necessary for their resolution[188,224]. Loss of function (LOF) mutations in DDX41, are associated with ineffective hematopoiesis and inherited myelodysplastic syndromes (MDS)[234]. Transgenic zebrafish models show that *ddx41* loss drive R-loop accumulation that can trigger cGAS-STING pathway dependent activation of inflammation[188,225]. In this model, *ddx41* LOF disrupts splicing of cell cycle genes and can drive the activation of ATM and ATR coordinated DDR that inhibit erythropoiesis. We found that in the context of acute MEF2A depletion cGAS, but not IFI16, coordinated the induction of downstream inflammatory responses. Our study demonstrates an expanded role for DDX41, as the accumulation of R-loops induces DDX41-dependent activation of STING and type I IFN-mediated inflammation. However, depletion of either DDX41 or cGAS did not result in a complete abrogation of responses. It is possible that the accumulation of RNA:DNA substrates or DNA breaks in *MEF2A*-deficient cardiac muscle cells could trigger PRR independently or trigger a cGAS/STING-independent inflammatory pathway[235].

The accumulation of transcriptional and mitotic R-loops has been shown to trigger ATR activation. ATR localizes to R-loops during mitosis to promote faithful chromosome segregation[130], and activation of the ATR/Chk1 pathway upon replication stress is important for the recruitment of nucleases into R-loops[197]. The loss of the splicing factor SRSF1 can promote R-loop accumulation and ATR activation[196,224]. Similarly, the disruption of DDX41 expression can enhance R-loop abundance and subsequent activate ATR[224]. Leveraging the MEF2A-depletion model, we showed that ATR kinase activity is necessary to coordinate the induction of DDX41/cGAS-dependent inflammatory responses upon increased R-loop abundance. Future studies will be crucial to gaining a better understanding of whether ATR promotes the recruitment and activation of RNA:DNA nucleases, such as DDX41, to R-loops to promote resolution, maintain genomic integrity, and drive inflammation.

Overall, this study bridges the activation of the transcriptional stress upon loss of MEF2A with DDX41-dependent activation of STING-mediated inflammation. Specifically, we demonstrate that ATR kinase activity is necessary for the activation of STING activation following R-loop accumulation. As such, our findings reveal a role for MEF2A in the regulation of cellular homeostasis and suggest a potential benefit for the use of specific ATR kinase inhibitors to mitigate deleterious inflammation in neurodegenerative and proliferative diseases defined by increases in R-loop abundance.

2.4 Materials and methods

Cell lines, cell culture conditions and treatments

Human cardiomyocyte (AC16) and derivate cell lines were grown in Dulbecco's modified Eagle's medium (DMEM) supplemented with 12.5% FBS, 2mM Glutamine, 100 U/ml Penicillin and 100 mg/ml Streptomycin and maintained at 37°C in 5% CO_2. Non-targeted (H1),

IRF3, STING, cGAS, IFI16 and DDX41-deficient AC16 cells were generated by CRISPR-Cas9 genome editing as previously described [236]. Transduced cells were enriched using antibiotic selection. BJ/TERT human fibroblasts were cultured in DMEM supplemented with 10% FBS, 2mM glutamine, 100 U/ml penicillin and 100 mg/ml streptomycin and maintained at 37°C in 5% CO_2. Huh7 human hepatoma cells and derivatives cell lines were cultured in DMEM supplemented with 10% FBS, 2mM Glutamine, 100 U/ml Penicillin and 100 mg/ml Streptomycin and maintained at 37°C in 5% CO_2. U937 monocytes were cultured in RPMI 1640 media supplemented with 10% FBS, 2mM glutamine, 100 U/ml penicillin and 100 mg/ml streptomycin and maintained at 37°C in 5% CO_2. THP-1 monocytes were maintained in RPMI 1640 media supplemented with 10% FBS, 2mM glutamine, 100 U/ml penicillin, 100 mg/ml streptomycin, 1 mM sodium pyruvate, 10 mM HEPES and 0.05 mM 2-mercaptoethanol and maintained at 37°C in 5% CO_2. U937 and THP-1 cells were differentiated for 48 hours (h) in their respective complete media containing 40 nM phorbol 12-myristate 13-acetate (PMA) followed by resting for 24 h in RPMI 1640 supplemented with 1% FBS.

Cells were stimulated with recombinant IFNβ (PBL Assay Science) and IFNλ3 (R&D Systems) at the indicated concentrations. Specific kinase inhibitors targeting, ATR (ETP-46465, AZD6738) (Cayman Chemicals), ATM (KU-55933) (SelleckChem), and DNA-PK (NU7441) (SelleckChem) were used at the indicated concentrations. Recombinant B18R (Life Technologies) was used at 1μg/ml. Etoposide and thapsigargin (Millipore Sigma) were used as indicated. Poly(deoxyadenylic-deoxythymidylic (polydA:dT) was transfected at 1μg/mL and host immune responses were measured after 24h. Actinomycin D treatment (0.5 μg/ml) was conducted 2h prior to fixation and immunostaining of AC16 cells transfected with either NC or *MEF2A*-targeting dsiRNA.

Viral models

VSV-GFP stock was a gift from Dr. Michael Gale Jr (University of Washington)[237]. Sendai Virus (Cantell strain) was acquired from Charles River. AC16 cells were seeded in 24-well plates at a density of 2 x 10^5 cells/well and transfected with negative control or MEF2A-targeting dsiRNA (IDT). Cells were infected with VSV-GFP at a multiplicity of infection (MOI) of 0.1, consistent with previous reports[236]. Following 24 h of infection, the culture medium was removed, cells were fixed with 4% PFA in PBS, and stained with Crystal violet stain (3% w/v) in 50% ethanol. Plates were imaged using the ChemiDoc XRS+ (BioRad) imaging system. Coxsackievirus B3 (CVB3)-Nancy infectious clone was a kind gift from Dr. Raul Andino (University of California San Francisco). Viral stocks were prepared by linearizing the plasmid by restriction digestion ClaI and *in vitro* transcribing viral RNA. The RNA was transfected into HeLa cells using Mirus X2 and cell supernatants (P0 stocks) were harvested. This supernatant was amplified in HeLa cells to generate P1 stocks that were quantified by plaque assay[238]. AC16 cells were seeded in 12-well plates at a density of 3.5 x 10^5 cells/well and transfected with negative control or *MEF2A*-targeting dsiRNA. After 24 h, cells were infected with CVB3 (MOI = 5) in a minimal volume for 1h at 37°C in 5% CO2 followed by washing with PBS and culturing in full serum media for 24 h. CVB3 RNA quantification was conducted via SYBR green based qPCR using primers specific to CVB3 VP1.

Plasmids and Oligonucleotides

CRISPR-Cas9 plasmids; pRRL-H1-PURO (non-targeting), pRRL-STING-PURO, pRRL-cGAS-PURO, pRRL-IRF3-PURO, pRRL-IFI16-PURO were a gift from Dr. Daniel Stetson (University of Washington)[239]. The ISRE reporter plasmid, pISRE-sfGFP, was a gift from Dr. Nicholas Heaton (Duke University) and has been previously described[220]. pRRL-DDX41-PURO

was generated by cloning single-guide RNA (sgRNA) targeting DDX41 (5'-CCTCATCTTCCGCCTCGGAG-3') into empty pRRL-Cas9-PURO plasmids as previously described[236,239]. pEGFP-RNASEH1 was a gift from Andrew Jackson & Martin Reijns (Addgene plasmid # 108699). Gene silencing was conducted using dicer-substrate interfering RNA (dsiRNA) specific to *MEF2A, MEF2C, MEF2D, TMEM173, MAVS, IRF1, STAT1* or non-targeting control. Transfection were carried out using 20 nM of dsiRNAs delivered intracellularly using TransIT-TKO (Mirus) according to manufacturer's guidelines. Additional *MEF2A* targeting was done using silencer siRNA (Dharmacon) or scramble control.

RNA extraction and quantification of gene expression

Total RNA was extracted using the NucleoSpin RNA extraction kit (Macherey-Nagel) as indicated by manufacturer guidelines. cDNA synthesis was performed using the QuantiTect RT kit (QIAGEN) or iScript cDNA synthesis kit (BioRad) according to the manufacturer guidelines. Relative quantification of mRNA was done by qPCR using the ViiA7 qPCR system with TaqMan reagents (Life Technologies) or CFX-384 with SSO Advanced Probes reagents (BioRad) using the *HPRT1* as reference gene. Primers and probes used for qPCR assays in this study were acquired from IDT or Life Technologies as indicated.

Western blot analysis

Whole cell lysates were prepared from cells using RIPA buffer (10 mM Tris-Cl (pH 8.0), 1 mM EDTA, 0.5 mM EGTA, 1% Triton X-100, 0.1% sodium deoxycholate, 0.1% SDS, 140 mM NaCl) supplemented with Halt protease and phosphatase inhibitor cocktail (Pierce). Protein quantification and normalization was done using the BCA Protein Assay Kit (Pierce). 10-30 ug total protein were resolved by SDS-PAGE and transferred to PVDF membranes (Bio-Rad). Primary antibody incubations were done overnight with antibodies diluted in 3% BSA in TBS-T

(Tris-buffered saline/Tween 20), and species-specific HRP conjugated secondary antibodies. Chemiluminescent image acquisition was performed using a ChemiDoc Touch (BioRad).

RNA sequencing, data processing, and analysis

AC16 cells were seeded in 24-well plates at a density of 2 x 10^5 cells/well and transfected with either negative control or *MEF2A*-targeting dsiRNA in triplicate. Total RNA was extracted 24 h post transfection as described above. Total RNA fluorometric quantification of was done using the Qubit RNA BR assay kit (Invitrogen) and assessment of RNA integrity was performed using the RNA 6000 Nano Kit in the 2100 Bioanalyzer (Agilent). Library preparation, QC, and sequencing was carried out by Seattle Genomics. Briefly, the synthesis of cDNA libraries was conducted using the TruSeq Stranded mRNA Library Prep Kit. Libraries were sequenced using the Ilumina NextSeq 500 sequencer. Human genome sequence (fasta) and gene transfer files (gtf) were obtained through iGenomes (https://support.illumina.com/sequencing/sequencing_software/igenome.html). Raw RNA-seq data (Fastq files) were demultiplexed prior to read quality determination (FastQC, version 0.11.3). Remaining ribosomal RNA reads were digitally removed using Bowtie2 (version 2.3.4). All samples had a minimum of twenty million reads per sample which were aligned to the human genome (GRCh37) using STAR (version 2.5.3a) and gene counts were derived using HTSeq (version 0.6.1). Library preparation, QC and sequencing of H1 and *DDX41* KO cells mRNA was done by Genewiz (Azenta Life Sciences). Gene counts were filtered (mean of ≥10 or greater across all samples) prior to statistical analysis using R statistical programming language (version 3.4.3) and 'edgeR' (version 3.20.9). Gene counts normalization was performed with voom and differential expression analysis was carried out with 'limma' (version 3.34.8). Gene Ontology

analysis of differentially expressed transcripts (lfc |0.26|; p-value < 0.01) was performed using EnrichR.

Micronuclei quantification assay

3 x 10^6 AC16 cells were plated in a 100-mm dish and treated with 100 ng/mL of nocodazole for 6h. Mitotic cells were harvested by shake-off and washed 3x with PBS. Mitotic cells were then counted and plated in on poly-L-ornithine (PLO)-coated #1.5 12 mm glass-coverslips (Thomas Scientific). Simultaneously, untreated AC16s were plated on PLO-coated coverslips and transfected with 40 nM of non-targeting dsiRNA or dsiRNA targeting *MEF2A* for 24 h. Cells were fixed with 4% Paraformaldehyde for 15 min at room temperature. Fixed cells were then washed 2 times with PBS and blocked in PBS containing 3% BSA and 0.3% Triton-X100. Cells were stained using Lamin B1 antibodies (CST) at 1:200 dilution for 1h at room temperature in PBS containing 1% BSA and 0.1% Triton X-100. Cells were washed 3 times and stained with Alexa-488 conjugated anti-rabbit secondary (Invitrogen) and DAPI (Thermo Scientific) for 1h at room temperature (RT) in PBS containing 1% BSA and 0.1% Triton X-100. Cells were washed and mounted with ProLong Glass Antifade mounting medium (Thermo Fisher). Samples were imaged using a Nikon Eclipse Ti laser scanning confocal microscope, 60x oil-immersion lens. Percent micronuclei was quantified by counting the number of micronuclei per nucleus in the field of view using FIJI[240].

***In vivo* and *in vitro* R-loop quantification assay**

RNA:DNA hybrid microscopy was conducted as previously described with some modifications[241]. AC16 cells were seeded at 0.5 x 105 cells/well on poly-L-ornithine (PLO)-coated #1.5 12 mm glass-coverslips (Thomas Scientific) and transfected with 40 nM of siNC or siMEF2A for 24 h. Cells were fixed as described above. Fixed cells were then washed 2 times

with PBS and blocked in PBS containing 3% BSA and 0.3% Triton-X100. Cells were immunostained using S9.6 antibody (Kerafast) at 1:500 dilution for 1h at RT in PBS containing 1% BSA and 0.1% Triton X-100. Cells were washed 3 times and stained with Alexa-488 conjugated anti-mouse secondary (Invitrogen) and DAPI (Thermo Scientific) for 1h at room temperature in PBS containing 1% BSA and 0.1% Triton X-100. Cells were washed and mounted with ProLong Glass Antifade Mountant (Thermo Fisher). Samples were imaged using a Nikon Eclipse Ti laser scanning confocal microscope, 60x oil-immersion lens. Images were quantified using CellProfiler[242] and presented as mean S9.6 foci intensity per nuclei.

RNA:DNA hybrid dot blots were performed as previously described[224]. In brief, total *MEF2A*-targeted and control cell DNA was extracted using NucleoSpin Tissue DNA kit (Machery-Nagel). DNA was digested with RNase III (Thermo Fisher Scientific) 1U/µg of DNA for 2h at 37°C followed by heat inactivation at 65°C for 20 min. Samples were then split in half and digested with RNaseH (Thermo Fisher Scientific) at 37°C overnight. RNAse treated DNA was then blotted on nitrocellulose membranes and UV-crosslinked using 1200 µJ x 100 cm^2. Membranes were blocked for 30 min in 3% BSA in TBS and 0.1% Tween-20. Membranes were probed overnight at 4°C with anti-RNA:DNA hybrid (S9.6) (Kerafast) at 1:2,000 dilution or dsDNA antibody (Abcam) at 1:2000 dilution. Membranes were incubated for 45 min with anti-mouse IgG HRP conjugated secondary antibodies for 45 min. Membranes were imaged using Bio-Rad Chemidoc.

ISGF3 Gaussia luciferase and ISRE GFP reporter assays

To generate the ISGF3 Gaussia Luciferase (Gluc) reporter construct, pTRIPZ-5xISGF3-BS-hGLuc-PEST, 5 tandem ISGF3 consensus sequences (5'-CGAAGAAATGAAACT-3')[243] were cloned with hGLuc-MODC-PEST into a pTRIPZ lentiviral plasmid. Lentivirus encoding

the reporter was packaged used to transduce human hepatoma Huh7 cells prior to single-cell cloning of reporter cells. To assess the presence of secreted IFN from dsiRNA transduced AC16 cells, cell supernatants from *MEF2*-depleted and non-targeting control were harvested 24 h post transfection and transferred onto 5xISGF3-GLuc Huh7 reporter cells. Reporter cells were then incubated at 37°C and 5% CO_2 for 24 h prior to assessment of Gaussia luciferase secretion into the media. Sample supernatants were diluted 1:1 with Gaussia Luciferase glow assay substrate (Thermo Fisher Scientific) and luminescence measured using a Synergy HTX (BioTek). To generate ISRE-GFP reporter cell lines, AC16 were stably transduced with lentivirus pISRE-sfGFP and pools were treated with 100IU/ml of recombinant IFNβ or transfected with non-targeting control or *MEF2A*-targeting dsiRNA in the presence of the indicated inhibitors prior to epifluorescent imaging using an EVOS cell imaging system (Thermo Fisher Scientific). For flow cytometric assessment of fluorescence expression, cells were recovered by trypsinization, labeled with Fixable Viability Dye eFluor™ 780 (Invitrogen) per manufacturer's guidelines and fixed with 4% methanol-free PFA. Fluorescence intensity was using a CANTO analyzer (BD). Flow cytometry data was analyzed using FlowJo (TreeStar).

ELISA quantification of 2′,3′-cGAMP production

H1 control AC16 cardiomyocytes and *cGAS* KO AC16s were seeded in 12-well plates and transfected with 5 μg of CT-DNA using Transit X2 (Mirus) at a 2:1 ratio for 8 h prior to harvest. Wild-type AC16 cells were seeded in 12-well plates prior to depletion of *MEF2A* with dsiRNA or non-targeting control as described above for 24 h prior to harvest. 2',3'-cyclic GMP-AMP (cGAMP) was quantified using the Direct 2′,3′-cGAMP ELISA Kit (Arbor Assays) according to manufactures protocol. Briefly, cells were lysed in 150ul of sample diluent solution for 15 min at room temperature. Cell lysates were recovered by scrapping and cell debris was

removed by centrifugation at 700 x g at 4°C. Absorbance was read at 450 nm using a Synergy HTX (BioTek).

Quantification and Statistical Analysis

Statistical analysis was performed using GraphPad Prism 9.0 (GraphPad software La Jolla, CA). Statistical significance was calculated as indicated for each experiment in the figure legends and across all experiments, p-values of < 0.05 were considered significant and are indicated by asterisks (∗). The number (N) of technical or biological replicates or individual cells and nuclei are indicated by data points in figures and/or descriptions in figure legends. Standard deviations (SD) or Standard Error of the Mean (SEM) are reported in figure legends.

Data and code availability

- The data generated in this study are available via the following accession identifiers on the NCBI-GEO database (GEO: GSE209601). The data used for gene expression analyses described in this manuscript were obtained from the GTEx Portal.
- This paper does not report original code.

Any additional information required to reanalyze the data reported in this work paper is available from the lead contact upon request.

2.5 Acknowledgements

We thank Daniel B. Stetson and Haitao Wen for sharing reagents and Richard Robinson and Eugene Oltz for manuscript feedback. This work was supported in part by the Award for Advancing Research in Infection and Immunity (A.F.), and the National Institutes of Health under grant number P30 CA016058 (The Ohio State University Comprehensive Cancer Center), R21AI141823 (R.S.), T32AI106677-6 (J.R.S.), and T32HL007312(A.F.). The content is solely the responsibility of the authors and does not necessarily represent the funding agency views.

Author contributions

Investigation and Formal Analysis (J.R.S, J.W.D, M.I.M, A.K., J.S., and A.F.); Conceptualization (J.R.S, J.W.D, A.F.), Writing (J.R.S, A.F.), Methodology (J.J.W), Supervision (R.S. and A.F.), Funding Acquisition (R.S. and A.F.).

Declaration of interests

These authors declare no competing interests.

2.6 Figures

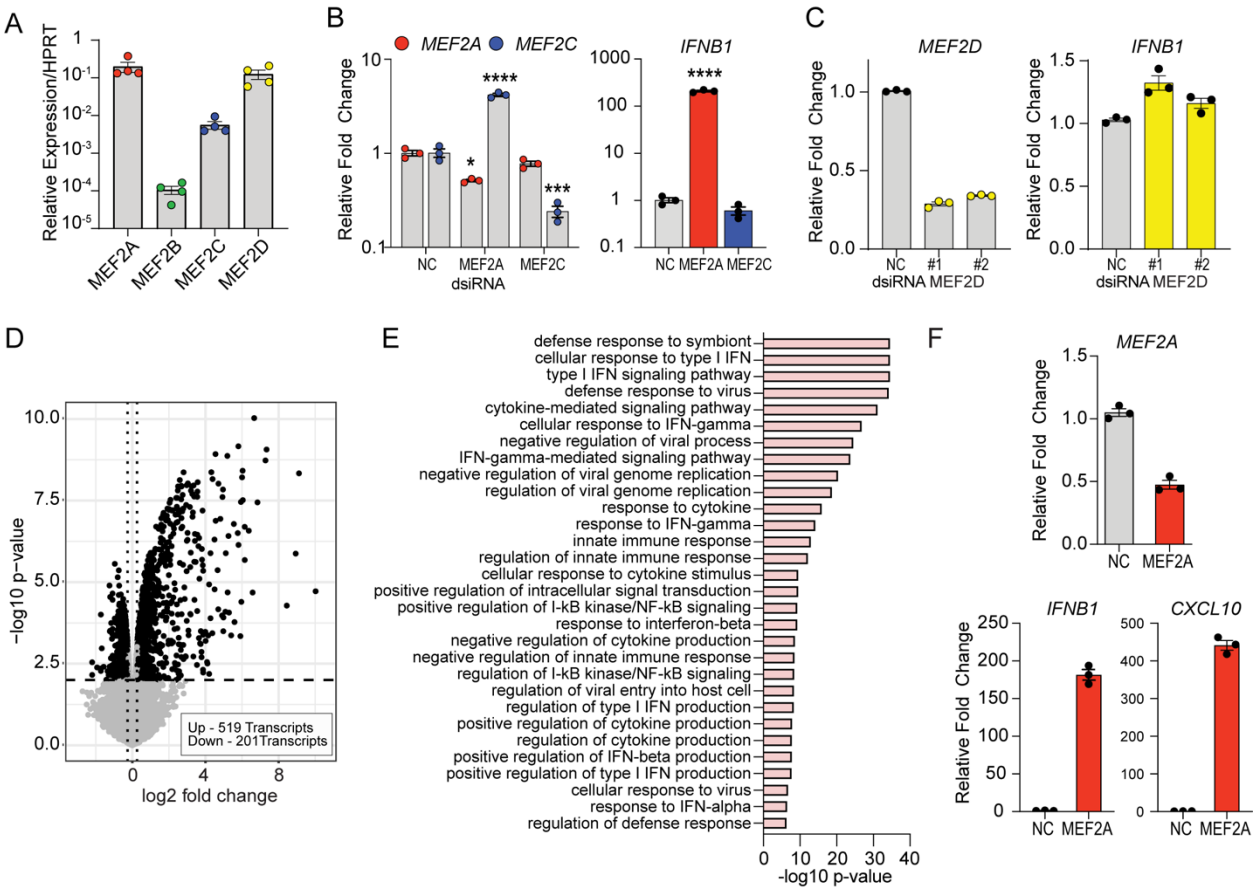

Figure 2.1. MEF2A silencing induces innate immune inflammation

A. Expression of MEF2 transcripts was calculated relative to *HPRT1*. Bars represent the average expression across 4 independent experiments and error bars represent SEM. **B.** Bar graphs represent relative expression of *MEF2A* (red) and *MEF2C* (blue) mRNA following dsiRNA

transfection (left). Expression of *IFNB1* mRNA following dsiRNA-mediated depletion of *MEF2A* (red) or *MEF2C* (blue). Relative fold change was calculated relative to NC transfected cells and normalized to *HPRT1* (value 1). **C.** Bar graphs represent the average relative expression of *MEF2D* (yellow, left) and *IFNB1* (right) mRNA following transfection of AC16 cells with two distinct MEF2D targeting dsiRNA or NC. Relative fold change in expression was calculated as described above. Experiments represent average of 3 individual experiments. Asterisks indicate **** $p \leq 0.0001$, *** $p \leq 0.001$ and * $p < 0.05$ as determined by one-way ANOVA. **D.** Volcano plot of differentially expressed genes (LFC |0.26|; adj p-value 0.01) following knockdown (KD) of *MEF2A* with dsiRNA. 519 transcripts were significantly upregulated, and 201 transcripts were downregulated (black) relative to NC transfected cells. Each dot represents a unique transcript, dashed lines indicate threshold of significance. Non-significant changes in gene expression are highlighted in grey. **E.** Bar graph represents the top 30 GO biological processes enriched amongst the genes upregulated by *MEF2A* depletion. **F.** Loss of MEF2A promotes the expression of *IFNB1* and *CXCL10* mRNA. Relative ISG expression was normalized to NC transfected cells (value of 1) and normalized to *HPRT1*. Data is representative of the average of 3 individual replicates ± SEM. See also Figure S1.

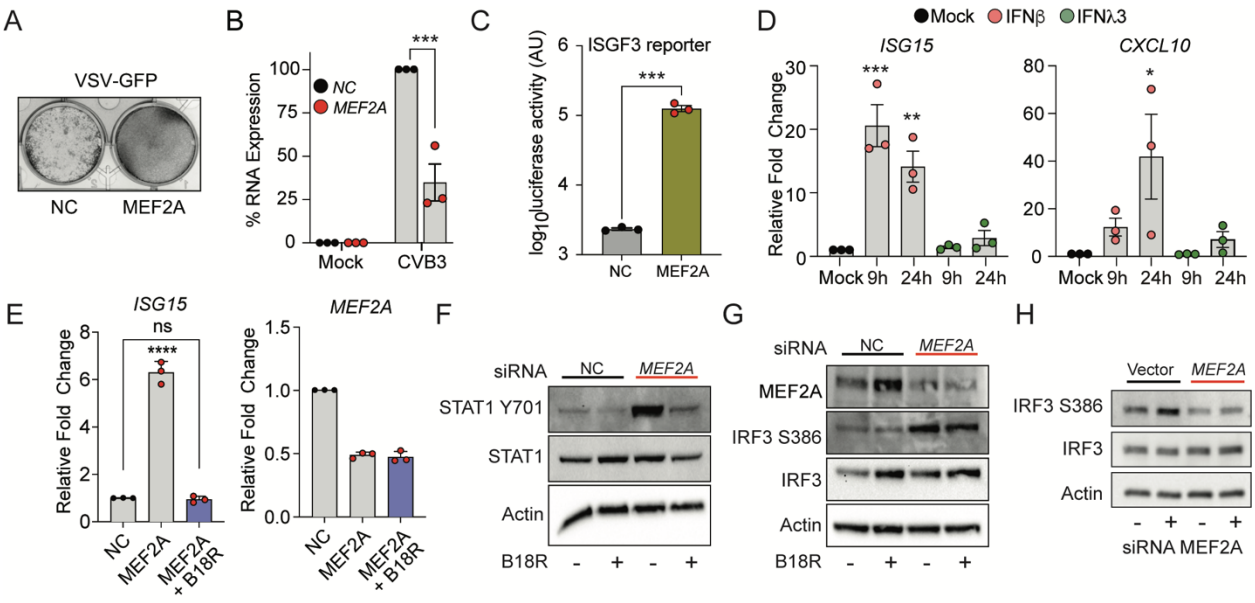

Figure 2.2. Type I IFN drive antiviral states upon MEF2A loss

A. Loss of *MEF2A* protects cells against the cytopathic effect of vesicular stomatitis virus (VSV). **B.** *MEF2A* loss protects against coxsackie virus B (CVB3). Bar graphs represent mean percent reduction of CVB3 viral RNA expression (VP1) in *MEF2A*-depleted cells (red) relative to NC-transfected cells (black) across 3 independent experiments ± SEM. **C.** Bar graphs represent average *Gaussia* luciferase activity from 5xISGF3-Gluc Huh7 reporter cells stimulated with supernatants derived from AC16 cells after *MEF2A* depletion. Data represents 3 independent experiments ± SEM. *** $p \leq 0.001$, as determined by students t-test. **D.** AC16 cells were stimulated with 25 IU/ml IFNβ (pink) or 100 ng/ml IFNλ3 (green) for the indicated times prior to total RNA harvest. Relative expression of *ISG15* and *CXCL10* mRNA was measured relative to *HPRT1* and normalized to mock-treated cells (value 1). Bar graphs represent average of 3 independent experiments ± SEM. *** $p \leq 0.001$, ** $p \leq 0.01$, * $p < 0.05$ as determined by two-way ANOVA. **E.** Type I IFN was blocked by pre-treatment of AC16 cells with 1 µg/mL of recombinant B18R prior to transfection with dsiRNA. Expression of *ISG15* (left) or *MEF2A* (right) mRNA was quantified relative to *HPRT1* and normalized to NC-transfected cells (value

of 1). Bar graphs represent average of 3 independent experiments ± SEM and **** represent $p \leq 0.0001$ as determined by one-way ANOVA. **F.** Activation of IFN signaling was probed by measuring phosphorylated STAT1 (Y701), STAT1, and Actin protein expression by Western blot. **G.** AC16 cells were treated as mentioned above and the levels of phosphorylated IRF3 (S386), IRF3, and Actin were measured by Western blot analysis. **H.** Vector control AC16 cells and cells overexpressing MEF2A were transfected with dsiRNA targeting the 3'UTR of the endogenous *MEF2A.* The levels of phosphorylated IRF3 (S386), IRF3, and Actin were measured by Western blot analysis. See also Figure S2.

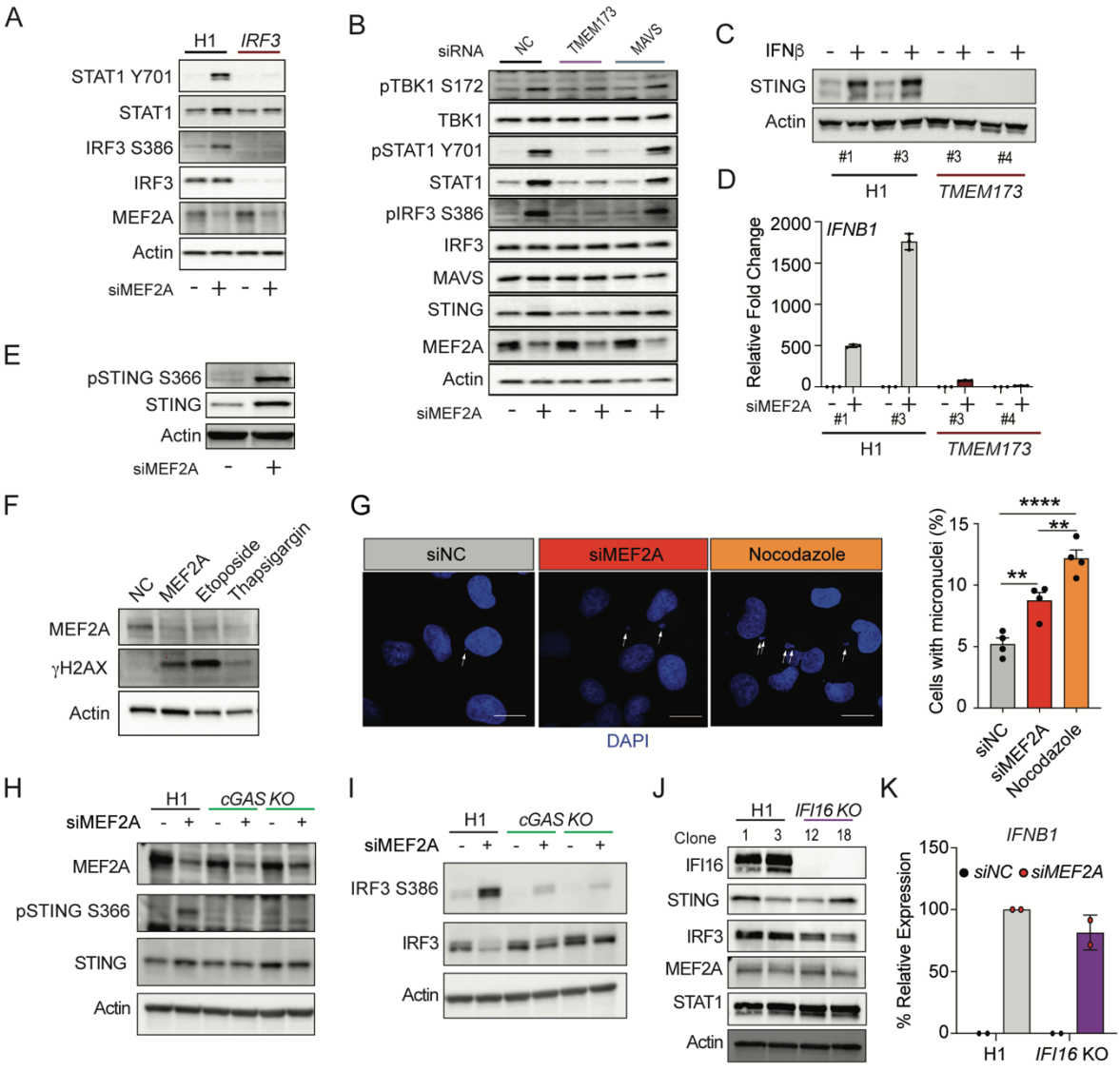

Figure 2.3. STING expression is necessary for the induction of IFN-mediated inflammation

A. AC16 cells stably transduced with non-targeting single-guide RNA (sgRNA) (H1) or IRF3-targeting sgRNA (IRF3) were transfected with NC or *MEF2A* targeting dsiRNA for 24 h. Analysis of protein expression of phosphorylated IRF3 (S386) and STAT1 (Y701), IRF3, STAT1, MEF2A, and Actin protein by Western Blot. **B.** Signal transduction through STING, but not MAVS, is required for IFN induction after the loss of MEF2A. AC16 cells were transfected with dsiRNA targeting *MAVS*, *TMEM173* (STING), or NC for 24 h. Cells were transfected with dsiRNA targeting *MEF2A* or NC for an additional 24 h. Whole cell protein lysates were probed

for phosphorylated TBK1 (S172), IRF3 (S386) and STAT1 (Y701), TBK1, STAT1, IRF3, MAVS, STING, MEF2A, and Actin. Western blot representative of 3 independent experiments. **C.** H1 and *TMEM173*-targeted cells were mock-treated or stimulated with IFNβ (25IU/ml) for 24 h. and Actin protein expression was measured by Western blot. Numbers indicate clonal cell populations. **D.** AC16 H1 and *TMEM173* (STING) KO cells transfected with dsiRNA targeting *MEF2A.* Bar graphs represent the average relative MEF2A mRNA expression relative to *HPRT1* expression and NC transfected cells (value 1) across 2 individual experiments. Numbers indicate clonal cell lines. **E.** AC16 cells were transfected with NC or MEF2A targeting siRNA for 24 h. Protein expression analysis for phosphorylated STING (S366), STING, and Actin. **F.** AC16 cells were transfected with either NC or *MEF2A* target dsiRNA. In parallel, cells were stimulated with Etoposide or thapsigargin. 24 h post treatment MEF2A, γH2AX, and Actin protein expression was measured by Western blot. Images are representative of 3 independent experiments. **G.** Representative micrographs of micronuclei detected by confocal microscopy of DAPI stained DNA in AC16 cells transfected with NC or *MEF2A*-targeting dsiRNA, or cells treated with nocodazole as positive control. Bar graphs represent the percentage of micronuclei positive cells following NC (grey), *MEF2A* KD (red), or treatment with nocodazole (orange). Data represents average of 4 independent experiments ± SEM. **** $p \leq 0.0001$ and ** $p \leq 0.01$ as determined by one-way ANOVA. **H.** AC16 expressing a non-targeting sgRNA (H1) or clones of cells in which *cGAS* has been targeted (cGAS KO) were transfected with NC or *MEF2A* targeting dsiRNA. 24 h post transfection, protein expression of MEF2A, phosphorylated STING (S366), total STING, and Actin was measured. **I.** Expression of phosphorylated IRF3 (S386), total IRF3, and Actin. Western blots are representative of at least 3 independent experiments. **J.** Clonal lines IFI16 knock-out were derived as indicated by individual numbers and expression of IFI16, STING,

IRF3, MEF2A, STAT1 and Actin was assessed by Western blot. **K.** AC16 H1 (clone1) and *IFI16* KO (clone 18) cells were transfected with NC or *MEF2A* targeting dsiRNA. 24 h post transfection relative expression of *IFNB1* mRNA was quantified by qPCR. Bar graphs represent *IFNB1* mRNA expression relative to *HPRT1* and H1 siMEF2A transfection (value 100). Data represents average of independent experiments ± SEM. See also Figure S3.

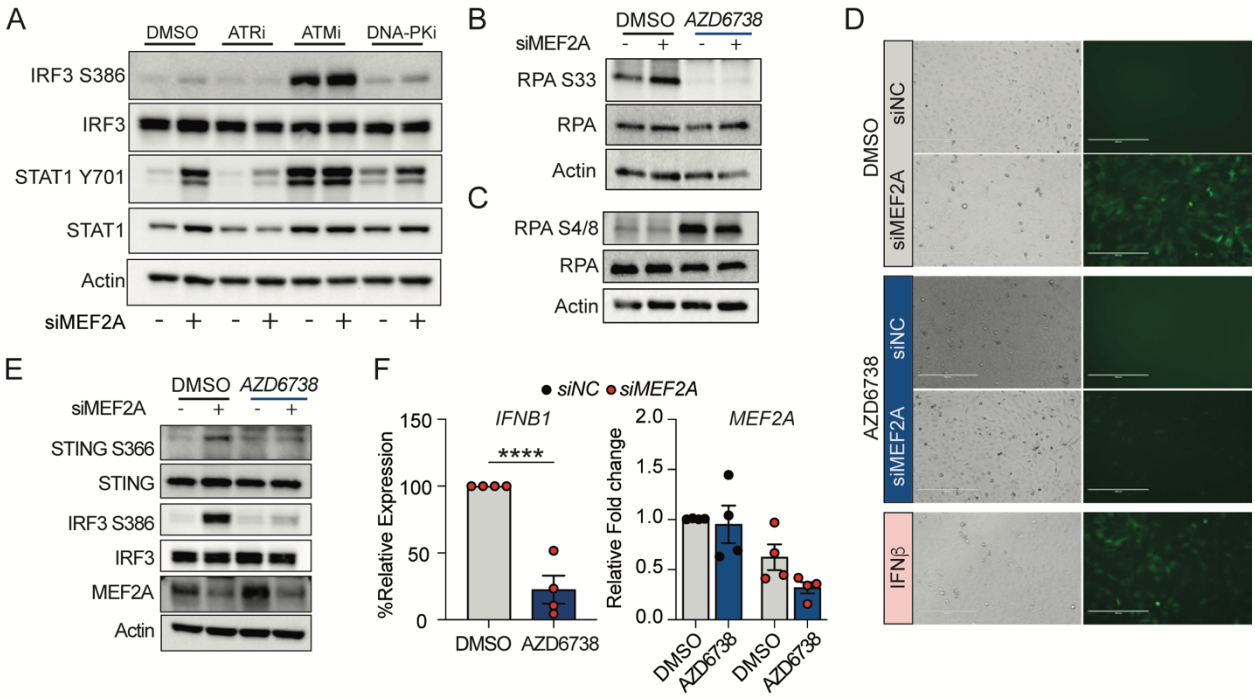

Figure 2.4. ATR kinase activity is required for IFN induction

A. Human fibroblast cells, BJ/TERT, were pre-treated with ATR (ETP-46464, 2μM) ATM (KU-55933, 30μM), DNA-PK (NU7441, 4μM) kinase inhibitors or DMSO as vehicle control for 2 h prior to dsiRNA transfection. Whole cell lysates were harvested 24 h post transfection and phosphorylated IRF3 (S386) and STAT1 (Y701), IRF3, STAT1, and Actin protein expression was measured. Data is representative of 3 independent experiments. **B.** BJ/TERT cells were pre-treated with AZD6738 (2μM) for 2 h prior to transfection with dsiRNA. Whole cell lysates were probed for phosphorylated RPA32(Ser33), total RPA32, and Actin by Western blot. **C.** Phosphorylation of ATM/DNA-Pk substrate RPA32 (Ser4/8) following *MEF2A* depletion and ATR kinase inhibition as determined by Western Blot. **D.** AC16 ISRE-GFP reporter cell lines were pre-treated with AZD6738 (2μM) for 2 h prior to dsiRNA transfection. Control cells were stimulated with 100 IU/ml of recombinant IFNβ. Fluorescent signal was detected by epifluorescent microscopy. **E.** AC16 cells were treated as described above. Expression of phosphorylated IRF3 (S386) and STING (S366), STING, IRF3, MEF2A, and Actin was

measured by Western blot. Data is representative of 3 independent experiments. **F.** Bar graphs represent the percent relative expression of endogenous *IFNB1* mRNA expression in transfected AC16 cells in response to ATR kinase inhibition. Relative *IFNB1* mRNA expression was calculated relative to expression in DMSO treated cells and normalized to *HPRT1* control (value 100%). Relative *MEF2A* expression was normalized to *HPRT1* expression and DMSO treated cells (value 1). Each represents average of 4 individual experiments ± SEM. **** $p \leq 0.0001$ as determined by student's t-test. See also Figure S4.

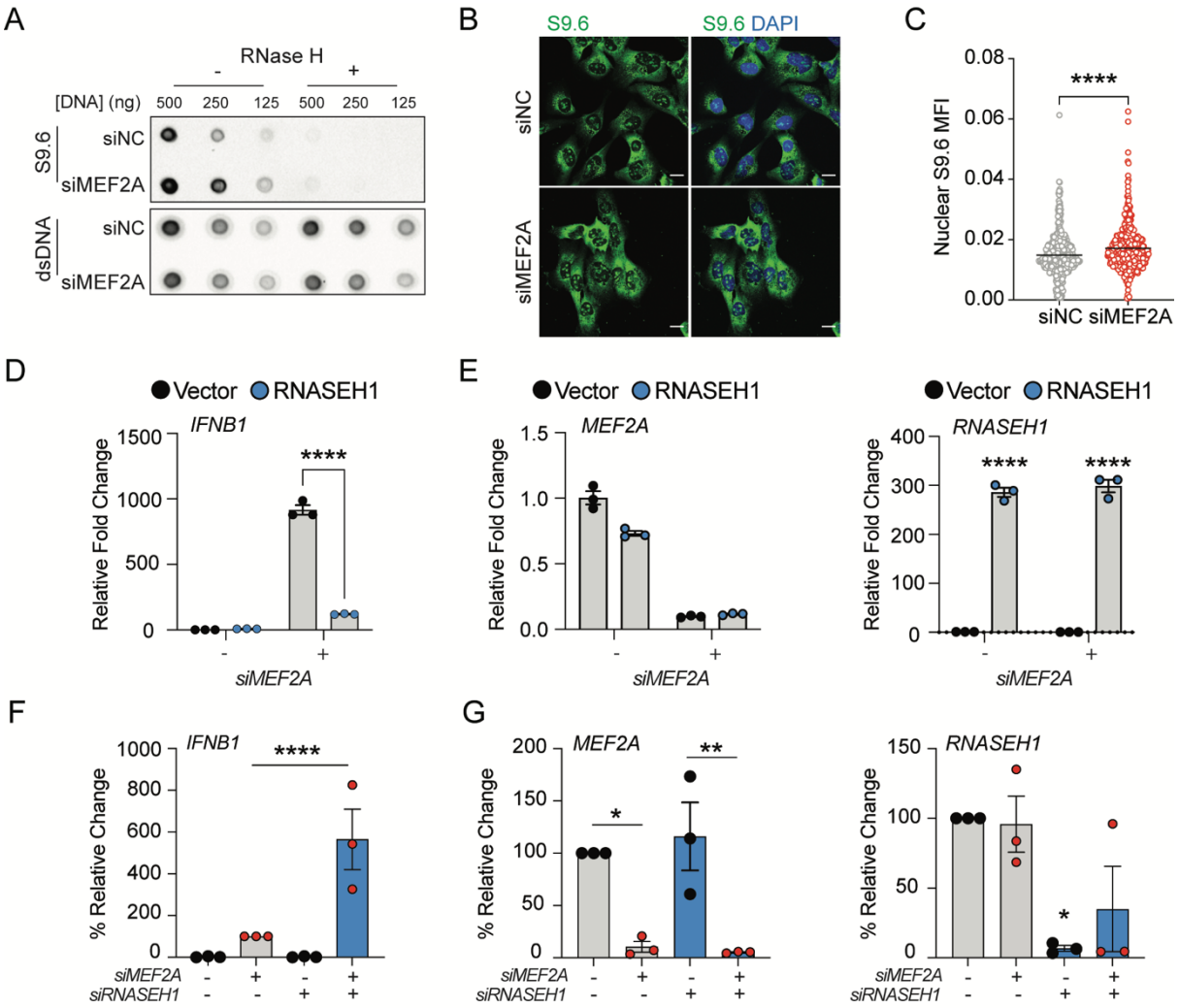

Figure 2.5. MEF2A depletion promotes R-loop accumulation.

A. RNA:DNA hybrid formation in AC16 cells transfected with NC or *MEF2A*-targeting dsiRNA. Serial dilutions of RNAse III treated nucleic acids were probed with S9.6 antibody or dsDNA-specific antibodies. RNaseH treatment was used for RNA:DNA hybrid degradation. **B.** Representative micrograph of S9.6 staining (green) in AC16 cells following dsiRNA transfection. DAPI staining (blue) indicates cell nucleus. Scale bar represents 20 µm. **C.** Quantification of nuclear S9.6 staining in cells transfected with NC or MEF2A-targeting dsiRNA. Data points represent individual nuclei. **D.** AC16 cells were transfected with *RNASEH1* expression plasmids of empty vector control (vector) overnight followed by dsiRNA

transfection. Bar graphs represent the fold change in *IFNB1* mRNA expression relative to vector/NC control and *HPRT1* (relative value of 1) ± SD. **** $p \leq 0.0001$ as determined by two-way ANOVA. Data is representative of experiments conducted in triplicate. **E.** Bar graphs represent the average expression of *MEF2A* and *RNASEH1* in transfected cells relative to HPRT1 ± SD. **** $p \leq 0.0001$ as determined by two-way ANOVA. **F.** Cells were co-transfected with dsiRNA targeting *MEF2A* and/or *RNASEH1* for 24 h prior to harvesting of total RNA. Bar graphs represent the percent fold change in *IFNB1* mRNA expression relative to *HPRT1* ± SD. Data was normalized to *IFNB1* mRNA expression in *MEF2A:NC* dsiRNA co-transfected cells (relative value of 100%). ** $p = 0.0015$ as determined by two-way ANOVA. Data representative of triplicate experiments. **G.** Bar graphs represent the average expression of *MEF2A* and *RNASEH1* in transfected cells relative to HPRT1 across triplicate experiments ± SD. Statistical significance was determined by two-way ANOVA. See also Figure S5.

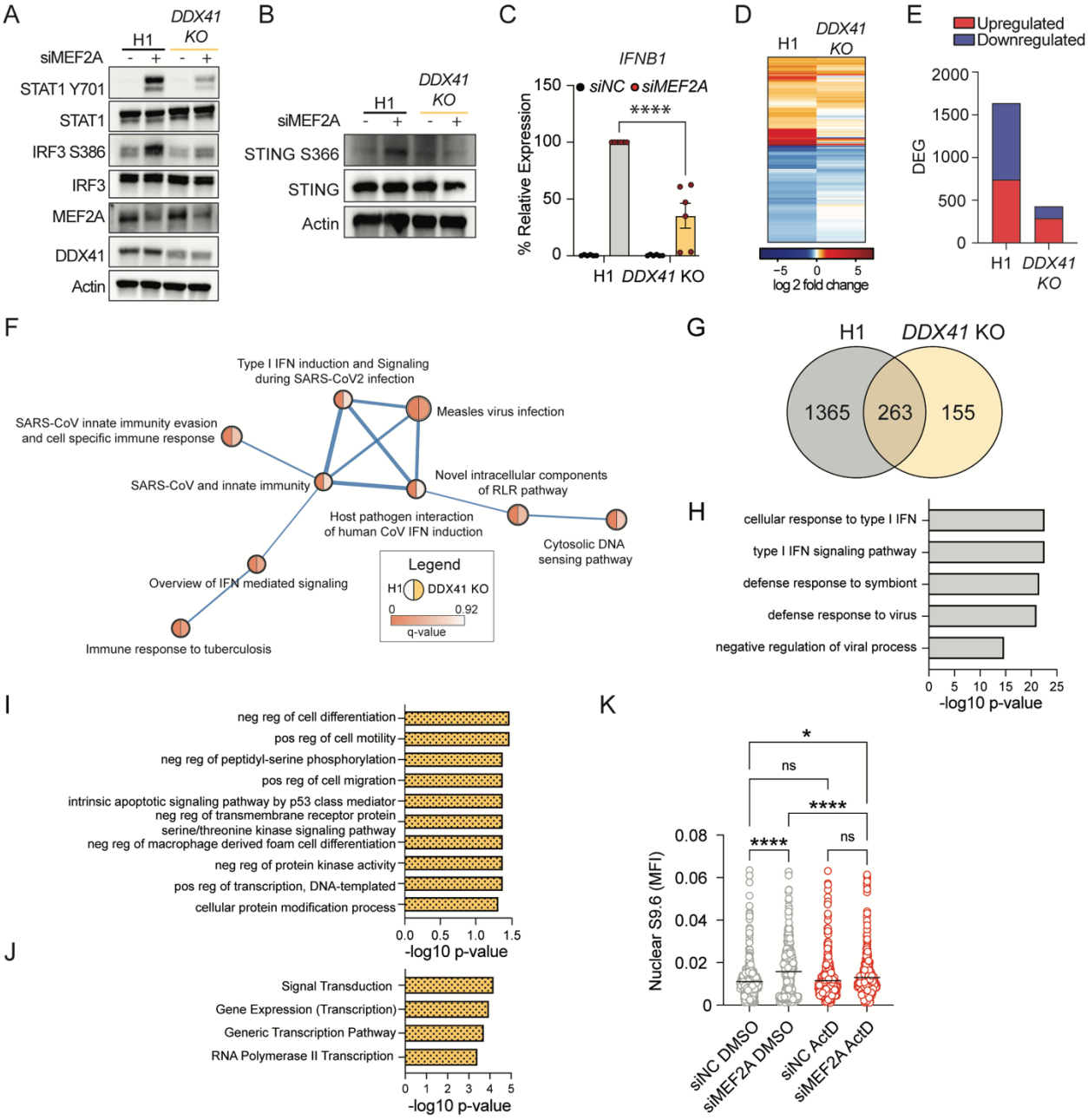

Figure 2.6. MEF2A depletion triggers DDX41-mediated inflammation and transcriptional stress.

A. AC16 DDX41-deficient cells were generated by CRISPR-Cas9 genome editing (DDX41 KO). Wild type (H1) and DDX41 KO cells were transfected with NC or MEF2A-targeting dsiRNA for 24 h post transfection. Whole cell lysates were probed for protein expression of

phosphorylated STAT1 (Y701) and IRF3 (S386), STAT1, IRF3, MEF2A, DDX41 and Actin. Data are representative of a minimum of 3 independent experiments. **B.** Control cells (H1) and DDX41 KO cells were transfected with NC or MEF2A-targeting dsiRNA as indicated above. Phosphorylated STING (S366), STING, DDX41 and Actin protein expression determined by Western blot. **C.** AC16 H1 and DDX41 KO cells were transfected with NC or MEF2A-targeting dsiRNA for 24 h prior to harvesting total RNA. Bar graphs represent percent IFNB1 mRNA expression relative to HPRT1 control and normalization to IFNB1 mRNA expression in H1 cells transfected with dsiMEF2A (100 %). Bar graphs represent average expression across 5 independent experiments ± SEM. **** $p \leq 0.0001$ as determined by two-way ANOVA. **D.** Hierarchical clustering and relative expression of 1793 differentially expressed genes (LFC |0.26|; adj p-value 0.01) following knockdown (KD) of MEF2A with dsiRNA in either wild-type (H1) or DDX41 KO cells. **E.** Bar graph represents upregulated (red) and downregulated (blue) genes following MEF2A silencing in each cell type. **F.** The affiliation network represents gene connectivity across 9 GO terms identified by GSEA. Each bubble represents a unique term with enrichment (adjusted p-value) represented by bubble color for in H1 (left) or DDX41 KO (right) cells. The weighed edges represent transcript overlap. **G.** Venn diagram of overlap of DE genes following *MEF2A* silencing. **H.** GO Biological process enrichment analysis of the 1385 DEG unique to WT cells. **I.** GO term enrichment analysis of the union of overlapping DEG across genotypes and DDX41 KO cells. Bar graphs represent the -log10 p-value of enrichment for each term. **J.** REACTOME pathway enrichment analysis of the overlap of DEG across genotypes and DDX41 KO cells. Bar graphs represent the -log10 p-value of enrichment for each term. **K.** *In vivo* assessment of RNA:DNA hybrids following *MEF2A* depletion and inhibition of *de novo* transcription by actinomycin D treatment.

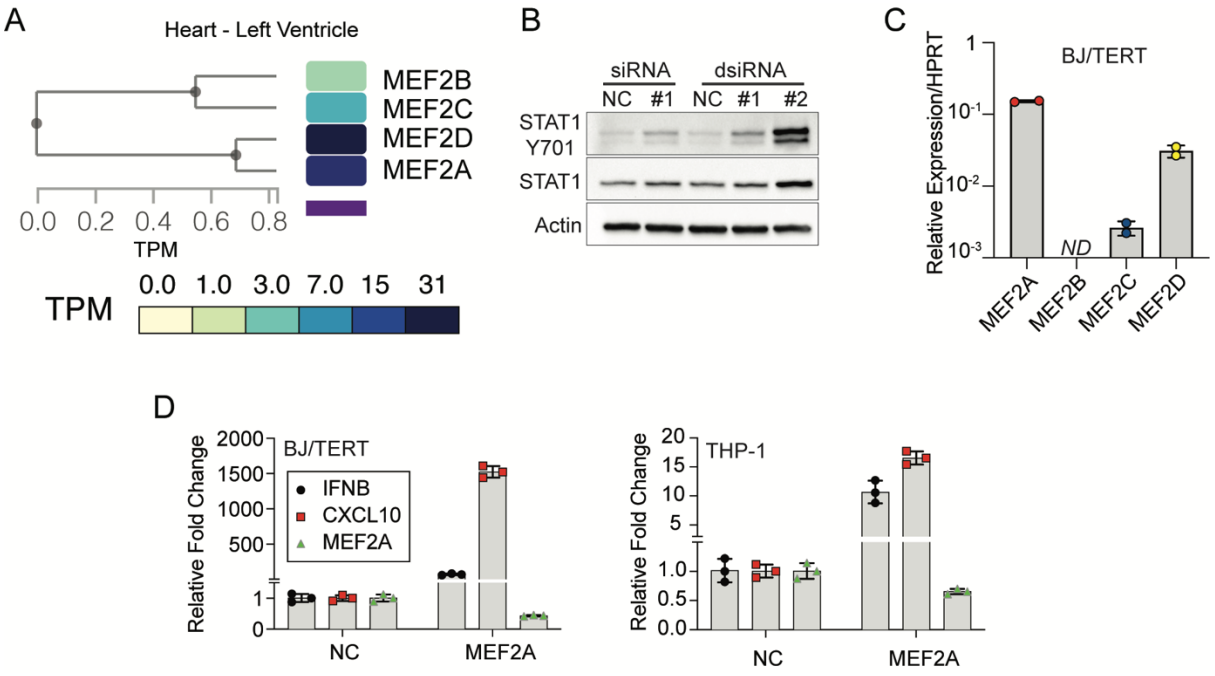

Figure 2.7. Supplemental figure related to Figure 2.1

A. Validation of IFN induction by various *MEF2A* siRNA sequences. AC16 cells were transfected with siRNA (Dharmacon) or dicer-substrate siRNA (dsiRNA) targeting distinct regions of *MEF2A* for 24 h prior to harvesting whole cell lysates. Control cells were transfected with equimolar concentrations of non-targeting siRNA. In all cases, silencing of *MEF2A* led to an increase in STAT1 phosphorylation (Y701). **B.** Expression of MEF2 transcription factor mRNA in human left ventricular cardiomyocytes. Heatmap represents the transcript per million detected by RNA sequencing as reported in GTEx. **C.** Expression of MEF2 transcripts in human fibroblast cell line, BJ/TERT. Bar graphs represent average *MEF2A* (red), *MEF2C* (blue) and *MEF2D* (yellow) mRNA expression relative to *HPRT1* across 2 independent experiments. *MEF2B* expression was not detected in these cells (ND). **D.** Depletion of *MEF2A* (green) promotes *IFNB1* (black) and *CXCL10* (red) in BJ/TERT cells relative to *HPRT1* and NC (left, value 1). Each data point represents an individual experiment, n=3. Depletion of *MEF2A* (green)

promotes *IFNB1* (black) and *CXCL10* (red) in PMA-differentiated THP-1 monocytes relative to *HPRT1* and NC (right, value 1). Each data point represents an individual experiment, n=3.

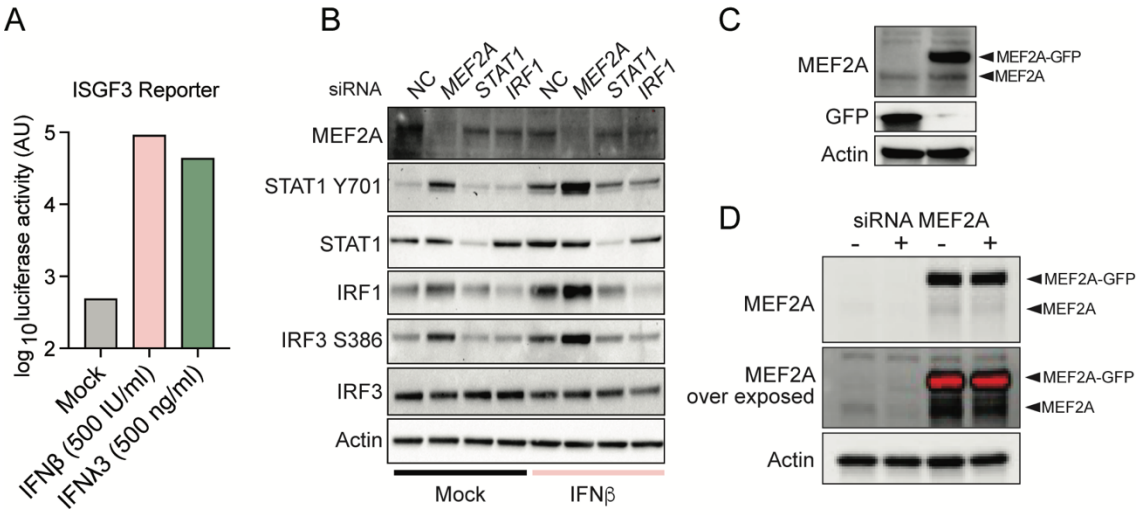

Figure 2.8. Supplemental figure related to Figure 2.2

A. Validation of ISGF3 responsiveness of reporter cell line. Bar graph represents *Gaussia* luciferase activity detected from 5xISGF3-Gluc Huh7 cells stimulated with recombinant IFNβ (500 U/mL, pink) or IFNλ3 (500 ng/mL, green) or mock treated for 24 h. **B.** AC16 cells were transfected with siRNA targeting MEF2A, STAT1, and IRF1 or NC. After 24 h of transfection, cells were stimulated with 25 IU/ml of recombinant IFNβ for 30 mins. Protein phosphorylation of IRF3 (S386) and STAT1 (Y701) was assessed by western blot. **C.** Generation of GFP vector control or MEF2A-GFP overexpressing AC16 cells. Cells were stably transduced with lentiviral vectors expressing the according transgenes. Expression of MEF2A, GFP, and Actin protein levels were determined by western blot analysis. **D.** Depletion of endogenous MEF2A using siRNA targeting the 3'UTR of *MEF2A*. AC16 cells were transfected with siRNA targeting MEF2A (Figure S1; dsiRNA #1) or NC. After 24 h of transfection, cells were Protein expression of MEF2A and Actin was assessed by western blot.

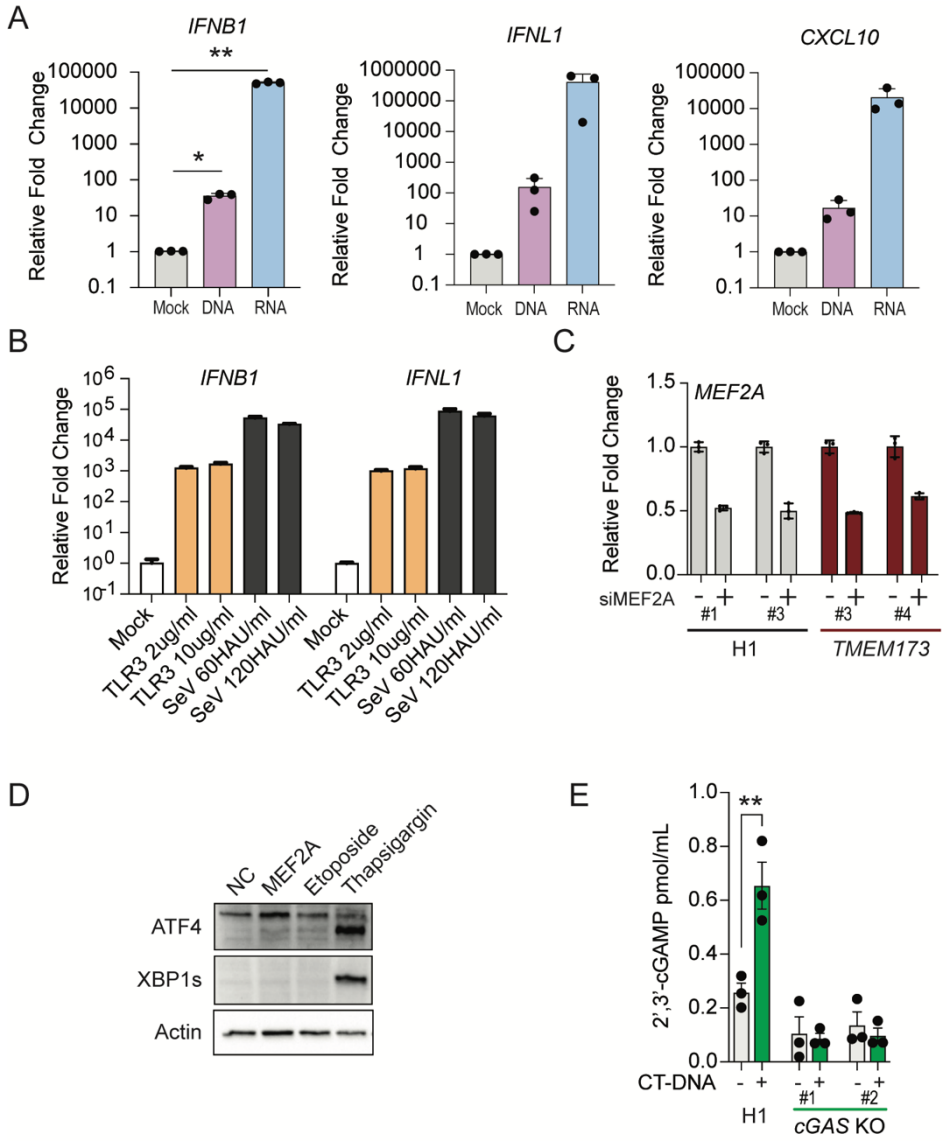

Figure 2.9. Supplemental figure related to Figure 2.3

A. Induction of type I and III IFN and IFN-stimulated genes by DNA and RNA transfection in AC16 cells. AC16 cells were transfected with calf-thymus DNA (DNA, purple) or HCV PAMP (RNA, blue) for 6 h prior to total RNA harvest. Bar graphs represent average relative fold changes in mRNA levels were calculated relative to *HPRT1* and normalized to mock-transfected cells (value 1). Bar graph represents 3 independent experiments and error bars represent SEM. **B.** Induction of IFN in response to exogenous dsRNA and virus infection. AC16 cells were treated with the indicated doses of floating poly(I:C) (TLR3 ligand) or Sendai Virus (Cantell strain). Bar

graphs represent relative fold changes in mRNA levels were calculated relative to *HPRT1* and normalized to mock-transfected cells (value 1). **C.** Confirmation of MEF2A knockdown in *TMEM173* KO cells. H1 non-targeting control and *TMEM173* targeted cells were transfected with *NC* or *MEF2A* targeting dsiRNA for 24 h. The expression of *MEF2A* was measured relative to *HPRT1* and normalized to NC transfected control for each clone (relative value 1). **D.** ER stress response elicited by treatment of AC16 cells with topoisomerase I (etoposide) and SERCA inhibitors (thapsigargin) or *MEF2A*-targeting. Cells were treated as described in Figure 4A. Whole cell lysates were probed for ATF4, spliced XBP1 (XBP1s), and Actin protein expression. Western blots representative of 3 independent experiments. **E.** 2'-3'-cGAMP ELISA in control (H1) and cGAS KO AC16 cells with and without CT-DNA transfection. Bar graphs represent average expression across 3 independent experiments ± SEM. ** $p \leq 0.01$, * $p \leq 0.05$ as determined by one-way ANOVA (A) and two-way ANOVA (E).

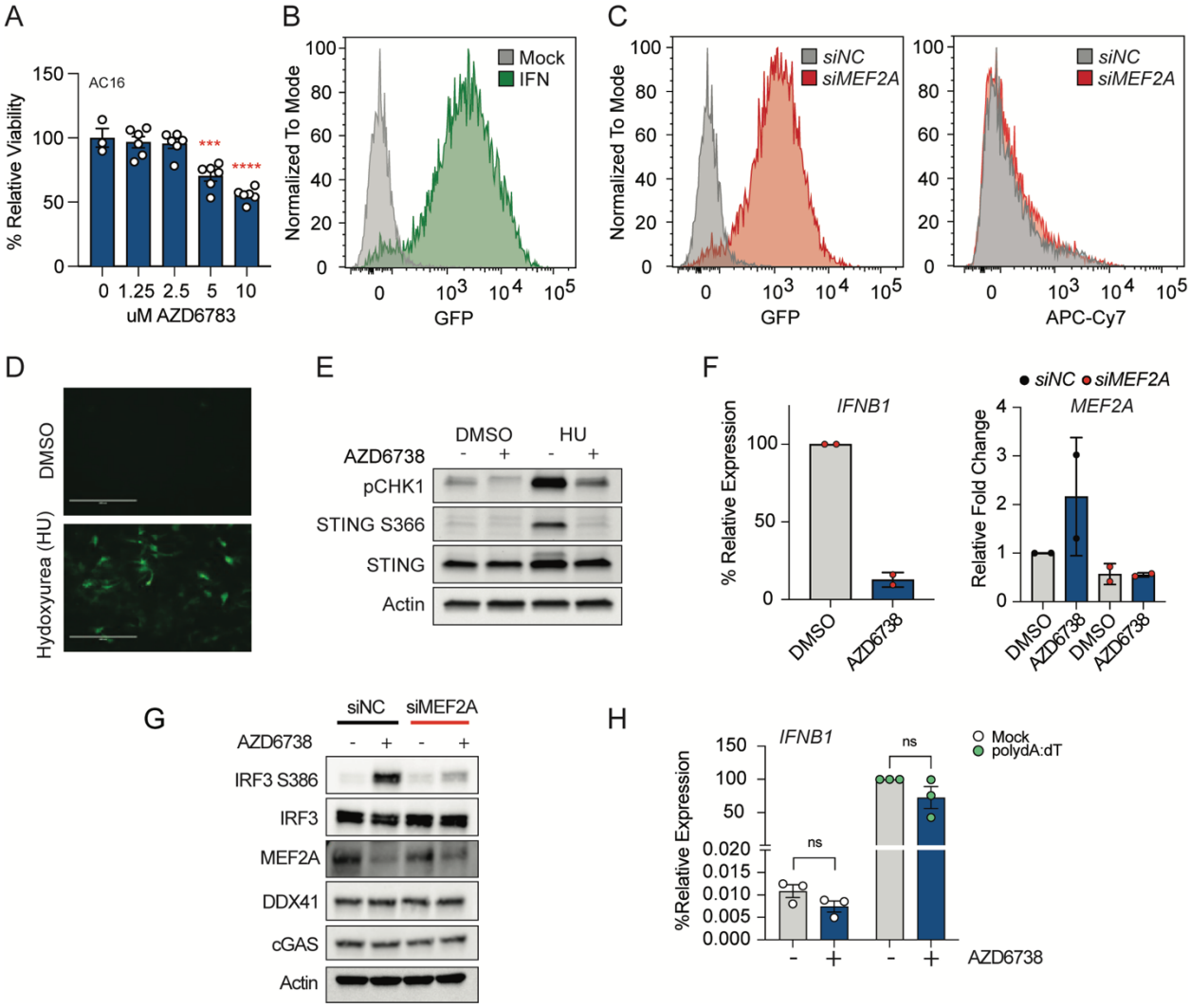

Figure 2.10. Supplemental figure related to Figure 2.4

A. Cytotoxicity of ATR kinase inhibitor AZD6783 in AC16 cells. AC16 cells were treated with increasing doses of ATR inhibitor as indicated. Cellular viability was measured by MT viability assay. Relative viability was calculated based on vehicle treated cells (100%) **B.** Characterization of AC16-ISRE-GFP reporter cell lines. Cells were treated with 500IU of recombinant IFNβ for 24 h prior to detection of FITC expression by FACS. **C.** Induction of ISRE activity by loss of MEF2A expression. AC16-ISRE-GFP cells were transfected with NC or MEF2A-targeting dsiRNA or 24 h prior to detection of FITC (left) or fluorescent-dye uptake (APC-Cy7) to assess

cellular viability (right). **D.** The induction of replicative stress by hydroxyurea treatment induces IFN responses. AC16-ISRE-GFP cells were stimulated with DMSO or 100nM hydroxyurea (HU) for 30 h. Fluorescent micrographs are representative of 3 independent experiments. **E.** The phosphorylation of STING following hydroxyurea treatment requires ATR kinase activity. AC16-ISRE-GFP cells were stimulated with DMSO or 100nM hydroxyurea (HU) for 30 h in the presence or absence of ATR inhibitor (AZD6738; 2μM). Whole cell lysates were harvested and protein expression of phosphorylated CHK1, phosphorylated STING, total STING and Actin were assessed by western blot. Images are representative of 3 independent experiments. **F.** Changes in endogenous *IFNB1* mRNA expression following ATR kinase inhibition in BJ/TERT cells transfected with NC or *MEF2A*-targeting siRNA. BJ/TERT cells were pre-treated with ATR kinase inhibitors (AZD6783; 2μM) for 2 h prior to 24 h transfection with NC or *MEF2A*-targeting siRNA. Bar graphs represent the average percent induction of *IFNB1* mRNA following *MEF2A* silencing in AZD6738 treated cells relative to DMSO (value 100%) or AZD6738 and expression level of *MEF2A* relative to DMSO (value 1) (left). Each data point represents values across 2 individual experiments and error bars represent SEM. **G.** Expression of DNA sensors in *MEF2A*-targeted and control cells treated with ATRi. **H.** *IFNB1* induction in cells treated with ATRi and polydA:dT. Each data point represents values across 3 individual experiments and error bars represent SEM.

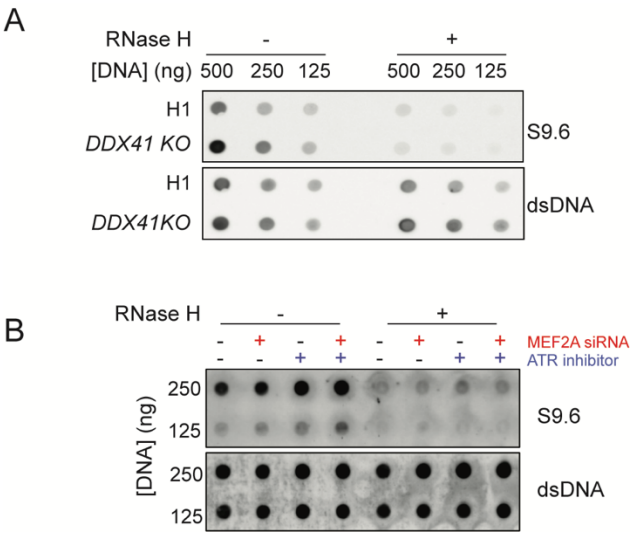

Figure 2.11. Supplemental figure related to Figure 2.6

A. In vitro assessment of RNA:DNA hybrid formation in DDX41 deficient cells. Genomic DNA was exracted from WT (H1) and *DDX41* KO AC16 cells. Serial dilutions of RNAse III treated DNA were dotted and cross-linked onto a nitrocellulose membrane as indicated. Membranes were incubated with S9.6 antibody to measure R-loops or dsDNA-specific antibodies as loading control. In addition, samples were mock-treated or digested with RNaseH to promote R-loop degradation. **B.** In vitro assessment of RNA:DNA hybrid formation in MEF2A-depleted AC16 cells with or without ATRi. Membranes were incubated with S9.6 antibody to measure R-loops or dsDNA-specific antibodies as loading control. In addition, samples were mock-treated or digested with RNaseH to promote R-loop degradation.

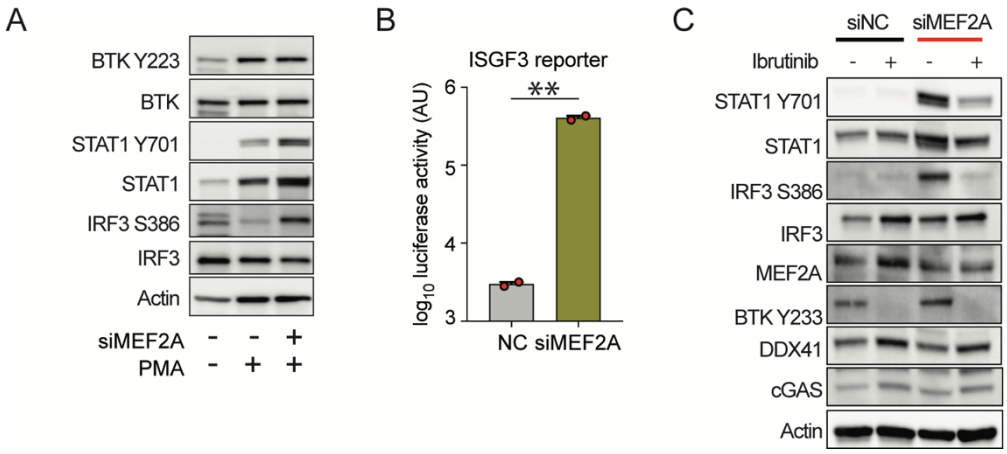

Figure 2.12. Supplemental figure related to figure 2.6

A. Bruton's tyrosine kinase (BTK) activity and MEF2A knockdown in U937 cells. Differentiation of U937 cells with 48 h PMA treatment (40 ng/ml) enhances BTK activity and STAT1 expression. PMA-differentiated cells were transfected with NC control or *MEF2A*-targeting dsiRNA for 24 h prior to harvesting whole cell lysates. Protein expression was assessed by western blot. **B.** IFN secretion from *MEF2A* depleted U937 cells. Bar graphs represent average *Gaussia* luciferase activity detected from 5xISGF3-GLuc Huh7 cells stimulated with supernatants from U937 human monocyte cells transfected with either NC or *MEF2A* targeting siRNA. Each data point represents an individual experiment, n=2. **C.** Inhibition of BTK abrogates the induction of IFN responses in U937 cells. U937 cells were treated with 4μM ibrutinib, specific kinase inhibitor for BTK, 2 h prior to dsiRNA transfection. Whole cell lysates were prepared 24 h post NC or *MEF2A* targeting and the expression of phosphorylated STAT1 (Y701), total STAT1, IRF3 (S386), total IRF3, MEF2A, phosphorylated BTK (Y233) and Actin. Image is representative of 3 independent experiments.

2.7 Tables

Table 2.7.1. Oligonucleotides and gBLOCKs used in this study

Oligos/gBLOCKs	SEQUENCE
5xISGF3_BS-hGLuc_PEST gBLOCK	5'-ATCTCGATCGAAGAAATGAAACTTGATCATCGCCGAAGAAATGAAACTGCGAATCTGACGAAGAAATGAAACTCGCTTCGTAACGAAGAAATGAAACTCGTAGACTACCGAAGAAATGAAACTCCCGGGTAGGGCCCAATTCGAGTCGAGGTAGGCGTGTACGGTGGGAGGTCTATATAAGCAGAGCTGGTTTAGTGAACCGTCAGATCGCCTGGAGAGATCTTTGTCGATCCTACCATCCACTCGACACACCCGCCAGCGACCACTGCCAAGCTTCCGAGCTCTCGCTCTAGAgccgccaccATGGGAGTCAAAGTTCTGTTTGCCCTGATCTGCATCGCTGTGGCCGAGGCCAAGCCCACCGAGAACAACGAAGACTTCAACATCGTGGCCGTGGCCAGCAACTTCGCGACCCACGGATCTCGATGCTGACCGCGGGAAGTTGCCCGGCAAGAAGCTGCCGCTGGAGGTGCTCAAAGAGATGGAAGCCAATGCCCGGAAAGCTGGCTGCACCAGGGGCTGTCTGATCTGCCTGTCCCACATCAAGTGCACGCCCAAGATGAAGAAGTTCATCCCAGGACGCTGCCACACCTACGAAGGCGACAAAGAGTCCGCACAGGGCGGCATAGGCGAGGCGATCGTCGACATTCCTGAGATTCCTGGGTTCAAGGACTTGGAGCCCATGGAGCAGTTCATCGCACAGGTCGATCTGTGTGTGGACTGCACAACTGGCTGCCTCAAAGGGCTTGCCAACGTGCAGTGTTCTGACCTGCTCAAGAAGTGGCTGCCGCAACGCTGTGCGACCTTTGCCAGCAAGATCCAGGGCCAGGTGGACAAGATCAAGGGGGCCGGTGGTGACAAGCTCCCTAGAAGTCATGGATTCCCACCTGCAGTGGCCGCGCAGGACGATGGTACCCTACCGATGTCTTGCGCTCAAGAGAGCGGAATGGACCGACATCCAGCGGCGTGTGCCTCAGCAAGAATTAACGTTTAG-3'
5xISGF3_BS GA fwd	5'-ATTTTATTATCTAACTGCTGATCGAGTGTAGCCAGATCTCCCGGGATCTCGATCGAAGAAATGAAACTTGATCA-3'
hLuc_PEST GA rev	5'-CTGTATTGCTACTTGTGATTGCTCCATGTTTTTCTAGGTCTCGAGCTAAACGTTAATTCTTGCTGAGGCACAC-3'

Chapter 3. CELF2 regulates RIG-I-like receptor activation by suppressing self-RNA ligands

Parts of this chapter were adapted from the following unpublished manuscript:

Smith, J.R., Etzyon, N., Somfleth, K., Gokhale, N.S., Schwerk, J., Nakamichi, K., Lindbloom-Brown, Z., Gale, M.Jr., Savan, R. (2023). CELF2 suppresses endogenous RNA ligands that activate RIG-I-mediated interferon induction. *In preperation.*

3.1 Introduction

Innate immunity is the first line of defense against viral infections, with interferons (IFNs) playing a dominant role in early defense[244]. RIG-I-like receptors (RLRs; retinoic acid-inducible gene I [RIG-I]), melanoma differentiation associated protein 5 [MDA5]) sense viral RNA in the cytosol and signal through the adaptor protein MAVS to activate NF-κB and IRF3 resulting in the robust transcription of type I and III IFNs [245,246]. These IFNs induce hundreds of antiviral defense molecules called interferon stimulated genes (ISGs)[4]. While type I IFNs are critical for controlling viral infection, unchecked IFN signaling can lead to damaging tissue pathology[247]. Precise transcriptional and post-transcriptional regulation effectively controls viral infection while preventing tissue damage.

There is strong support for RLR activation through "self"-RNA ligands which can potentiate the induction of interferons. Virus infections can promote the unmasking of ribosomal RNA pseudogenes and vault RNA from ribonuclear proteins to expose 5'-ppp motifs recognized by RIG-I and promote antiviral signaling and viral clearance[37,38]. On the other hand, sensing of endogenous RNA ligands can result in IFN mediated autoimmune diseases. Such is the case with loss-of-function ADAR1 mutations and gain-of-function MDA5 mutations leading to the sensing

of endogenous RNAs such as inverted *Alu* element repeats[48,49,248,249]. In addition, 7SL RNA, an RNA polymerase III (Pol III) transcript harboring a 5'-ppp motif, is normally protected from recognition by RLRs through its interactions with signal recognition particle (SRP) 9 and 14, whose homeostatic function is to coordinate translation termination of nascent peptides. However, 7SL RNA transferred in exosomes from fibroblasts to cancer cells, can be sensed by RIG-I and induce interferons, leading to chemotherapy resistance of certain tumors[56,57]. Together these finding support the idea that self-RNA can act as damage associated molecular patterns (DAMPs) and, depending on the context, induce sterile inflammation driven by RLRs. However, our understanding of how immunostimulatory self-RNA are generated and the factors that suppress them are not fully understood.

RNA splicing factors play important roles in post-transcriptional programming of immune responses[250–252]. Indeed, viruses often co-opt or disrupt the function of splicing factors to support their own replication, positioning these factors as key regulators of the inflammatory response[253–256]. Depletion of splicing factors has also been shown to result in generation or unmasking of endogenous RNA ligands and IFN activation[54,257]. How splicing factors contribute to the maintenance of immune homeostasis by suppression of immunostimulatory RNA is not completely understood. The splicing factor CELF2 is highly expressed in the developing heart and muscles, leukocytes and the central nervous system. The increased expression of CELF2 in immune cells implies a role in immune responses[258]. CELF2 and other CELF proteins bind to G/U-rich elements primarily found in introns and 3'-untranslated regions (UTRs) via three conserved RNA recognition motifs to mediate splicing and alternative polyadenylation in the nucleus as well as mRNA translation in the cytosol[148,152]. The role of CELF2 in regulating innate immune activation in monocytes or endogenous RNA ligands has not been studied despite

evidence that CELF2 modulates immune activation in T cells and non-coding RNA processing in macrophages[156–158,161].

In this study, we show that CELF2 plays a central role in the suppression of spontaneous IFN production in monocytes/macrophages. CELF2, which we found to be constitutively expressed in monocyte and macrophages is critical for maintaining homeostatic splicing and translation in these cells. The absence of CELF2 results in the generation of immunostimulatory self-RNA which is sufficient to activate host RLR responses. We specifically show increased RNA:RIG-I interactions in the absence of CELF2 and activation of IRF3 and downstream IFN signaling. These data provide a novel role for CELF2 in suppressing the innate immune activation of macrophages through suppression of immunostimulatory self-RNA.

3.2 Results

3.2.1 Loss of CELF2 results in spontaneous production of type I IFN

To understand the contributions of CELF2 to innate immunity and splicing in macrophages we utilized dicer-substrate interfering RNA (DsiRNA, henceforth siRNA) to transiently deplete CELF2 in U937 monocytes (**Figure 3.1A**). We performed long-read RNA-sequencing using the Nanopore technology to assess differential gene expression and alternative isoform usage. We found that depletion of CELF2 in the absence of any innate immune stimulus resulted in a robust induction of type I IFNs and associated interferon-stimulated genes (ISGs) signature (**Figure 3.1B**). Pathway analysis of differential genes confirmed that IFN signaling was significantly upregulated (**Figure 3.1C**). Conversely, we observed a significant downregulation of ribosomal protein genes along with decreased pathways involved in translation (**Figure 3.1B-C, Figure 3.4A**). These findings were striking as CELF2 has not previously been implicated in the spontaneous production of IFN and thus required further investigation.

To confirm our RNA-seq results, we measured *IFNB1* and *ISG15* transcription (**Figure 3.1D**) and STAT1 phosphorylation (**Figure 3.1E**) following CELF2 depletion and observed significant increases compared to control cells. These findings were also confirmed using a pooled siRNA for CELF2 from a separate source which targeted distinct sites (**Figure 3.4A-C**). We also confirmed CELF2-dependent IFN and ISG induction in an additional macrophage-like cell line, THP1 cells (**Figure 3.4E-G**). Finally, we incubated supernatants from CELF2-depleted and control cells on ISGF3 *Gaussia* luciferase reporter cell line[259] and measured luciferase activity. We found that supernatants from CELF2-depleted cells resulted in a robust increase in luciferase activity, demonstrating that IFN is secreted from CELF2-deficient monocytes (**Figure 3.1F**). Together, these data suggest that loss of CELF2 in monocytes results in the spontaneous production of IFN.

We next tested if complementation of CELF2 in CELF2-deficient cells could prevent spontaneous type I IFN production. We engineered U937 cells to constitutively express wild-type CELF2 ($CELF2^{WT}$) or an RNA-binding mutant CELF2 ($CELF2^{mut}$), as well as GFP as a control. As expected, knockdown (KD) of CELF2 in GFP expressing cells resulted in IFN production as measured by our ISGF3 reporter cells (**Figure 3.1G**). However, cells which constitutively express $CELF2^{WT}$ demonstrated a significant reduction in reporter activity compared to control cells (**Figure 3.1G**). Interestingly, KD of CELF2 in $CELF2^{mut}$ expressing cells also resulted in IFN production indicating that CELF2 RNA-binding is required to suppress IFN production in monocytes (**Figure 3.1G**). The expression of most CELF proteins is tissue restricted following development with CELF1 having the most promiscuous expression. CELF2 is robustly expressed in immune cells, cells of the central nervous system, the developing heart and stem cells[149]. We do not detect CELF2 expression in a hepatocyte cell-line (Huh7, **Figure**

3.4G) and therefore tested if introducing the siRNA into these cells also induced IFN production as an off-target effect. We observed no significant difference in *IFNB1* or *CXCL10* expression as well as no STAT1 phosphorylation following siCELF2 transfection in Huh7 suggesting that the spontaneous production of IFN is not due to an off target effect of the siRNA (**Figure 3.4G-I**). Together these data demonstrate that CELF2 in monocytes plays a central role in suppression of type I IFN at homeostasis.

3.2.2 CELF2 suppresses mRNA translation

Our RNA sequencing data showed that genes downregulated following CELF2 depletion affect pathways involved in translation including 87% ribosomal protein (RP) genes (**Figure 3.1B-C, Figure 3.5A and C**). Leveraging long-read RNA sequencing data, we analyzed the changes in isoform usage in CELF2-depleted cells vs control cells. While there were significantly alternatively spliced transcripts in several differentially expressed genes, we discovered that 31% of RP genes were significantly alternatively spliced (change in isoform usage, p value < 0.05) (**Figure 3.5A-C**). Indeed, of the 24 alternatively spliced RP genes, 22 of them were also significantly down regulated (p value < 0.05) (**Figure 3.5A and C**). This suggests that CELF2 plays a key role in splicing of RP genes and aberrant splicing likely leads to degradation of these mRNAs.

To test if loss of CELF2 did in fact lead to a loss of translation we performed a puromycin uptake assay[260]. CELF2-depleted monocytes exhibited reduced uptake of puromycin, confirming or RNA-seq pathway analysis that loss of CELF2 results in decreased translation (**Figure 3.5D**). Addition of the pan-type I IFN blocker, B18R, did in fact partially restore the levels of puromycin uptake but not to the levels of control cells treated with B18R (**Figure 3.5D**)[261]. These data suggests that CELF2 is required for mRNA translation in monocytes that is

partially independent of type I IFN. Under cellular stress such as during viral infection or serum starvation, cells block of translation via the integrated stress response (ISR) kinases that phosphorylates eIF2α blocking translation initiation[262]. To test if loss of CELF2 was activating ISR kinases to block translation we measured eIF2α phosphorylation in the absence of CELF2 in the presences or absence of type I IFN signaling. We did not observe eIF2α phosphorylation in the absence of CELF2 with or without type I IFN signaling (**Figure 3.5E**). Together, these data suggest that CELF2 is required for mRNA translation in monocytes independent of ISR activation, likely through splicing of RP genes.

3.2.3 Spontaneous IFN signature is dependent on the RIG-I-like receptor pathway

IFN production in monocytes can be triggered by nucleic acid sending through RIG-I-like receptors (RLRs), toll-like receptors (TLRs) or the cGAS-STING pathway. As IRF3 is the major transcription factor induced downstream of these sensors we generated *IRF3* knockout (KO) U937 cells using CRISPR-Cas9 technology. We depleted CELF2 in *IRF3* KO cells and measured *IFNB1* transcription and STAT1 phosphorylation. As expected, non-targeting control cells exhibited a significant increase in *IFNB1* transcription and STAT1 phosphorylation following CELF2 depletion (**Figure 3.2A**). However, loss of CELF2 in *IRF3* KO cells ablated the production of *IFNB1* or STAT1 phosphorylation (**Figure 3.2A**). Indeed, we observe IRF3 phosphorylation in CELF2-depleted cells supporting the conclusion that CELF2 depletion results in the activation of IRF3 (**Figure 3.2E**). These data suggest that loss of CELF2 induces IFNs through IRF3.

We next set out to determine the upstream adaptor that activates IRF3 in the absence of CELF2. As both RNA and DNA sensing pathways activate IRF3 we deleted the adaptor proteins MAVS and STING required for RNA and DNA sensing, respectively. CELF2 depletion in

STING (*STING1*) KO cells resulted in production of *IFNB1* and STAT1 phosphorylation identical to Cas9 control cells (**Figure 3.2B**). However, deletion of *MAVS* resulted in a complete loss of *IFNB1* transcription and STAT1 phosphorylation following CELF2 depletion (**Figure 3.2C**). Taken together these data suggest that loss of CELF2 in monocytes activates the RLR and not DNA sensing pathway.

3.2.4 Loss of CELF2 results in the production of immunostimulatory RNA which is sensed by RIG-I

We next tested if RNA derived from CELF2-depleted cells could induce interferons in naïve cells. We isolated RNA from CELF2-depleted and control cells and transfected the RNA into ISRE-GFP reporter A549 cells, which fluoresce green upon the transcription of IFNs[263]. As a control transfecting the ISRE-GFP reporter cells with a RIG-I ligand induces robust GFP expression by flow cytometry compared to non-transfected cells or treated with transfection reagent alone, indicating that these cells robustly respond to immunostimulatory RNA and not to transfection reagents (**Figure 3.6A**). RNA degradation by the RNase L pathway following viral infection can serve as RLR ligands[40]. Therefore, we validated the integrity of the RNA isolated from CELF2-depleted and control cells by gel electrophoresis to ensure we are not transfecting fragmented RNA which could trigger RLR responses. We observed equivalent integrity of RNA derived from either condition (**Figure 3.6B**). We then transfected RNA from CELF2-depleted and control cells into the ISRE-GFP reporter cells and observed a dose dependent increase in the percent of GFP positive cells upon transfection of RNA isolated from CELF2-depleted cells and not from control cells (**Figure 3.3A**). These data suggested that loss of CELF2 results in the aberrant production of immunostimulatory RNAs that induce IFNs.

IFN induction following CELF2 depletion relies on MAVS and IRF3, and RNA derived from CELF2 KD cells can induce IFN reporter expression. Therefore, we reasoned that immunostimulatory self-RNA generated in the absence of CELF2 2 must trigger the activation of either RIG-I or MDA5. To test if RIG-I is required for IFN production following CELF2 depletion, we depleted CELF2 in *RIGI* KO cells and measured production of *IFNB1* and downstream IFN signaling activation. We observed a complete loss of *IFNB1* induction and STAT1 phosphorylation following CELF2 depletion in *RIGI* KO cells (**Figure 3.3B**), suggesting that RIG-I is the primary sensor of RNA induced following CELF2 depletion.

To test if a self-RNA ligand interacted with RIG-I, we performed irCLIP, a method of visualizing RBP-RNA interactions via fluorescence nucleic acid probe ligation to RNA in complex with RBPs[264]. CELF2 was depleted in wild-type and *RIGI* KO U937s followed by UV exposure to crosslink RNA to proteins they may be interacting with. We then performed an immunoprecipitation (IP) with polyclonal rabbit serum directed against RIG-I. Following IP, we performed an on-bead incomplete digest followed by fluorescent adapter which will allow for visualization of RIG-I:RNA complexes after SDS-PAGE electrophoresis. We observed laddering of RIG-I:RNA complexes following CELF2 depletion, indicating that in the absence of CELF2 RIG-I is bound to RNA (**Figure 3.3C**). We did not observe RNA interaction in control cells or cells which lack RIG-I (**Figure 3.3C**), indicating increased specific RIG-I:RNA interactions following CELF2 depletion.

We next set out to determine the biochemical make up of RNA derived from CELF2 depleted cells. For this, we isolated RNA from CELF2 depleted cells and subjected the RNA to RNase I and RNase III to degrade single-stranded and double-stranded RNA, respectively. Additionally, we treated RNA with alkaline phosphatase to dephosphorylate the ends of the

RNA. Treated RNA were transfected into cells to find RNase I and III completely prevented *IFNB1* productions (**Figure 3.6C**). Surprisingly, alkaline phosphatase treatment did not influence immune activation by transfected RNA as alkaline phosphatase treated RNA exhibited the same induction of *IFNB1* as RNA not treated with any RNase or cell transfected with a specific RIG-I agonist (**Figure 3.6C**). Together these data suggest that the loss of CELF2 results in dsRNA accumulation that specifically activates RIG-I to induce the production of type I IFN.

3.3 Discussion

Here we show that loss of an RNA splicing factor, CELF2, in monocytes results in the spontaneous production of type I IFN and subsequent ISG signature. We show that the CELF2 generated ligand is a dsRNA as RNase III treatment ablated IFN production following transfection. Deletion of MAVS, and not STING, ablates the induction of interferons, indicating CELF2 regulates the RNA sensing pathway. Finally, we found that the immunostimulatory RNA generated after CELF2 depletion was sensed by RIG-I, as we observed increased RIG-I:RNA interactions and genetic deletion of *RIGI* completely ablated immune activation. Taken together, we show that CELF2 is a novel suppressor of endogenous dsRNA that can activate the RIG-I pathway.

Host factors that suppress endogenous self RNA are critical to prevent IFN activation and development autoinflammatory diseases known as interferonopathies[6]. ADAR1 is the most well-known regulator of self RNA. However, we show CELF2 is involved in suppression of ligands generated during mRNA splicing in human macrophages. CELF2-driven alternative splicing is critical for development of several tissues, with is expression decreasing postnatally, and global deletion of *Celf2* in mice is embryonic lethal likely affecting development[265,149,151]. As *Celf2*$^{-/-}$ have developmental defects are embryonically lethal, previous *in vivo* studies have not focused

on immune responses elicited by the loss of CELF2. However, several tissues including CNS, small intestine, and immune cells express high levels of CELF2 postnatally[148,149,266]. Indeed, in humans, mutations in CELF2 result in severe neurological dysfunction[267,268]. CELF2 has been shown to be critical for alternative splicing and alternative poly adenylation in human T cells following T cell receptor activation[156,158,153]. In addition, CELF2 has been shown to regulate immune responses downstream of IL-10 stimulation in mouse macrophages, but studies of CELF2 regulation of IFN in macrophages is lacking[161]. While CELF2 is expressed in other immune cells such as T cells and plasmacytoid dendritic cells, which are major producers of type I IFN, we do not observe robust IFN production in the absence of CELF2 in these cell types (data not shown) leading us to believe that this phenotype is specific to monocytes/macrophages. This is perhaps due to the fact that monocytes and macrophages are critical reservoirs for virus and thus are primed to respond to viral infection through RLR stimulation[269]. Whether CELF2 suppression of immunostimulatory dsRNA in macrophage/monocyte specific function is conserved between human and mice is unknown. Future *in vivo* studies utilizing macrophage/monocyte specific conditional deletion studies could help elucidate the role of CELF2 in these cells and maybe discover species specific regulation immunostimulatory RNA generation.

We found that overexpression of CELF2 abrogated spontaneous IFN production in CELF2 depleted cells, while RNA binding mutant of CELF2 failed to suppress IFNs. These data suggest that the RNA-binding capacity of CELF2 is required for the suppression of IFN activation. *De novo* missense mutations in CELF2 have been shown to mislocalize CELF2 into the cytoplasm resulting in perturbations of neuronal precursor development [268]. While these mutations lead to mislocalization and developmental phenotypes, it did not result in disruption of

CELF2-mediated splicing, suggesting that perhaps mutations in CELF2 that affect splicing or RNA-binding are selected against. This could likely be contributed to the importance of CELF2-mediated splicing requirements during development but also perhaps due to the role of CELF2 in suppressing immunostimulatory RNA leading to autoimmunity. Rather the localization mutations discovered affected translation through interactions with mRNA in the cytoplasm[268]. Indeed, CELF2 and CELF1 have been shown to regulate translation of various genes in the cytoplasm through interaction with mRNA or ribosomal initiation factors[154,155,270]. However, this is the first reporting of CELF2 suppressing translation via alternative splicing of ribosomal protein (RP) genes opening the door for investigation into fundamental aspects of posttranscriptional regulation of translation machinery and ribosome biogenesis. If perturbations of RP gene splicing contributes to the spontaneous IFN phenotype is unknown but previous studies have shown that ribosomal RNA can serve as RIG-I ligands[271]. Future investigations will elucidate the RP gene alternative splicing on the access of ribosomal RNA by RIG-I and induction of IFN.

Cancers often disrupt homeostatic functions within the cell to evade cell death and spread, including disrupting RNA splicing[272–274,50]. As such, spliceosome-targeted therapies (STTs) have shown promising efficacy in a variety of cancers[55,275–277]. Recently, the mechanism of a STT to treat triple-negative breast cancer targeting SF3B1 demonstrated that SF3B1 inhibition led to dsRNA accumulation and activation of innate immune responses, leading to cell death and better immune cell recruitment into tumors[55]. CELF2 expression is often dysregulated in cancers and this dysregulation is often associated with pro-cancer survival[278–280]. Increased expression of the related RRM-containing splicing factor, HNRNPC1, was shown in cancer cells to promote survival, and targeting HNRNPC1 for depletion resulted in the production of type I

IFN via increased dsRNA and cell death[54]. It has been shown that CELF2 and HNRNPC1 mutually regulate the expression of each other in T cells as well as coordinate splicing together following TCR activation[160,270]. It is exciting to think that CELF2 could play a similar role as HNRNPC1 or SF3B1 in cancers making CELF2 a novel therapeutic target in anti-tumor therapy via induction of inflammatory signaling within tumor cells.

Collectively, our study reveals a novel role for CELF2 in the suppression of immunostimulatory RNA that is sensed by RIG-I and provides a novel target to combat diseases such as autoinflammation, viral infection and cancer.

3.4 Materials and methods

Cell lines, cell culture conditions and treatments

U937 monocytes were cultured in RPMI 1640 media supplemented with 10% FBS, 2mM glutamine, 100 U/ml penicillin and 100 mg/ml streptomycin and maintained at 37°C in 5% CO_2. Non-targeted (H1), IRF3, STING, MAVS and RIG-I-deficient U937 cells were generated by CRISPR-Cas9 genome editing by spiculation lentiviral transduction and FLAG-GFP, FLAG-CELF2^{WT} and FLAG-CELF2^{mut} U937 cells were generated by lentiviral transduction through spinoculation. Briefly, cells were incubated with specific lentiviruses packaged with pPAX and VSV-G, spun for 1 hour (h) at room temperature at 800 x g. Cells were then transferred and grown for 24h. Media was then changed and incubated for another 24 h before transduced cells were enriched using antibiotic selection. THP-1 monocytes were maintained in RPMI 1640 media supplemented with 10% FBS, 2mM glutamine, 100 U/ml penicillin, 100 mg/ml streptomycin, 1 mM sodium pyruvate, 10 mM HEPES and 0.05 mM, 2-mercaptoethanol and maintained at 37°C in 5% CO_2. U937 and THP-1 cells were differentiated for 48 h in their respective complete media containing 40 nM phorbol 12-myristate 13-acetate (PMA) followed

by resting for 24 h in RPMI 1640 supplemented with 1% FBS. Huh7 human hepatoma cells, A549 human lung epithelial cells and derivatives cell lines were cultured in DMEM supplemented with 10% FBS, 2mM Glutamine, 100 U/ml Penicillin and 100 mg/ml Streptomycin and maintained at 37°C in 5% CO_2. Gene silencing was conducted using dicer-substrate interfering RNA (dsiRNA, IDT) or siGENOME SMARTpool siRNA (Dharmacon) specific to *CELF2* or non-targeting control (Table 3.1). Transfection were carried out using 20 nM of dsiRNA or siRNA delivered intracellularly using TransIT-X2 according to manufacturer's guidelines (Mirus).

Plasmids and Oligonucleotides

CRISPR-Cas9 plasmids; pRRL-H1-PURO (non-targeting), pRRL-STING-PURO and pRRL-MAVS-PURO were a gift from Dr. Daniel Stetson (University of Washington) [239]. pRRL-IRF3-PURO was generated in the lab as previously described[281]. pRRL-*RIGI*-PURO was generated by cloning single-guide RNA (sgRNA) targeting *RIGI* (5'-GTTCCTGTTGGAGCTCCAGG -3') into empty pRRL-Cas9-PURO plasmids as previously described [236,239]. The ISRE reporter plasmid, pISRE-sfGFP, was a gift from Dr. Nicholas Heaton (Duke University) and has been previously described [220]. pcDNA-FLAG-CELF2 (wild-type) was purchased from addgene. pCDNA-FLAG-CELF2^{mut} was generated using QuickChange Lightning Multi site-directed mutagenesis kit (Agilent) according to manufacturer's guidelines. Primers for site directed mutagenesis can be found in Table 3.1. pLEX- FLAG-CELF2^{WT} and pLEX- FLAG-CELF2^{mut} were generated using infusion cloning (Takara), primers can be found in Table 1. Fluorescent oligo for irCLIP can be found in Table 3.1.

RNA extraction and quantification of gene expression

Total RNA was extracted using the NucleoSpin RNA extraction kit (Macherey-Nagel) or TRIzol reagent as indicated by manufacturer guidelines. cDNA synthesis was performed using the Prime Script RT (Takara Bio) according to the manufacturer guidelines. Relative quantification of mRNA was done by qPCR using the ViiA7 qPCR system with TaqMan reagents (Life Technologies) using the *HPRT1* as reference gene. Primers and probes used for qPCR assays in this study were acquired from IDT or Life Technologies as indicated in Table 3.2.

RNA transfer experiments

RNA was isolated from CEFL2-depleted or control cells as described. RNA was either digested with 1 U of RNase I/μg of total RNA, 1 U of RNase III/μg of total RNA or treated with 1 U of Shrimp Alkaline Phosphatase (NEB)/μg of total RNA for 1h at 37°C or left untreated. RNase treated RNA was repurified using Phenol:Chloroform:Isoamyl alcohol extraction. RNA was transfected at indicated doses using Mirus TransIT X2 (Mirus) according to manufacturer guidelines.

Western blot analysis

Whole cell lysates were prepared from cells using RIPA buffer (10 mM Tris-Cl (pH 8.0), 1 mM EDTA, 0.5 mM EGTA, 1% Triton X-100, 0.1% sodium deoxycholate, 0.1% SDS, 140 mM NaCl) supplemented with Halt protease and phosphatase inhibitor cocktail (Pierce). Protein quantification and normalization was done using the Quick-Start Bradford assay (Bio-Rad). 10-30 ug total protein were resolved by SDS-PAGE and transferred to PVDF membranes (Bio-Rad). Primary antibody incubations were done overnight with antibodies diluted in 3% BSA in TBS-T (Tris-buffered saline/Tween 20), and species-specific HRP

conjugated secondary antibodies. Chemiluminescent image acquisition was performed using a ChemiDoc XRS+ (Bio-Rad).

irCLIP

irCLIP protocol carried out as previously described[264]. Briefly, CELF2-depleted and control wild-type or *RIGI* KO cells were UV-crosslinked at 150 μJ x 100/cm^2 then lysed. RIG-I was immunoprecipitated (IP) using polyclonal rabbit serum overnight at 4°C. The next day samples were stringently washed, RNA was digested on bead using 25ng/mL RNase A for 15 min at 30°C. RNA ends were then dephosphorylated and an IR-dye oligo (Table xxx) was ligated onto the free ends of the RNA. RNA:Protein complexes were then run on an SDS-PAGE gel and transferred to a nitrocellulose membrane. IR-RNA:protein complexes were imaged on a LI-COR Odyssey CLx (LI-COR). HRP-conjugated antibody imaging was done as described.

RNA sequencing, data processing, and analysis

Total RNA was isolated as previously described. Total RNA was subject to polyA mRNA purification using oligo dT Dynabead mRNA purification kit (ThermoFisher) according to manufacture guildlines. 1 ng of polyA enriched RNA underwent PCR-cDNA barcoding using the PCR-cDNA barcoding kit (Nanopore) according to manufacturer guildlines. Briefly, RNA was reverse transcribed using VN primers and strand-switching primers provided in kit. cDNA was then amplified using barcoded cDNA primers provided in kit then subject to exonuclease I treatment. cDNA was purified using AMPure XP beads (Beckman Coulter) according to manufacture guildlines and cDNA was checked for size and quality using the Agilent Bioanalyzer System (Agilent Technologies). The rapid adapter provided with kit was added to

the barcoded cDNA. Minon flowcell quality check, priming and loading was conducted according to manufacture guildlines and sequencing allowed to progress for 72h. Reads were basecalled using Guppy basecaller (Nanopore). Basecalled reads were trimmed using pychopper version 2.2.0 (Nanopore) and aligned to the GRCh38 genome. Differential gene expression and alternative splicing analysis was conducted using FLAIR, as previously described[282].

ISGF3 Gaussia luciferase and ISRE GFP reporter assays

5xISGF3 Huh7 cells were generated as previously described[259]. Briefly, to generate the ISGF3 Gaussia Luciferase (Gluc) reporter construct, pTRIPZ-5xISGF3-BS-hGLuc-PEST, 5 tandem ISGF3 consensus sequences (5'-CGAAGAAATGAAACT-3') were cloned with hGLuc-MODC-PEST into a pTRIPZ lentiviral plasmid. Lentivirus encoding the reporter was packaged used to transduce human hepatoma Huh7 cells prior to single-cell cloning of reporter cells. To assess the presence of secreted IFN from dsiRNA transfected U937 cells, cell supernatants from CELF2-depleted and non-targeting control were harvested 24 h post transfection and transferred onto 5xISGF3-GLuc Huh7 reporter cells. Reporter cells were then incubated at 37°C and 5% CO_2 for 24 h prior to assessment of Gaussia luciferase secretion into the media. Sample supernatants were diluted 1:1 with Gaussia Luciferase glow assay substrate (Thermo Fisher Scientific) and luminescence measured using a Synergy HTX (BioTek). To generate ISRE-GFP reporter cell lines, A549s were stably transduced with lentivirus pISRE-sfGFP and pools were transfected with RNA from CELF2-depleted or control cells as described and GFP expression was measured using a CANTO analyzer (BD). Flow cytometry data was analyzed using FlowJo (TreeStar).

Quantification and Statistical Analysis

Statistical analysis was performed using GraphPad Prism 9.0 (GraphPad software La Jolla, CA). Statistical significance was calculated as indicated for each experiment and across all experiments, p-values of < 0.05 were considered significant and are indicated by asterisks ($*$).

Public data availability

The data generated in this study are available upon request from corresponding author.

3.5 Acknowledgements

We thank Michael Gale Jr., Daniel B. Stetson and Nicholas Heaton for sharing reagents. We thank Jennifer Hyde, Daniel Blanco-Melo, Tristan Jordan and Emmanuelle Genoyer for helpful discussions. This work was supported in part by the National Institutes of Health (R.S.: AI176442, J.R.S.: 2T32AI106677-6).

AUTHOR CONTRIBUTIONS

Investigation and Formal Analysis (J.R.S., N.E., K.S., N.G., J.S.); Conceptualization (J.R.S., R.S.), Writing (J.R.S., R.S.), Supervision (R.S.), Funding Acquisition (J.R.S., R.S.).

3.6 Figures

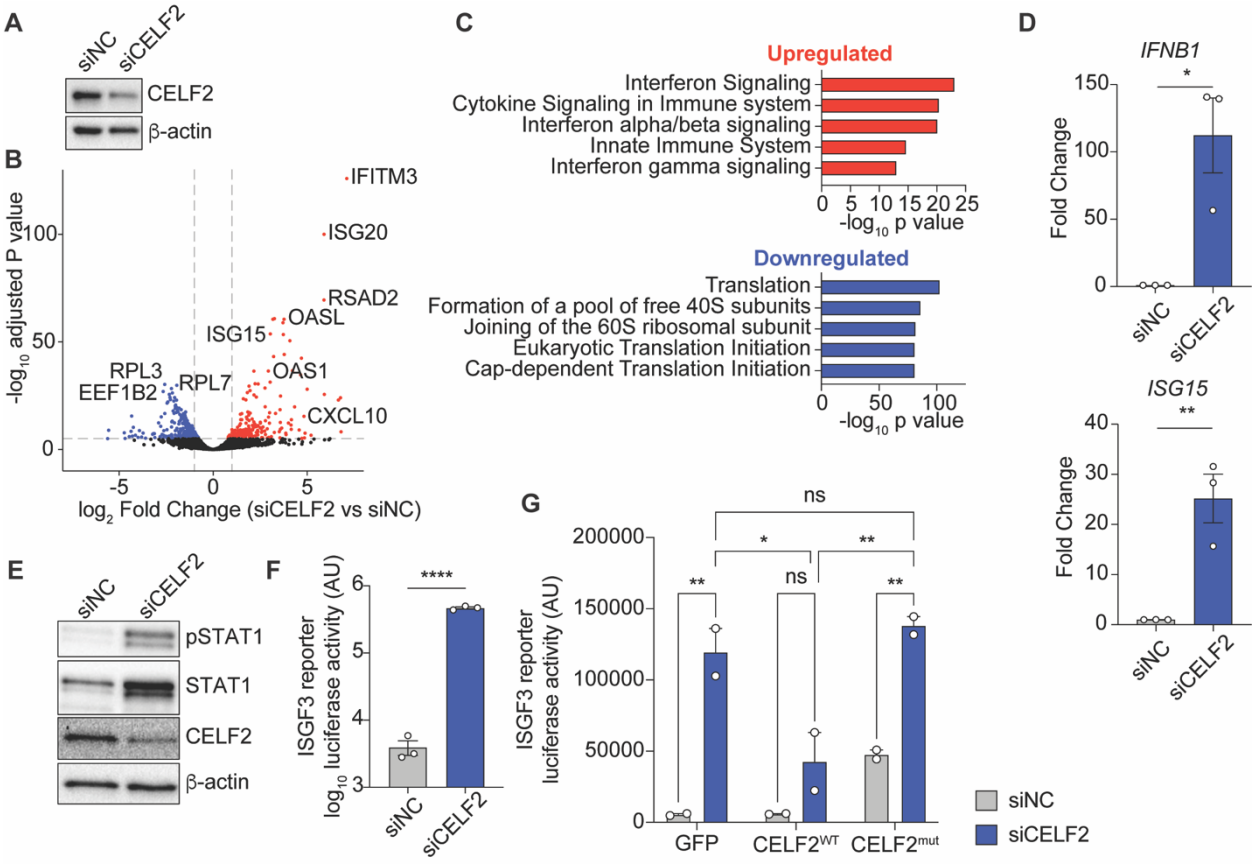

Figure 3.1. CELF2-depleted monocytes exhibit a spontaneous interferon-stimulated gene signature

A. Representative immunoblot analysis of CELF2-depleted (siCELF2) and control (siNon-targeting Control (NC)) monocytes. **B.** Volcano plot of differentially expressed genes in CELF2-depleted monocytes compared to control monocytes from Nanopore MinION long-read RNA sequencing. Red indicates significantly upregulated genes; blue indicates significantly downregulated genes. $p < 0.05$, n=3. **C.** Reactome pathway analysis of significantly up- (red) and down- (blue) regulated genes from long-read RNA sequencing analysis. **D.** RT-qPCR analysis of *IFNB1* and *ISG15* induction following CELF2 depletion. **E.** Immunoblot analysis of STAT1 phosphorylation following CELF2 depletion. **F.** 5xISGF3 *Gaussia* Luciferase reporter activity of

supernatants from CELF2-depleted cells. Supernatants were taken from CELF2-depleted monocytes and transferred onto ISGF3 luciferase reporter cells and luciferase activity was measured after 24h. **G.** 5xISGF3 *Gaussia* luciferase reporter activity from CELF2-depleted cells engineered to express GFP, $CELF2^{WT}$ or CELF2 RNA-binding mutants ($CELF2^{mut}$). Data in all panel are representative of n=2-3 independent experiments. Each symbol represents individual biological replicates. Graphs display mean ± SEM. Student's t-test (D and F), Two-way ANOVA (G); * represents $p < 0.05$, ** represents $p \leq 0.01$ **** represents $p \leq 0.0001$, ns represents $p > 0.05$. A and E immunoblots representative of n=3 independent experiments.

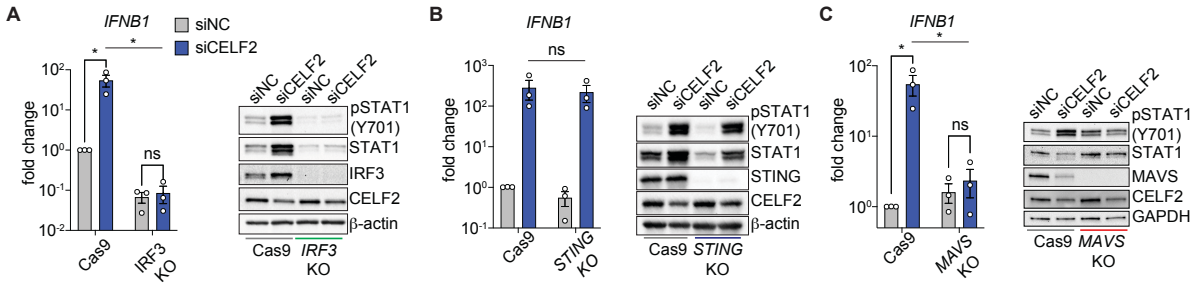

Figure 3.2. Spontaneous type I IFN and ISG expression following CELF2-depletion is RLR-dependent.

A. RT-qPCR of *IFNB1* expression and representative immunoblot analysis in *IRF3* KO control or CELF2-depleted cells. **B-C.** RT-qPCR of *IFNB1* expression and representative immunoblot analysis in STING (*TMEM173*) (B) or *MAVS* (C) KO control or CELF2-depleted cells. Data in all panels are n=3 independent experiments. Each symbol represents individual biological replicate. Graphs display mean ± SEM. All data analyzed by two-way ANOVA; ns represents $p > 0.05$, * represents $p < 0.05$. Immunoblots representative of n=3 independent experiments.

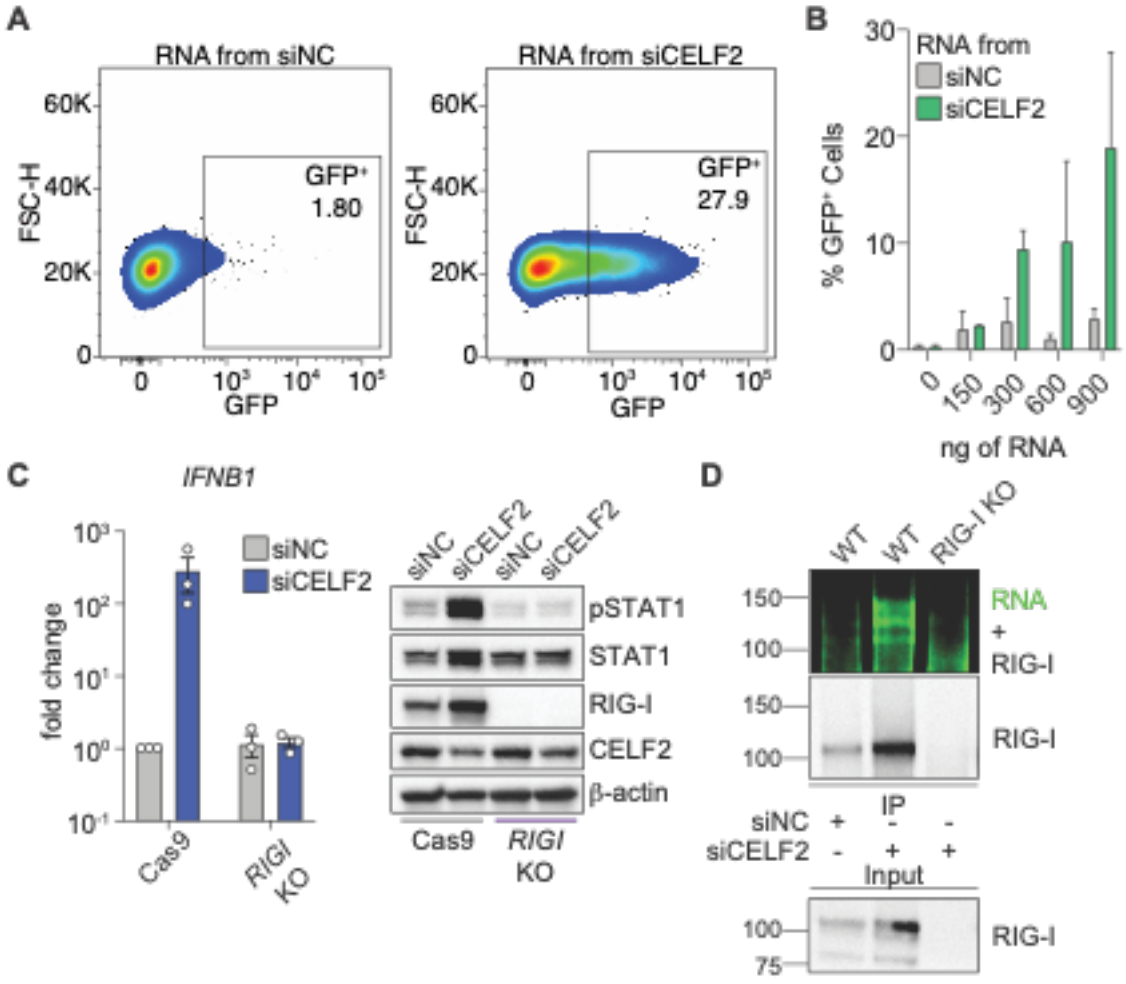

Figure 3.3. Loss of CELF2 results in the production of immunostimulatory RNA which is sensed by RIG-I.

A. RNA transfer from CELF2-depleted and control cells into ISRE-GFP A549 cells. Flow plots (left) are representative of 900 ng of transferred RNA and representative of 2 independent biological replicates. **B.** %GFP+ cells enumerated (right) and representative of 2 independent biological replicates. **C.** RT-qPCR of *IFNB1* expression and representative immunoblot analysis in *RIGI* KO control or CELF2-depleted cells. **C.** irCLIP analysis of RIG-I:RNA complexes following CELF2-depletion. Immunoblots and fluorescent readout are representative of 3

independent replicates. Data in all panels unless otherwise stated are n=3 independent experiments. Each symbol represents individual biological replicate. Graphs display mean ± SEM. B: two-way ANOVA, ns represents $p > 0.05$, * represents $p < 0.05$. Immunoblots representative of n=3 independent experiments.

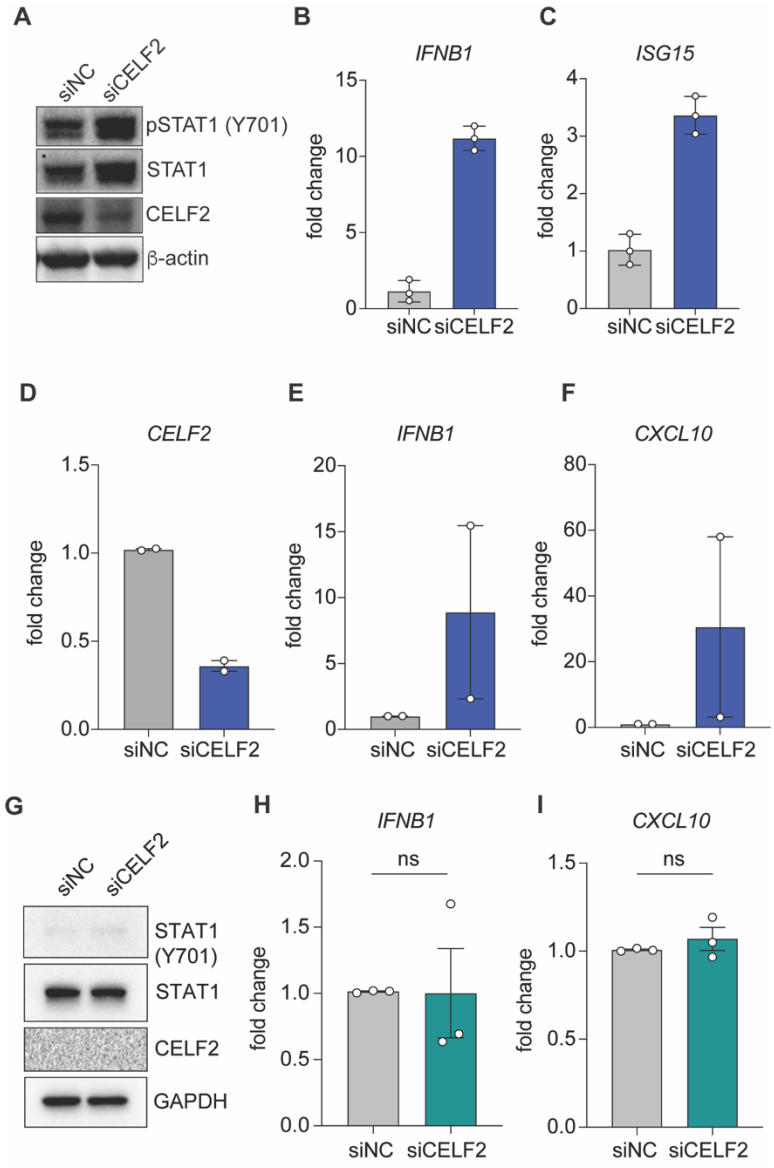

Figure 3.4. Supplemental figure related to Figure 3.1

A. Representative micrographs of CELF2 depletion using pool of siRNA from Dharmacon. **B-C.** RT-qPCR of *IFNB1* (B) and *ISG15* (C) expression and representative immunoblot analysis in CELF2-depleted and control cells using Dharmacon siRNA. n=3 independent replicates. **D-F.** RT-qPCR of *CELF2* (D), *IFNB1* (E) and *CXCL10* (F) expression in CELF2-depleted THP-1 monocytes. n=2 independent replicates. **G.** Representative immunoblot analysis of CELF2 targeting in Huh7 cells. Blots representative of n=3 independent replicates. **H-I**. RT-qPCR of

IFNB1 (H) and *CXCL10* (I) expression in CELF2-targeted Huh7 hepatocytes. n=3 independent replicates, students t-test; ns represents $p > 0.05$.

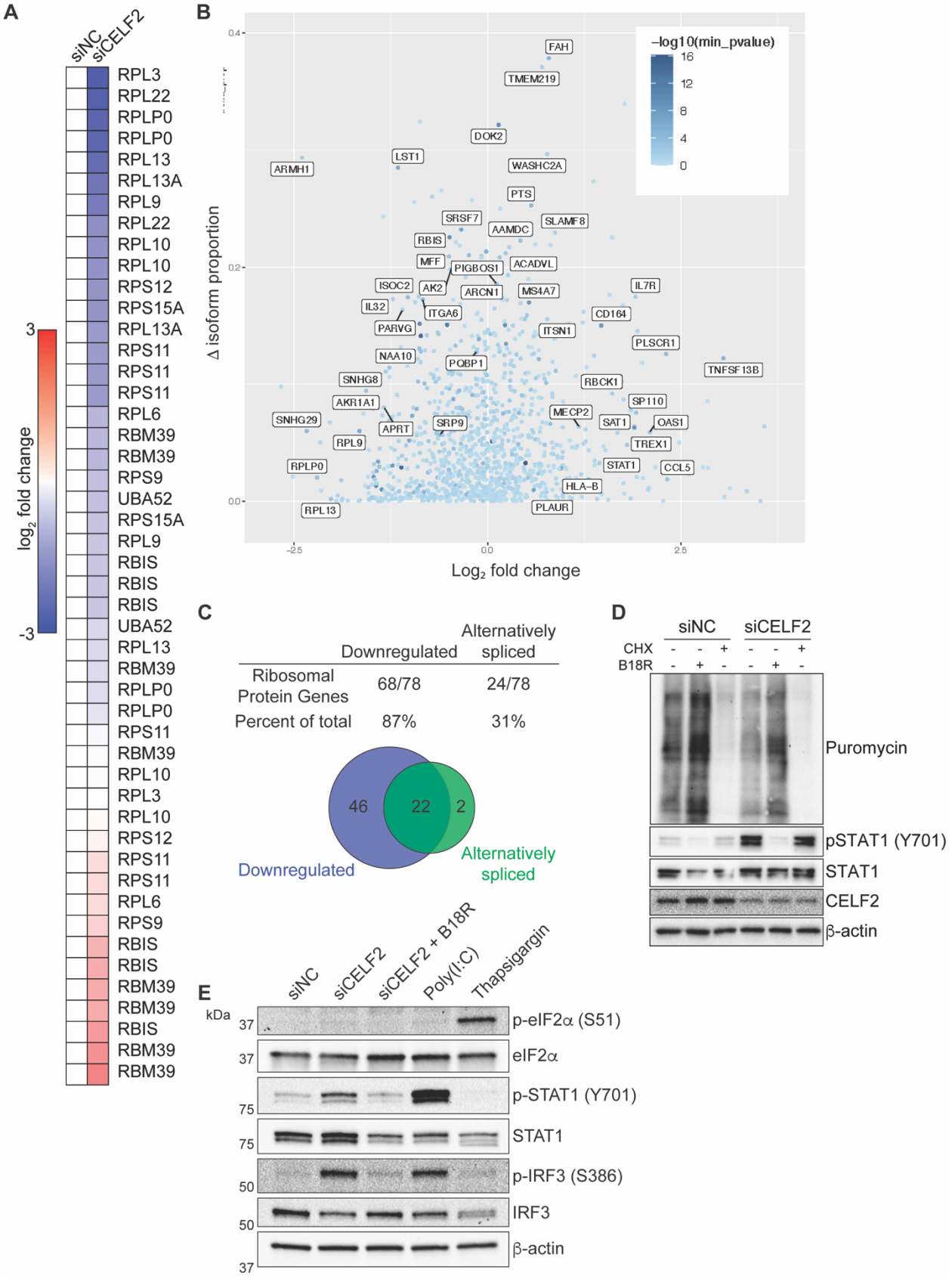
A
siNC
siCELF2
RPL3
RPL22
RPLP0
RPLP0
RPL13
RPL13A
RPL9
RPL22
RPL10
RPL10
RPS12
RPS15A
RPL13A
RPS11
RPS11
RPS11
RPL6
RBM39
RBM39
RPS9
UBA52
RPS15A
RPL9
RBIS
RBIS
RBIS
UBA52
RPL13
RBM39
RPLP0
RPLP0
RPS11
RBM39
RPL10
RPL3
RPL10
RPS12
RPS11
RPS11
RPL6
RPS9
RBIS
RBIS
RBM39
RBM39
RBIS
RBM39
RBM39
3
-3
log2 fold change
B
−log10(min_pvalue)
16
12
8
4
0
FAH
TMEM219
DOK2
LST1
ARMH1
WASHC2A
PTS
SRSF7
AAMDC
SLAMF8
RBIS
MFF
PIGBOS1
ACADVL
ISOC2
AK2
ARCN1
MS4A7
IL7R
IL32
ITGA6
CD164
PARVG
ITSN1
PLSCR1
NAA10
PQBP1
TNFSF13B
SNHG8
RBCK1
AKR1A1
SP110
SNHG29
APRT
SRP9
MECP2
SAT1
OAS1
RPL9
TREX1
RPLP0
STAT1
CCL5
HLA-B
RPL13
PLAUR
0.4
0.2
0.0
−2.5
0.0
2.5
Δ isoform proportion
Log2 fold change
C
Downregulated
Alternatively spliced
Ribosomal Protein Genes
68/78
24/78
Percent of total
87%
31%
46
22
2
Downregulated
Alternatively spliced
D
siNC
siCELF2
CHX
B18R
Puromycin
pSTAT1 (Y701)
STAT1
CELF2
β-actin
E
siNC
siCELF2
siCELF2 + B18R
Poly(I:C)
Thapsigargin
kDa
37
p-eIF2α (S51)
37
eIF2α
75
p-STAT1 (Y701)
75
STAT1
50
p-IRF3 (S386)
50
IRF3
37
β-actin

Figure 3.5. Supplemental figure related to Figure 3.1

A. Heatmap of ribosomal protein (RP) gene isoform expression in CELF2-depleted vs control cells from long-read RNA sequencing. **B.** Change in isoform proportion compared to changes in expression in CELF2-depleted cells. **C.** Ribosomal protein (RP) gene expression and splicing analysis from long-read RNA sequencing. 68 of 78 RP genes are downregulated and 24 of 78 RP genes are alternatively spliced (table/top). Of the downregulated and alternatively spliced RP genes, 22 overlap (venn diagram/bottom). **D.** Representative immunoblot analysis of puromycin uptake assay. CHX was used to block translation and B18R was used to block type I IFN signaling. **E.** Immunoblot analysis of the integrative stress response via eIF2α phosphorylation analysis. Thapsigargin was used as a positive control for eIF2α phosphorylation.

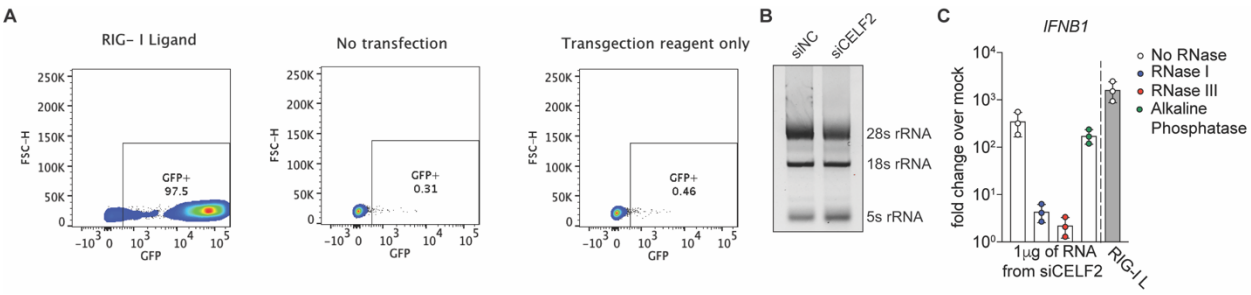

Figure 3.6. Supplemental figure related to Figure 3.3

A. Representative flow blots of ISRE-GFP reporter using RIG-I Ligand and negative controls (no transfection or transfection reagent only). **B.** Representative gel analysis of RNA integrity of RNA from CELF2-depleted and control cells. 28s, 18s and 5s abundance was used to indicate RNA integrity. **C.** RT-qPCR for *IFNB1* from cells following RNA transfer from CELF2-depleted cells after RNase treatment.

3.7 Tables

Table 3.2. Oligonucleotides and gBLOCKs used in this study

Oligos/gBLOCKs	SEQUENCE
sgRNA-*RIGI* sense	5'-AAAGGACGAAACACCGTTCCTGTTGGAGCTCCAGGGTTTTAGAGCTAGAAATAGCAAG-3'
sgRNA-*RIGI* anti-sense	5'-CTTGCTATTTCTAGCTCTAAAACCCTGGAGCTCCAACAGGAACGGTGTTTCGTCCTTT-3'
5xISGF3_BS-hGLuc_PEST gBLOCK	5'-ATCTCGATCGAAGAAATGAAACTTGATCATCGCCGAAGAAATGAAACTGCGAATCTGACGAAGAAATGAAACTCGCTTCGTAACGAAGAAATGAAACTCGTAGACTACCGAAGAAATGAAACTCCCGGGTAGGGCCCAATTCGAGTCGAGGTAGGCGTGTACGGTGGGAGGTCTATATAAGCAGAGCTGGTTTAGTGAACCGTCAGATCGCCTGGAGAGATCTTTGTCGATCCTACCATCCACTCGACACACCCGCCAGCGACCACTGCCAAGCTTCCGAGCTCTCGCTCTAGAgccgccaccATGGGAGTCAAAGTTCTGTTTGCCCTGATCTGCATCGCTGTGGCCGAGGCCAAGCCCACCGAGAACAACGAAGACTTCAACATCGTGGCCGTGGCCAGCAACTTCGCGACCCACGGATCTCGATGCTGACCGCGGGAAGTTGCCCGGCAAGAAGCTGCCGCTGGAGGTGCTCAAAGAGATGGAAGCCAATGCCCGGAAAGCTGGCTGCACCAGGGGCTGTCTGATCTGCCTGTCCCACATCAAGTG

	CACGCCCAAGATGAAGAAGTTCATCCCAGGACGCTGCCACACCTA CGAAGGCGACAAAGAGTCCGCACAGGGCGGCATAGGCGAGGCGA TCGTCGACATTCCTGAGATTCCTGGGTTCAAGGACTTGGAGCCCAT GGAGCAGTTCATCGCACAGGTCGATCTGTGTGTGGACTGCACAACT GGCTGCCTCAAAGGGCTTGCCAACGTGCAGTGTTCTGACCTGCTCA AGAAGTGGCTGCCGCAACGCTGTGCGACCTTTGCCAGCAAGATCC AGGGCCAGGTGGACAAGATCAAGGGGGCCGGTGGTGACAAGCTCC CTAGAAGTCATGGATTCCCACCTGCAGTGGCCGCGCAGGACGATG GTACCCTACCGATGTCTTGCGCTCAAGAGAGCGGAATGGACCGAC ATCCAGCGGCGTGTGCCTCAGCAAGAATTAACGTTTAG-3'
5xISGF3_BS GA fwd	5'-ATTTTATTATCTAACTGCTGATCGAGTGTAGCCAGATCTCCCGGGA TCTCGATCGAAGAAATGAAACTTGATCA-3'
hLuc_PEST GA rev	5'-CTGTATTGCTACTTGTGATTGCTCCATGTTTTTCTAGGTCTCGAGCT AAACGTTAATTCTTGCTGAGGCACAC-3'
CELF2 G21A fwd	5'-CATTAAGATGTTTGTCGCACAGATCCCCCGGTCAT-3'
CELF2 G21A rev	5'-ATGACCGGGGGATCTGTGCGACAAACATCTTAATG-3'
CELF2 C61G fwd	5'-CCCTCCGCAGAGTAAAGGTGGTTGTTTCGTAACATTTTAT-3'
CELF2 C61G rev	5'-ATAAAATGTTACGAAACAACCACCTTTACTCTGCGGAGGG-3'
CELF2 G113A fwd	5'-GGAAGACAGAAAATTGTTCATAGCAATGGTTTCGAAGAAATGTAA TG-3'
CELF2 G113A rev	5'-CATTACATTTCTTCGAAACCATTGCTATGAACAATTTTCTGTCTTCC -3'
CELF2 C150G fwd	5'-GGCTGAGTCGAGGCGGTGCGTTTGTCACA-3'
CELF2 C150G rev	5'-TGTGACAAACGCACCGCCTCGACTCAGCC-3'
CELF2 G449A fwd	5'-CAATCTGAGCAAGTGCTTTGCTTTTGTTAGCTACGACAATC-3'
CELF2 G449A rev	5'-GATTGTCGTAGCTAACAAAAGCAAAGCACTTGCTCAGATTG-3'
pLEX-F-C2_F	5'-GACTCTACTAGAGGATCCGCCACCATGGATTACAAGGATGACGAT GACAAGG-3'
F-C2-pLEX_R	5'-CGGGCCCTCTAGACTCGAGTCAGTAAGGTTTGCTGTCGTTTTTGG-3'

Chapter 4. Conclusions

4.1 Summary

MEF2A suppresses stress responses that trigger DDX41-dependent IFN production

The MEF2 family of transcription factors are critical for cardiac development and have recently been implemented in IFN regulation. However, the extent of MEF2A regulation of IFN in differentiated cells has yet to be fully elucidated. In this study we demonstrate that acute loss of MEF2A results in the spontaneous production of IFN and establishment of an antiviral state in cardiomyocytes, fibroblasts and monocytes. The antiviral state induced following MEF2A depletion is sufficient to suppress viral infection, and although both type I and type III IFNs are made, type I IFNs play the dominant role in establishing viral protection. IFN production was found to be a result of STING activation and required both cGAS as well as the DEAD-box helicase, DDX41. Loss of MEF2A resulted in robust DNA damage likely triggering cGAS. Interestingly, we found that MEF2A depletion also resulted in the generation of RNA:DNA hybrids or R-loops, which likely contribute to the accumulation of DNA damage. DDX41 has been shown to not only resolve genomic R-loops to prevent DNA damage but can also initiate an immune response through STING in response to RNA:DNA hybrids. We propose that R-loop accumulation leads to a DDX41/cGAS dependent immune response. Indeed, RNASEH1 overexpression prevented STING activation and IFN production following MEF2A depletion, suggesting that IFN production following the loss of MEF2A is due to R-loop accumulation. Finally, we found that DNA damage following MEF2A depletion activated the DNA damage response kinase, ATR, and that inhibition of ATR kinase activity prevented activation of STING. Therefore, our study positions MEF2A as a suppressor of transcriptional stress, leading to R-loop accumulation and DNA damage that triggers IFN responses.

CELF2 suppresses self-RNA ligands that activate RIG-I-mediated interferon induction

Perturbations in RNA splicing can have profound effects on innate immune signaling and can lead to immunostimulatory dsRNA accumulation. However, the factors that control these various aspects of RNA metabolism are largely unknown. Here, we find that loss of the splicing factor, CELF2, results in the spontaneous production of IFN in monocytes. Depletion of CELF2 from monocytes resulted in the production of IFN and an ISG signature. Reintroduction of wild-type CELF2 into CELF2 depleted monocytes reduced the production of IFN, but introduction of RNA-binding mutant CELF2 did not. IFN production was due to RLR pathway activation as deletion of IRF3, MAVS or RIG-I prevented the induction of IFN. Transfer of RNA from CELF2-depleted cells into IFN reporter cells caused reporter activation suggesting that CELF2 is required to suppress immunostimulatory RNA. Indeed, using a fluorescence-based RNA-RBP visualization approach known as irCLIP we were able to show RIG-I association with RNA in the absence of CELF2. Together this data suggests that CELF2 suppresses immunostimulatory RNA in monocytes and loss of CELF2 results in self-RNA-dependent activation of RLRs.

4.2 Discussion and future directions

MEF2A induced transcriptional stress and DDX41 activation of STING

This dissertation demonstrates a critical role for MEF2A in the suppression of transcriptional stress that leads to DNA damage and innate immune signaling. An immediate future direction would be to investigate precisely how the loss of MEF2A leads to R-loop formation. Evaluation of our RNA-seq analysis reveals that cells deficient in MEF2A exhibit an increase in pathways associate with transcription. Indeed, increased transcription has been associated with aberrant R-loop accumulation[283]. We showed that preventing translation with the transcription inhibitor, actinomycin D, we could reverse the R-loop accumulation observed

following MEF2A depletion. However, this still leaves the question as to how MEF2A is resulting in increased transcription? One hypothesis is that at steady state MEF2A sits on promotors and enhancers and prevents the aberrant transcription by promiscuous transcription factors. Indeed, we observed pathway enhancement of "generic transcription pathways" as well as RNA polymerase II transcription. Hypertranscription is a hallmark of cancer cells and can be driven by general transcription factors and oncogenes, such as MYC, recruiting RNA polymerases to drive robust transcription[284]. Alternatively, MEF2A could be responsible for inducting expression of a gene involved in transcription suppression, however, we were able to find such a gene in our RNA-seq data set. Nonetheless, both hypotheses could be tested molecularly by utilizing DNA-binding mutant MEF2A and TAD mutant MEF2A expression constructs. We were able to prevent spontaneous IFN production by reconstituting wild-type MEF2A. Utilizing the same assay with DNA-binding or TAD mutant would allow us to understand the requirement for MEF2A enhancer/promotor occupancy or MEF2A transcriptional activity respectively, on R-loop suppression. Interestingly, we observed a significant increase in MEF2C expression when MEF2A was depleted. It is possible that increased MEF2C expression is contributing to hypertranscription in the absence of MEF2A. Future studies looking at the role of increased MEF2C expression could begin to answer these questions. Furthermore, investigating the regions of the genome experiencing increased R-loop accumulation will allow us to better understand how MEF2A is suppressing R-loop formation. The two major methods for investigating genomic R-loop sequences are; DNA:RNA immunoprecipitation sequencing (DRIP-seq) which utilizes the S9.6 DNA:RNA hybrid antibody, and R-ChIP, which utilizes a catalytic dead RNASEH1 to pull down R-loops, followed by sequencing[285,286]. Both have benefits and draw backs, for instance the S9.6 antibody can also interact with dsRNA and ssRNA

and therefore requires treatment with various RNases to prevent nonspecific pulldown of non-R-loop sequences[287]. In addition, both methods exhibit differences in the size and localization of R-loops within the genome[288]. Regardless, either method would be sufficient to begin mapping the area of R-loop accumulation in the absence of MEF2A to allow us to better understand how MEF2A suppresses R-loop formation. These findings present an interesting phenotype that may extend beyond MEF2A and even MEF2 transcription factors. Investigation into other transcription factors that at the surface do not play a role in immune suppression could play roles in maintaining homeostatic functions that prevent aberrant immune activation.

This dissertation also presents a previously undescribed role for DDX41 in activating an immune response following transcriptional stress. DDX41 has previously been shown to activate STING in both a cGAS-dependent and -independent manner but in responses to pathogenic DNA[123,126]. In addition, DDX41 has been shown to help resolve R-loops and prevent transcriptional stress[136,137]. Indeed, we observe increased R-loops in the absence of DDX41 like these previous reports. The key difference is that rather than increased R-loops perpetuating the IFN phenotype by inducing more DNA damage that is sensed by cGAS, we observe a dampening of the inflammatory response and decreased STING activation, suggesting that DDX41 is acting as a sensor rather than a resolver in this context. These findings provoke two major questions revolving around DDX41. Is DDX41 sensing R-loops or DNA damage and how is DDX41 functioning as a sensor rather than resolver of R-loops? Addressing the first question is tricky as untangling DNA damage from increased R-loops is near impossible. We were able to demonstrate that resolving R-loops by RNASEH1 overexpression could prevent IFN production and inversely, knocking down RNASEH1 increased IFN production in the absence of MEF2A, but it is likely that we are also preventing DNA damage or enhancing DNA damage in these

experiments. We attempted to block R-loop formation with actinomycin D prior to immune activation after MEF2A depletion but prolonged actinomycin D treatment proved toxic to cells resulting in robust cell death. Therefore, *in cellulo* approaches are not useful in addressing if DDX41 can activate STING signaling in response to R-loops and alternative approaches must be developed. *In vitro* assays to investigating IRF3 activation by MAVS have been utilized by extracting mitochondria and cytosolic extracts, combining with *in vitro* translated [^{35}S] IRF3 and looking at [^{35}S] IRF3 phosphorylation in the presence of immunostimulatory RNA[289]. A similar approach whereby purification of ER membranes, cytosolic, and nuclear extracts from DDX41 KO and wild-type cells, followed by spiking in R-loops derived from MEF2A-depleted cells treated with or without RNase H and measuring STING phosphorylation, could be used to test if R-loops function as a ligand for DDX41 to activate STING. This assay could not only be used to determine DDX41 ligands but expanded to investigate multiple STING activating molecules. Conceptually, understanding the factors that govern the role of DDX41 in immune activation could allow for a wide variety of translational approaches towards antiviral therapeutics, vaccine adjuvants and anti-cancer therapies.

The second question of how DDX41 functions as an innate immune sensor rather than R-loops resolver could involve another finding the from this dissertation which is that the DNA-damage response kinase, ATR, is required for immune activation following MEF2A depletion. ATR activation by replicative stress or ssDNA break induces a cascade of phosphorylation of a wide variety of targets[102]. Indeed DDX41 and ATR pathways interact, however DDX41 often induces the activation of induces activation of ATR[136,138]. Perhaps in some context ATR activation can drive DDX41 aways from R-loop resolution and towards STING activation. This would likely be through ATR-mediated activation of BTK, which has previously shown to be

important for DDX41-STING activation[125]. This hypothesis would link the observation that ATR and DDX41 are both required for IFN production in the absence of MEF2A. ATR has been previously found to be required for IFN and ISG induction by SV40, a tumor causing polyomavirus, derived large T antigen, establishing an interplay between ATR and IFN[290]. Perhaps the threat of genotoxic stress triggers ATR to push the cell into an antiviral state as an evolutionary mechanism to defend against oncogenic viruses. Further investigation into the role MEF2A, DDX41 and ATR play in IFN production could elucidate key mechanism that link the innate immune response to DNA damage and genotoxic stress, findings that could have wide reached implication for autoinflammatory and cancer research.

CELF2 suppression of self-RNA ligands in monocytes

This dissertation demonstrates a role for CELF2 in the suppression of immunostimulatory RNA ligands. While the concept of perturbations in splicing leading to the accumulation of endogenous-RNA ligands is not novel and spliceosome-targeted therapies are already in clinical use demonstrating dsRNA-driven immune activation[55], this is the first description of CELF2 perturbation causing such a phenomenon. Perhaps the lack of reports that describe CELF2 involvement in innate immune activation are due to the fact that the loss of *Celf2* is embryonic lethal in mice and *de novo* mutations are rare and cause severe neurological defects making innate immunological phenotypes more difficult to detect[151,268]. However, a 2016 report found that several single nucleotide polymorphisms (SNPs) in the *CELF2* gene are associated with acute respiratory distress syndrome (ARDS) in children with pneumonia[291]. This report found 4 SNPs in two cohorts of African American and non-Hispanic Caucasian children were associated with increased risk of developing ARDS but did not investigate a mechanism of action. Three of the SNPs, rs7068124, rs3814634 and rs10905928, reside within introns of the CELF2 gene, and

one, rs2277212, is within a coding exon. How these SNPs affect CELF2 expression and function is unknown but further investigation could provide novel insights into CELF2 function and potentially link the observed self-RNA ligand generation observed in this dissertation to development of ARDS or other human disease.

CELF2 has been shown to not only coordinate splicing with the splicing factor hnRNPC, but also regulate the translation of hnRNPC in T cells[160,270]. It is noteworthy that hnRNPC, like CELF2, contains RRM domains. In data not shown, we did not observe decreased expression of hnRNPC in the absence of CELF2 in macrophages, suggesting that the regulation of hnRNPC translation by CELF2 could be cell-type specific. HnRNPC suppresses inverted *Alu* element repeats which form cytoplasmic dsRNAs in breast cancer cells and depletion of hnRNPC results in RIG-I driven immune activation and cancer cell death[54]. Indeed, RIG-I is the driver of innate immune activation in the absence of CELF2 as well. As CELF2 and hnRNPC target RNA overlap it is possible that CELF2 serves the same role in macrophages, but the exact self-RNA ligand generated in the absence of CELF2 is unknown. Ongoing studies aimed at sequencing the RNA associated with RIG-I in the absence of CELF2 using irCLIP[264], the method used in this dissertation to visualize RIG-I-RNA complexes, are currently underway and will provide an answer to what the exact RNA ligand is. We are also using an orthogonal approach, STAMP (surveying targets by APOBEC-mediated profiling)[292], to investigate what RNAs are activating RIG-I in the absence of CELF2. Here, by fusing APOBEC to RIG-I we can see what RNAs come in close proximity to RIG-I by looking at C to U editing in bulk RNA-seq samples. Comparing this data set to the data set generated by irCLIP we can narrow down precisely what RNAs are activating RIG-I in the absence of CELF2. Discovery of these RNAs will provide new avenues for discovery of self-RNAs that can be targets for antiviral therapies.

An interesting observation reported in this dissertation is that loss of CELF2 results in significant alternative splicing of ribosomal protein (RP) genes. Pathway analysis of both downregulated genes and alternatively spliced genes in CELF2-depleted monocytes show translation defects. Indeed, using a puromycin uptake assay to tag nascent peptides we showed a functional decrease in translation. Alternative splicing of RP genes rarely results in an alternative protein isoform, rather alternative splicing of RP genes results in degradation and thus alterative splicing of RP genes likely modulates the available pool of accessible RPs[293]. Indeed, a significant amount of alternatively spliced RP genes in CELF2-depleted cells are also significantly downregulated. This suggests that CELF2 is required in monocytes to maintain homeostatic levels of ribosome biogenesis and maintain translation. Long-read RNA sequencing in this dissertation was conducted on poly-A purified RNA and non-coding ribosomal RNA (rRNA) is not poly-adenylated. Therefore, we did not assess the expression levels of rRNA. The loss of ribosomal protein expression can lead to impaired rRNA processing[294]. It is possible that in the absence of RPs, improperly processed rRNA is degraded by cellular RNases. Indeed, RNase degraded rRNA can serve as a RIG-I ligand[271]. Degraded rRNA could be serving as an RNA ligand in the absence of CELF2 due to improper ribosome biogenesis and degradation of rRNA. Future studies are necessary to test the link between CELF2-mediated splicing of RP gens, rRNA integrity and RIG-I mediated IFN production.

The “guard hypothesis” is the idea that the host detects the virulence of a pathogen by monitoring disruptions within the cells rather than the pathogen itself and launching a secondary immune response, a mechanism of defense utilized primarily by plants[295]. However, human monocytes launch a similar form of defense against herpes simplex virus 1 (HSV-1). The HSV-1 virulence factor, infected cell protein 0 (ICP0), targets MORC3 for degradation, but loss of

MORC3 results in the spontaneous production of type I IFN, thus controlling HSV-1 infection[296]. Interestingly, MORC3 has also been shown to be an direct suppressor of HSV-1 infection, suggesting that the targeting of MORC3 by HSV-1 is a trip-wire for a more robust antiviral IFN response[297]. Splicing factors are often a target of manipulation by viruses, either causing their degradation or relocalization to disrupt their function or co-opting them for their own replication[298,254,256,299]. Given the fact that the loss of CELF2 results in the robust production of type I IFN, it is possible that CELF2 is also a tripwire for viruses to succumb to. As of now there are no reports of viruses that target CELF2 expression of function. Investigating viruses that replicate in the nucleus, such as DNA viruses or influenza virus would be excellent places to start looking for viruses that alter CELF2 expression and function. Indeed, DNA viruses can induce the expression of host RNAs to induce RLR activation thus expanding the host response beyond DNA sensing pathways and restrict viruses[37,38]. Perturbations in CELF2 by nuclear replicating DNA virus could also promote an RLR response to aid in viral restriction. Therefore, investigation into viruses that modulate the expression of CELF2 expression could prove rewarding in discovering new biology surrounding the role of CELF2 in immune cells.

In conclusion, this dissertation demonstrates the role of two factors in suppressing the expression and endogenous nucleic acid ligands to suppress IFN production. The transcription factor MEF2A prevents R-loop accumulation which can be sensed by the DDX41-cGAS-STING pathway and the splicing factor CELF2 suppresses endogenous RNAs that activate the RIG-I-MAVS pathway. Further investigation of these factors could provide basic research that can aid in the discovery of novel antiviral therapeutics, vaccine adjuvants and aid in anti-cancer immunotherapies.

BIBLIOGRAPHY

1. Medzhitov, R. & Janeway, C. Innate Immunity. *N Engl J Med* **343**, 338–344 (2000).
2. Janeway, C. A. Approaching the asymptote? Evolution and revolution in immunology. *Cold Spring Harb Symp Quant Biol* **54 Pt 1**, 1–13 (1989).
3. Mogensen, T. H. Pathogen Recognition and Inflammatory Signaling in Innate Immune Defenses. *Clin Microbiol Rev* **22**, 240–273 (2009).
4. Schneider, W. M., Chevillotte, M. D. & Rice, C. M. Interferon-Stimulated Genes: A Complex Web of Host Defenses. *Annual Review of Immunology* **32**, 513–545 (2014).
5. Lee-Kirsch, M. A. The Type I Interferonopathies. *Annu. Rev. Med.* **68**, 297–315 (2017).
6. Crow, Y. J. & Manel, N. Aicardi–Goutières syndrome and the type I interferonopathies. *Nat Rev Immunol* **15**, 429–440 (2015).
7. Rehwinkel, J. & Gack, M. U. RIG-I-like receptors: their regulation and roles in RNA sensing. *Nature Reviews Immunology* **20**, 537–551 (2020).
8. Vazquez, C. & Horner, S. M. MAVS Coordination of Antiviral Innate Immunity. *J Virol* **89**, 6974–6977 (2015).
9. Schoggins, J. W. Interferon-Stimulated Genes: What Do They All Do? *Annual Review of Virology* **6**, 567–584 (2019).
10. Lazear, H. M., Schoggins, J. W. & Diamond, M. S. Shared and Distinct Functions of Type I and Type III Interferons. *Immunity* **50**, 907–923 (2019).
11. Forero, A. *et al.* Differential Activation of the Transcription Factor IRF1 Underlies the Distinct Immune Responses Elicited by Type I and Type III Interferons. *Immunity* **51**, 451-464.e6 (2019).

12. Ivashkiv, L. B. & Donlin, L. T. Regulation of type I interferon responses. *Nature Reviews Immunology* **14**, 36–49 (2014).

13. Kato, H. *et al.* Length-dependent recognition of double-stranded ribonucleic acids by retinoic acid-inducible gene-I and melanoma differentiation-associated gene 5. *J Exp Med* **205**, 1601–1610 (2008).

14. Kato, H. *et al.* Differential roles of MDA5 and RIG-I helicases in the recognition of RNA viruses. *Nature* **441**, 101–105 (2006).

15. Feng, Q. *et al.* MDA5 detects the double-stranded RNA replicative form in picornavirus-infected cells. *Cell Rep* **2**, 1187–1196 (2012).

16. Roth-Cross, J. K., Bender, S. J. & Weiss, S. R. Murine coronavirus mouse hepatitis virus is recognized by MDA5 and induces type I interferon in brain macrophages/microglia. *J Virol* **82**, 9829–9838 (2008).

17. Yin, X. *et al.* MDA5 Governs the Innate Immune Response to SARS-CoV-2 in Lung Epithelial Cells. *Cell Rep* **34**, 108628 (2021).

18. Goubau, D. *et al.* Antiviral immunity via RIG-I-mediated recognition of RNA bearing 5'-diphosphates. *Nature* **514**, 372–375 (2014).

19. Hornung, V. *et al.* 5'-Triphosphate RNA is the ligand for RIG-I. *Science* **314**, 994–997 (2006).

20. Pichlmair, A. *et al.* RIG-I-mediated antiviral responses to single-stranded RNA bearing 5'-phosphates. *Science* **314**, 997–1001 (2006).

21. Jiang, F. *et al.* Structural basis of RNA recognition and activation by innate immune receptor RIG-I. *Nature* **479**, 423–427 (2011).

22. Schuberth-Wagner, C. *et al.* A Conserved Histidine in the RNA Sensor RIG-I Controls Immune Tolerance to N1-2'O-Methylated Self RNA. *Immunity* **43**, 41–51 (2015).

23. Devarkar, S. C. *et al.* Structural basis for m7G recognition and 2′-O-methyl discrimination in capped RNAs by the innate immune receptor RIG-I. *Proceedings of the National Academy of Sciences* **113**, 596–601 (2016).

24. Züst, R. *et al.* Ribose 2'-O-methylation provides a molecular signature for the distinction of self and non-self mRNA dependent on the RNA sensor Mda5. *Nat Immunol* **12**, 137–143 (2011).

25. Diamond, M. S. IFIT1: A dual sensor and effector molecule that detects non-2'-O methylated viral RNA and inhibits its translation. *Cytokine Growth Factor Rev* **25**, 543–550 (2014).

26. Ray, D. *et al.* West Nile virus 5'-cap structure is formed by sequential guanine N-7 and ribose 2'-O methylations by nonstructural protein 5. *J Virol* **80**, 8362–8370 (2006).

27. Zhou, Y. *et al.* Structure and function of flavivirus NS5 methyltransferase. *J Virol* **81**, 3891–3903 (2007).

28. Dong, H. *et al.* Biochemical and genetic characterization of dengue virus methyltransferase. *Virology* **405**, 568–578 (2010).

29. Kaiser, J. A. *et al.* Genotypic and phenotypic characterization of West Nile virus NS5 methyltransferase mutants. *Vaccine* **37**, 7155–7164 (2019).

30. Menachery, V. D. *et al.* Attenuation and restoration of severe acute respiratory syndrome coronavirus mutant lacking 2'-o-methyltransferase activity. *J Virol* **88**, 4251–4264 (2014).

31. Menachery, V. D. *et al.* Middle East Respiratory Syndrome Coronavirus Nonstructural Protein 16 Is Necessary for Interferon Resistance and Viral Pathogenesis. *mSphere* **2**, (2017).

32. Williams, G. D., Gokhale, N. S. & Horner, S. M. Regulation of Viral Infection by the RNA Modification N6-methyladenosine. *Annu Rev Virol* **6**, 235–253 (2019).

33. Durbin, A. F., Wang, C., Marcotrigiano, J. & Gehrke, L. RNAs Containing Modified Nucleotides Fail To Trigger RIG-I Conformational Changes for Innate Immune Signaling. *mBio* **7**, e00833-16 (2016).

34. Karikó, K., Buckstein, M., Ni, H. & Weissman, D. Suppression of RNA recognition by Toll-like receptors: the impact of nucleoside modification and the evolutionary origin of RNA. *Immunity* **23**, 165–175 (2005).

35. Kim, G.-W., Imam, H., Khan, M. & Siddiqui, A. N6-Methyladenosine modification of hepatitis B and C viral RNAs attenuates host innate immunity via RIG-I signaling. *J Biol Chem* **295**, 13123–13133 (2020).

36. Lu, M. *et al.* N6-methyladenosine modification enables viral RNA to escape recognition by RNA sensor RIG-I. *Nat Microbiol* **5**, 584–598 (2020).

37. Chiang, J. J. *et al.* Viral unmasking of cellular 5S rRNA pseudogene transcripts induces RIG-I-mediated immunity. *Nat Immunol* **19**, 53–62 (2018).

38. Zhao, Y., Ye, X., Dunker, W., Song, Y. & Karijolich, J. RIG-I like receptor sensing of host RNAs facilitates the cell-intrinsic immune response to KSHV infection. *Nat Commun* **9**, 4841 (2018).

39. Hornung, V., Hartmann, R., Ablasser, A. & Hopfner, K.-P. OAS proteins and cGAS: unifying concepts in sensing and responding to cytosolic nucleic acids. *Nat Rev Immunol* **14**, 521–528 (2014).

40. Malathi, K., Dong, B., Gale, M. & Silverman, R. H. Small self-RNA generated by RNase L amplifies antiviral innate immunity. *Nature* **448**, 816–819 (2007).

41. Burke, J. M., Kincaid, R. P., Nottingham, R. M., Lambowitz, A. M. & Sullivan, C. S. DUSP11 activity on triphosphorylated transcripts promotes Argonaute association with noncanonical viral microRNAs and regulates steady-state levels of cellular noncoding RNAs. *Genes Dev* **30**, 2076–2092 (2016).

42. Dhir, A. *et al.* Mitochondrial double-stranded RNA triggers antiviral signalling in humans. *Nature* **560**, 238–242 (2018).

43. Deininger, P. Alu elements: know the SINEs. *Genome Biology* **12**, 236 (2011).

44. Chen, L.-L., DeCerbo, J. N. & Carmichael, G. G. Alu element-mediated gene silencing. *The EMBO Journal* **27**, 1694–1705 (2008).

45. Ahmad, S. *et al.* Breaching Self-Tolerance to Alu Duplex RNA Underlies MDA5-Mediated Inflammation. *Cell* **172**, 797-810.e13 (2018).

46. Chung, H. *et al.* Human ADAR1 Prevents Endogenous RNA from Triggering Translational Shutdown. *Cell* **172**, 811-824.e14 (2018).

47. Rice, G. I. *et al.* Gain-of-function mutations in IFIH1 cause a spectrum of human disease phenotypes associated with upregulated type I interferon signaling. *Nat Genet* **46**, 503–509 (2014).

48. Oda, H. *et al.* Aicardi-Goutières syndrome is caused by IFIH1 mutations. *Am J Hum Genet* **95**, 121–125 (2014).

49. Pestal, K. *et al.* Isoforms of RNA-Editing Enzyme ADAR1 Independently Control Nucleic Acid Sensor MDA5-Driven Autoimmunity and Multi-organ Development. *Immunity* **43**, 933–944 (2015).

50. Kahles, A. *et al.* Comprehensive Analysis of Alternative Splicing Across Tumors from 8,705 Patients. *Cancer Cell* **34**, 211-224.e6 (2018).

51. Park, Y. M. *et al.* Heterogeneous nuclear ribonucleoprotein C1/C2 controls the metastatic potential of glioblastoma by regulating PDCD4. *Mol Cell Biol* **32**, 4237–4244 (2012).

52. Pino, I. *et al.* Altered patterns of expression of members of the heterogeneous nuclear ribonucleoprotein (hnRNP) family in lung cancer. *Lung Cancer* **41**, 131–143 (2003).

53. Zarnack, K. *et al.* Direct Competition between hnRNP C and U2AF65 Protects the Transcriptome from the Exonization of Alu Elements. *Cell* **152**, 453–466 (2013).

54. Wu, Y. *et al.* Function of HNRNPC in breast cancer cells by controlling the dsRNA-induced interferon response. *EMBO J* **37**, (2018).

55. Bowling, E. A. *et al.* Spliceosome-targeted therapies trigger an antiviral immune response in triple-negative breast cancer. *Cell* **184**, 384-403.e21 (2021).

56. Boelens, M. C. *et al.* Exosome transfer from stromal to breast cancer cells regulates therapy resistance pathways. *Cell* **159**, 499–513 (2014).

57. Nabet, B. Y. *et al.* Exosome RNA Unshielding Couples Stromal Activation to Pattern Recognition Receptor Signaling in Cancer. *Cell* **170**, 352-366.e13 (2017).

58. Akopian, D., Shen, K., Zhang, X. & Shan, S. Signal Recognition Particle: An Essential Protein-Targeting Machine. *Annu. Rev. Biochem.* **82**, 693–721 (2013).

59. Stetson, D. B. & Medzhitov, R. Recognition of cytosolic DNA activates an IRF3-dependent innate immune response. *Immunity* **24**, 93–103 (2006).

60. Ishikawa, H. & Barber, G. N. STING is an endoplasmic reticulum adaptor that facilitates innate immune signalling. *Nature* **455**, 674–678 (2008).

61. Abe, T. *et al.* STING recognition of cytoplasmic DNA instigates cellular defense. *Mol Cell* **50**, 5–15 (2013).

62. Burdette, D. L. *et al.* STING is a direct innate immune sensor of cyclic di-GMP. *Nature* **478**, 515–518 (2011).

63. Ablasser, A. *et al.* cGAS produces a 2'-5'-linked cyclic dinucleotide second messenger that activates STING. *Nature* **498**, 380–384 (2013).

64. Gao, P. *et al.* Cyclic [G(2',5')pA(3',5')p] is the metazoan second messenger produced by DNA-activated cyclic GMP-AMP synthase. *Cell* **153**, 1094–1107 (2013).

65. Diner, E. J. *et al.* The innate immune DNA sensor cGAS produces a noncanonical cyclic dinucleotide that activates human STING. *Cell Rep* **3**, 1355–1361 (2013).

66. Sun, L., Wu, J., Du, F., Chen, X. & Chen, Z. J. Cyclic GMP-AMP synthase is a cytosolic DNA sensor that activates the type I interferon pathway. *Science* **339**, 786–791 (2013).

67. Mankan, A. K. *et al.* Cytosolic RNA:DNA hybrids activate the cGAS-STING axis. *EMBO J* **33**, 2937–2946 (2014).

68. Herzner, A.-M. *et al.* Sequence-specific activation of the DNA sensor cGAS by Y-form DNA structures as found in primary HIV-1 cDNA. *Nat Immunol* **16**, 1025–1033 (2015).

69. Luecke, S. *et al.* cGAS is activated by DNA in a length-dependent manner. *EMBO Rep* **18**, 1707–1715 (2017).

70. Zhang, X. *et al.* The cytosolic DNA sensor cGAS forms an oligomeric complex with DNA and undergoes switch-like conformational changes in the activation loop. *Cell Rep* **6**, 421–430 (2014).

71. Li, X. *et al.* Cyclic GMP-AMP synthase is activated by double-stranded DNA-induced oligomerization. *Immunity* **39**, 1019–1031 (2013).

72. Du, M. & Chen, Z. J. DNA-induced liquid phase condensation of cGAS activates innate immune signaling. *Science* **361**, 704–709 (2018).

73. Liu, Z.-S. *et al.* G3BP1 promotes DNA binding and activation of cGAS. *Nat Immunol* **20**, 18–28 (2019).

74. Yoh, S. M. *et al.* PQBP1 Is a Proximal Sensor of the cGAS-Dependent Innate Response to HIV-1. *Cell* **161**, 1293–1305 (2015).

75. Shannon, J. L. *et al.* Polyglutamine binding protein 1 (PQBP1) inhibits innate immune responses to cytosolic DNA. *Molecular Immunology* **99**, 182–190 (2018).

76. Morchikh, M. *et al.* HEXIM1 and NEAT1 Long Non-coding RNA Form a Multi-subunit Complex that Regulates DNA-Mediated Innate Immune Response. *Molecular Cell* **67**, 387-399.e5 (2017).

77. Lahaye, X. *et al.* NONO Detects the Nuclear HIV Capsid to Promote cGAS-Mediated Innate Immune Activation. *Cell* **175**, 488-501.e22 (2018).

78. Volkman, H. E., Cambier, S., Gray, E. E. & Stetson, D. B. Tight nuclear tethering of cGAS is essential for preventing autoreactivity. *eLife* **8**, e47491 (2019).

79. Gentili, M. *et al.* The N-Terminal Domain of cGAS Determines Preferential Association with Centromeric DNA and Innate Immune Activation in the Nucleus. *Cell Rep* **26**, 2377-2393.e13 (2019).

80. Zhao, B. *et al.* The molecular basis of tight nuclear tethering and inactivation of cGAS. *Nature* **587**, 673–677 (2020).

81. Li, T. *et al.* Phosphorylation and chromatin tethering prevent cGAS activation during mitosis. *Science* **371**, (2021).

82. Yang, Y.-G., Lindahl, T. & Barnes, D. E. Trex1 exonuclease degrades ssDNA to prevent chronic checkpoint activation and autoimmune disease. *Cell* **131**, 873–886 (2007).

83. Stetson, D. B., Ko, J. S., Heidmann, T. & Medzhitov, R. Trex1 Prevents Cell-Intrinsic Initiation of Autoimmunity. *Cell* **134**, 587–598 (2008).

84. Ablasser, A. *et al.* TREX1 deficiency triggers cell-autonomous immunity in a cGAS-dependent manner. *J Immunol* **192**, 5993–5997 (2014).

85. Gray, E. E., Treuting, P. M., Woodward, J. J. & Stetson, D. B. Cutting Edge: cGAS Is Required for Lethal Autoimmune Disease in the Trex1-Deficient Mouse Model of Aicardi-Goutières Syndrome. *J Immunol* **195**, 1939–1943 (2015).

86. Ablasser, A. *et al.* Cell intrinsic immunity spreads to bystander cells via the intercellular transfer of cGAMP. *Nature* **503**, 530–534 (2013).

87. Gentili, M. *et al.* Transmission of innate immune signaling by packaging of cGAMP in viral particles. *Science* **349**, 1232–1236 (2015).

88. Li, L. *et al.* Hydrolysis of 2’3’-cGAMP by ENPP1 and design of nonhydrolyzable analogs. *Nat Chem Biol* **10**, 1043–1048 (2014).

89. Carozza, J. A. *et al.* ENPP1’s regulation of extracellular cGAMP is a ubiquitous mechanism of attenuating STING signaling. *Proc Natl Acad Sci U S A* **119**, e2119189119 (2022).

90. Maltbaek, J. H., Cambier, S., Snyder, J. M. & Stetson, D. B. ABCC1 transporter exports the immunostimulatory cyclic dinucleotide cGAMP. *Immunity* **55**, 1799-1812.e4 (2022).

91. Shang, G. *et al.* Crystal structures of STING protein reveal basis for recognition of cyclic di-GMP. *Nat Struct Mol Biol* **19**, 725–727 (2012).

92. Zhang, C. *et al.* Structural basis of STING binding with and phosphorylation by TBK1. *Nature* **567**, 394–398 (2019).

93. Zhao, B. *et al.* A conserved PLPLRT/SD motif of STING mediates the recruitment and activation of TBK1. *Nature* **569**, 718–722 (2019).

94. Dobbs, N. *et al.* STING Activation by Translocation from the ER Is Associated with Infection and Autoinflammatory Disease. *Cell Host Microbe* **18**, 157–168 (2015).

95. Petrasek, J. *et al.* STING-IRF3 pathway links endoplasmic reticulum stress with hepatocyte apoptosis in early alcoholic liver disease. *Proc Natl Acad Sci U S A* **110**, 16544–16549 (2013).

96. Harding, S. M. *et al.* Mitotic progression following DNA damage enables pattern recognition within micronuclei. *Nature* **548**, 466–470 (2017).

97. Crasta, K. *et al.* DNA breaks and chromosome pulverization from errors in mitosis. *Nature* **482**, 53–58 (2012).

98. Mackenzie, K. J. *et al.* cGAS surveillance of micronuclei links genome instability to innate immunity. *Nature* **548**, 461–465 (2017).

99. Zhang, C.-Z. *et al.* Chromothripsis from DNA damage in micronuclei. *Nature* **522**, 179–184 (2015).

100. Flynn, P. J., Koch, P. D. & Mitchison, T. J. Chromatin bridges, not micronuclei, activate cGAS after drug-induced mitotic errors in human cells. *Proc Natl Acad Sci USA* **118**, e2103585118 (2021).

101. Giordano, A. M. S. *et al.* DNA damage contributes to neurotoxic inflammation in Aicardi-Goutières syndrome astrocytes. *Journal of Experimental Medicine* **219**, e20211121 (2022).

102. Blackford, A. N. & Jackson, S. P. ATM, ATR, and DNA-PK: The Trinity at the Heart of the DNA Damage Response. *Molecular Cell* **66**, 801–817 (2017).

103. Dunphy, G. *et al.* Non-canonical Activation of the DNA Sensing Adaptor STING by ATM and IFI16 Mediates NF-κB Signaling after Nuclear DNA Damage. *Molecular Cell* **71**, 745-760.e5 (2018).

104. Orvain, C. *et al.* Hair follicle stem cell replication stress drives IFI16/STING-dependent inflammation in hidradenitis suppurativa. *J Clin Invest* **130**, 3777–3790 (2020).

105. Ammann, A. J. & Hong, R. Autoimmune phenomena in ataxia telangiectasia. *J Pediatr* **78**, 821–826 (1971).

106. Härtlova, A. *et al.* DNA Damage Primes the Type I Interferon System via the Cytosolic DNA Sensor STING to Promote Anti-Microbial Innate Immunity. *Immunity* **42**, 332–343 (2015).

107. Feng, X. *et al.* ATR inhibition potentiates ionizing radiation-induced interferon response via cytosolic nucleic acid-sensing pathways. *EMBO J* **39**, e104036 (2020).

108. Tang, Z. *et al.* ATR Inhibition Induces CDK1–SPOP Signaling and Enhances Anti–PD-L1 Cytotoxicity in Prostate Cancer. *Clin Cancer Res* **27**, 4898–4909 (2021).

109. Ferguson, B. J., Mansur, D. S., Peters, N. E., Ren, H. & Smith, G. L. DNA-PK is a DNA sensor for IRF-3-dependent innate immunity. *Elife* **1**, e00047 (2012).

110. Burleigh, K. *et al.* Human DNA-PK activates a STING-independent DNA sensing pathway. *Science Immunology* **5**, (2020).

111. Rocak, S. & Linder, P. DEAD-box proteins: the driving forces behind RNA metabolism. *Nat Rev Mol Cell Biol* **5**, 232–241 (2004).

112. Taschuk, F. & Cherry, S. DEAD-Box Helicases: Sensors, Regulators, and Effectors for Antiviral Defense. *Viruses* **12**, (2020).

113. Cargill, M., Venkataraman, R. & Lee, S. DEAD-Box RNA Helicases and Genome Stability. *Genes* **12**, 1471 (2021).

114. Gorbalenya, A. E. & Koonin, E. V. Helicases: amino acid sequence comparisons and structure-function relationships. *Current Opinion in Structural Biology* **3**, 419–429 (1993).

115. Linder, P. *et al.* Birth of the D-E-A-D box. *Nature* **337**, 121–122 (1989).

116. Ribeiro de Almeida, C. *et al.* RNA Helicase DDX1 Converts RNA G-Quadruplex Structures into R-Loops to Promote IgH Class Switch Recombination. *Mol Cell* **70**, 650-662.e8 (2018).

117. Andrisani, O. *et al.* Biological functions of DEAD/DEAH-box RNA helicases in health and disease. *Nat Immunol* **23**, 354–357 (2022).

118. Perčulija, V. & Ouyang, S. Chapter 9 - Diverse Roles of DEAD/DEAH-Box Helicases in Innate Immunity and Diseases. in *Helicases from All Domains of Life* (ed. Tuteja, R.) 141–171 (Academic Press, 2019). doi:10.1016/B978-0-12-814685-9.00009-9.

119. Zheng, Q., Hou, J., Zhou, Y., Li, Z. & Cao, X. The RNA helicase DDX46 inhibits innate immunity by entrapping m 6 A-demethylated antiviral transcripts in the nucleus. *Nature Immunology* **18**, 1094–1103 (2017).

120. Roundtree, I. A. *et al.* YTHDC1 mediates nuclear export of N6-methyladenosine methylated mRNAs. *eLife* **6**, e31311 (2017).

121. Shi, P. *et al.* SUMOylation of DDX39A Alters Binding and Export of Antiviral Transcripts to Control Innate Immunity. *J.I.* **205**, 168–180 (2020).

122. Zhang, Z. *et al.* DDX1, DDX21, and DHX36 helicases form a complex with the adaptor molecule TRIF to sense dsRNA in dendritic cells. *Immunity* **34**, 866–878 (2011).

123. Zhang, Z. *et al.* The helicase DDX41 senses intracellular DNA mediated by the adaptor STING in dendritic cells. *Nat Immunol* **12**, 959–965 (2011).

124. Parvatiyar, K. *et al.* The helicase DDX41 recognizes the bacterial secondary messengers cyclic di-GMP and cyclic di-AMP to activate a type I interferon immune response. *Nat Immunol* **13**, 1155–1161 (2012).

125. Lee, K.-G. *et al.* Bruton's Tyrosine Kinase Phosphorylates DDX41 and Activates Its Binding of dsDNA and STING to Initiate Type 1 Interferon Response. *Cell Reports* **10**, 1055–1065 (2015).

126. Singh, R. S. *et al.* DDX41 is required for cGAS-STING activation against DNA virus infection. *Cell Rep* **39**, 110856 (2022).

127. Stavrou, S., Aguilera, A. N., Blouch, K. & Ross, S. R. DDX41 Recognizes RNA/DNA Retroviral Reverse Transcripts and Is Critical for In Vivo Control of Murine Leukemia Virus Infection. *mBio* **9**, e00923-18 (2018).

128. Yu, K., Chedin, F., Hsieh, C.-L., Wilson, T. E. & Lieber, M. R. R-loops at immunoglobulin class switch regions in the chromosomes of stimulated B cells. *Nat Immunol* **4**, 442–451 (2003).

129. Aguilera, A. & Gómez-González, B. DNA–RNA hybrids: the risks of DNA breakage during transcription. *Nat Struct Mol Biol* **24**, 439–443 (2017).

130. Kabeche, L., Nguyen, H. D., Buisson, R. & Zou, L. A mitosis-specific and R loop–driven ATR pathway promotes faithful chromosome segregation. *Science* (2018) doi:10.1126/science.aan6490.

131. Brickner, J. R., Garzon, J. L. & Cimprich, K. A. Walking a tightrope: The complex balancing act of R-loops in genome stability. *Molecular Cell* (2022) doi:10.1016/j.molcel.2022.04.014.

132. Cristini, A. *et al.* RNase H2, mutated in Aicardi-Goutières syndrome, resolves co-transcriptional R-loops to prevent DNA breaks and inflammation. *Nat Commun* **13**, 2961 (2022).

133. Park, K. *et al.* Aicardi-Goutières syndrome-associated gene SAMHD1 preserves genome integrity by preventing R-loop formation at transcription–replication conflict regions. *PLOS Genetics* **17**, e1009523 (2021).

134. Sollier, J. *et al.* Transcription-Coupled Nucleotide Excision Repair Factors Promote R-Loop-Induced Genome Instability. *Molecular Cell* **56**, 777–785 (2014).

135. Nguyen, H. D. *et al.* Functions of Replication Protein A as a Sensor of R Loops and a Regulator of RNaseH1. *Molecular Cell* **65**, 832-847.e4 (2017).

136. Mosler, T. *et al.* R-loop proximity proteomics identifies a role of DDX41 in transcription-associated genomic instability. *Nat Commun* **12**, 7314 (2021).

137. Weinreb, J. T. *et al.* Excessive R-loops trigger an inflammatory cascade leading to increased HSPC production. *Developmental Cell* **56**, 627-640.e5 (2021).

138. Weinreb, J. T., Gupta, V., Sharvit, E., Weil, R. & Bowman, T. V. Ddx41 inhibition of DNA damage signaling permits erythroid progenitor expansion in zebrafish. *Haematologica* **107**, 644–654 (2022).

139. Wilkinson, M. E., Charenton, C. & Nagai, K. RNA Splicing by the Spliceosome. *Annual Review of Biochemistry* **89**, null (2020).

140. Wang, E. T. *et al.* Alternative isoform regulation in human tissue transcriptomes. *Nature* **456**, 470–476 (2008).

141. WANG, Y. *et al.* Mechanism of alternative splicing and its regulation. *Biomed Rep* **3**, 152–158 (2015).

142. Carpenter, S., Ricci, E. P., Mercier, B. C., Moore, M. J. & Fitzgerald, K. A. Post-transcriptional regulation of gene expression in innate immunity. *Nature Reviews Immunology* **14**, 361–376 (2014).

143. Schaub, A. & Glasmacher, E. Splicing in immune cells—mechanistic insights and emerging topics. *Int Immunol* **29**, 173–181 (2017).

144. Kastner, B., Will, C. L., Stark, H. & Lührmann, R. Structural Insights into Nuclear pre-mRNA Splicing in Higher Eukaryotes. *Cold Spring Harb Perspect Biol* **11**, a032417 (2019).

145. Steitz, T. A. & Steitz, J. A. A general two-metal-ion mechanism for catalytic RNA. *Proc Natl Acad Sci U S A* **90**, 6498–6502 (1993).

146. Galej, W. P. *et al.* Cryo-EM structure of the spliceosome immediately after branching. *Nature* **537**, 197–201 (2016).

147. Ule, J. & Blencowe, B. J. Alternative Splicing Regulatory Networks: Functions, Mechanisms, and Evolution. *Mol Cell* **76**, 329–345 (2019).

148. Dasgupta, T. & Ladd, A. N. The importance of CELF control: molecular and biological roles of the CUG-BP, Elav-like family of RNA binding proteins. *Wiley Interdiscip Rev RNA* **3**, 104–121 (2012).

149. Blech-Hermoni, Y., Stillwagon, S. & Ladd, A. Diversity and conservation of CELF1 and CELF2 RNA and protein expression patterns during embryonic development. *Dev Dyn* **242**, 767–777 (2013).

150. Barreau, C., Paillard, L., Méreau, A. & Osborne, H. B. Mammalian CELF/Bruno-like RNA-binding proteins: molecular characteristics and biological functions. *Biochimie* **88**, 515–525 (2006).

151. Chen, L. *et al.* CELF RNA binding proteins promote axon regeneration in C. elegans and mammals through alternative splicing of Syntaxins. *eLife* **5**, e16072 (2016).

152. St. Louis, I. V., Dickson, A. M., Bohjanen, P. R. & Wilusz, C. J. CELFish ways to modulate mRNA decay. *Biochim Biophys Acta* **1829**, 695–707 (2013).

153. Chatrikhi, R. *et al.* RNA Binding Protein CELF2 Regulates Signal-Induced Alternative Polyadenylation by Competing with Enhancers of the Polyadenylation Machinery. *Cell Reports* **28**, 2795-2806.e3 (2019).

154. Timchenko, N. A., Wang, G.-L. & Timchenko, L. T. RNA CUG-binding Protein 1 Increases Translation of 20-kDa Isoform of CCAAT/Enhancer-binding Protein β by Interacting with the α and β Subunits of Eukaryotic Initiation Translation Factor 2*. *Journal of Biological Chemistry* **280**, 20549–20557 (2005).

155. Sureban, S. M. *et al.* Functional antagonism between RNA binding proteins HuR and CUGBP2 determines the fate of COX-2 mRNA translation. *Gastroenterology* **132**, 1055–1065 (2007).

156. Mallory, M. J. *et al.* Induced transcription and stability of CELF2 mRNA drives widespread alternative splicing during T-cell signaling. *PNAS* **112**, E2139–E2148 (2015).

157. Martinez, N. M. *et al.* Widespread JNK-dependent alternative splicing induces a positive feedback loop through CELF2-mediated regulation of MKK7 during T-cell activation. *Genes Dev.* **29**, 2054–2066 (2015).

158. Ajith, S. *et al.* Position-dependent activity of CELF2 in the regulation of splicing and implications for signal-responsive regulation in T cells. *RNA Biology* **13**, 569–581 (2016).

159. Michel, M., Wilhelmi, I., Schultz, A.-S., Preussner, M. & Heyd, F. Activation-induced Tumor Necrosis Factor Receptor-associated Factor 3 (Traf3) Alternative Splicing Controls the Noncanonical Nuclear Factor κB Pathway and Chemokine Expression in Human T Cells. *J. Biol. Chem.* **289**, 13651–13660 (2014).

160. Schultz, A.-S., Preussner, M., Bunse, M., Karni, R. & Heyd, F. Activation-Dependent TRAF3 Exon 8 Alternative Splicing Is Controlled by CELF2 and hnRNP C Binding to an Upstream Intronic Element. *Mol. Cell. Biol.* **37**, e00488-16, /mcb/37/7/e00488-16.atom (2017).

161. Yoon, J. S. J. *et al.* Interleukin-10 control of pre-miR155 maturation involves CELF2. *PLoS ONE* **15**, e0231639 (2020).

162. Pon, J. R. & Marra, M. A. MEF2 transcription factors: developmental regulators and emerging cancer genes. *Oncotarget* **7**, 2297–2312 (2015).

163. Chen, X., Gao, B., Ponnusamy, M., Lin, Z. & Liu, J. MEF2 signaling and human diseases. *Oncotarget* **8**, 112152–112165 (2017).

164. Lisek, M., Przybyszewski, O., Zylinska, L., Guo, F. & Boczek, T. The Role of MEF2 Transcription Factor Family in Neuronal Survival and Degeneration. *International Journal of Molecular Sciences* **24**, 3120 (2023).

165. Desjardins, C. A. & Naya, F. J. Antagonistic regulation of cell-cycle and differentiation gene programs in neonatal cardiomyocytes by homologous MEF2 transcription factors. *Journal of Biological Chemistry* **292**, 10613–10629 (2017).

166. Lin, Q., Schwarz, J., Bucana, C. & N. Olson, E. Control of Mouse Cardiac Morphogenesis and Myogenesis by Transcription Factor MEF2C. *Science* **276**, 1404–1407 (1997).

167. Naya, F. J. *et al.* Mitochondrial deficiency and cardiac sudden death in mice lacking the MEF2A transcription factor. *Nat Med* **8**, 1303–1309 (2002).

168. Deczkowska, A. *et al.* Mef2C restrains microglial inflammatory response and is lost in brain ageing in an IFN-I-dependent manner. *Nat Commun* **8**, 717 (2017).

169. Xue, F., Tian, J., Yu, C., Du, H. & Guo, L. Type I interferon response-related microglial Mef2c deregulation at the onset of Alzheimer's pathology in 5×FAD mice. *Neurobiology of Disease* **152**, 105272 (2021).

170. Lu, F. *et al.* Regulation of IFN-Is by MEF2D Promotes Inflammatory Homeostasis in Microglia. *JIR* **Volume 14**, 2851–2863 (2021).

171. Cilenti, F. *et al.* A PGE2-MEF2A axis enables context-dependent control of inflammatory gene expression. *Immunity* **0**, (2021).

172. Black, B. L. & Olson, E. N. Transcriptional Control of Muscle Development by Myocyte Enhancer Factor-2 (mef2) Proteins. *Annual Review of Cell and Developmental Biology* **14**, 167–196 (1998).

173. Wang, L., Fan, C., Topol, S. E., Topol, E. J. & Wang, Q. Mutation of MEF2A in an Inherited Disorder with Features of Coronary Artery Disease. *Science* **302**, 1578–1581 (2003).

174. King, K. R. *et al.* IRF3 and type I interferons fuel a fatal response to myocardial infarction. *Nat Med* **23**, 1481–1487 (2017).

175. Chemudupati, M. *et al.* From APOBEC to ZAP: Diverse mechanisms used by cellular restriction factors to inhibit virus infections. *Biochimica et Biophysica Acta (BBA) - Molecular Cell Research* **1866**, 382–394 (2019).

176. Crow, Y. J. & Manel, N. Aicardi–Goutières syndrome and the type I interferonopathies. *Nat Rev Immunol* **15**, 429–440 (2015).

177. Harding, S. M. *et al.* Mitotic progression following DNA damage enables pattern recognition within micronuclei. *Nature* **548**, 466–470 (2017).

178. Mackenzie, K. J. *et al.* cGAS surveillance of micronuclei links genome instability to innate immunity. *Nature* **548**, 461–465 (2017).

179. Dunphy, G. *et al.* Non-canonical Activation of the DNA Sensing Adaptor STING by ATM and IFI16 Mediates NF-κB Signaling after Nuclear DNA Damage. *Molecular Cell* **71**, 745-760.e5 (2018).

180. Brickner, J. R., Garzon, J. L. & Cimprich, K. A. Walking a tightrope: The complex balancing act of R-loops in genome stability. *Molecular Cell* (2022) doi:10.1016/j.molcel.2022.04.014.

181. Crow, Y. J., Shetty, J. & Livingston, J. H. Treatments in Aicardi–Goutières syndrome. *Developmental Medicine & Child Neurology* **62**, 42–47 (2020).

182. Cargill, M., Venkataraman, R. & Lee, S. DEAD-Box RNA Helicases and Genome Stability. *Genes* **12**, 1471 (2021).

183. Andrisani, O. *et al.* Biological functions of DEAD/DEAH-box RNA helicases in health and disease. *Nat Immunol* **23**, 354–357 (2022).

184. Zhang, Z. *et al.* The helicase DDX41 senses intracellular DNA mediated by the adaptor STING in dendritic cells. *Nat Immunol* **12**, 959–965 (2011).

185. Singh, R. S. *et al.* DDX41 is required for cGAS-STING activation against DNA virus infection. *Cell Reports* **39**, (2022).

186. Lee, K.-G. *et al.* Bruton's Tyrosine Kinase Phosphorylates DDX41 and Activates Its Binding of dsDNA and STING to Initiate Type 1 Interferon Response. *Cell Reports* **10**, 1055–1065 (2015).

187. Stavrou, S., Aguilera, A. N., Blouch, K. & Ross, S. R. DDX41 Recognizes RNA/DNA Retroviral Reverse Transcripts and Is Critical for In Vivo Control of Murine Leukemia Virus Infection. *mBio* **9**, e00923-18 (2018).

188. Weinreb, J. T. *et al.* Excessive R-loops trigger an inflammatory cascade leading to increased HSPC production. *Developmental Cell* **56**, 627-640.e5 (2021).

189. Forero, A. *et al.* Simian Virus 40 Large T Antigen Induces IFN-Stimulated Genes through ATR Kinase. *The Journal of Immunology* **192**, 5933–5942 (2014).

190. Blackford, A. N. & Jackson, S. P. ATM, ATR, and DNA-PK: The Trinity at the Heart of the DNA Damage Response. *Molecular Cell* **66**, 801–817 (2017).

191. Burleigh, K. *et al.* Human DNA-PK activates a STING-independent DNA sensing pathway. *Science Immunology* **5**, (2020).

192. Ferguson, B. J., Mansur, D. S., Peters, N. E., Ren, H. & Smith, G. L. DNA-PK is a DNA sensor for IRF-3-dependent innate immunity. *eLife* **1**, e00047 (2012).

193. Justice, J. L. & Cristea, I. M. Nuclear antiviral innate responses at the intersection of DNA sensing and DNA repair. *Trends in Microbiology* (2022) doi:10.1016/j.tim.2022.05.004.

194. Ragu, S., Matos-Rodrigues, G. & Lopez, B. S. Replication Stress, DNA Damage, Inflammatory Cytokines and Innate Immune Response. *Genes* **11**, 409 (2020).

195. Saldivar, J. C., Cortez, D. & Cimprich, K. A. The essential kinase ATR: ensuring faithful duplication of a challenging genome. *Nat Rev Mol Cell Biol* **18**, 622–636 (2017).

196. Matos, D. A. *et al.* ATR Protects the Genome against R Loops through a MUS81-Triggered Feedback Loop. *Molecular Cell* **77**, 514-527.e4 (2020).

197. Hodroj, D. *et al.* An ATR-dependent function for the Ddx19 RNA helicase in nuclear R-loop metabolism. *The EMBO Journal* **36**, 1182–1198 (2017).

198. Lu, F. *et al.* Regulation of IFN-Is by MEF2D Promotes Inflammatory Homeostasis in Microglia. *JIR* **Volume 14**, 2851–2863 (2021).

199. Cilenti, F. *et al.* A PGE2-MEF2A axis enables context-dependent control of inflammatory gene expression. *Immunity* **0**, (2021).

200. Xue, F., Tian, J., Yu, C., Du, H. & Guo, L. Type I interferon response-related microglial Mef2c deregulation at the onset of Alzheimer's pathology in 5×FAD mice. *Neurobiology of Disease* **152**, 105272 (2021).

201. Deczkowska, A. *et al.* Mef2C restrains microglial inflammatory response and is lost in brain ageing in an IFN-I-dependent manner. *Nat Commun* **8**, 717 (2017).

202. Chen, X., Gao, B., Ponnusamy, M., Lin, Z. & Liu, J. MEF2 signaling and human diseases. *Oncotarget* **8**, 112152–112165 (2017).

203. Naya, F. J. *et al.* Mitochondrial deficiency and cardiac sudden death in mice lacking the MEF2A transcription factor. *Nat Med* **8**, 1303–1309 (2002).

204. King, K. R. *et al.* IRF3 and type I interferons fuel a fatal response to myocardial infarction. *Nat Med* **23**, 1481–1487 (2017).

205. Majidi, S. P. *et al.* Chromatin Environment and Cellular Context Specify Compensatory Activity of Paralogous MEF2 Transcription Factors. *Cell Reports* **29**, 2001-2015.e5 (2019).

206. Soveg, F. W. *et al.* Endomembrane targeting of human OAS1 p46 augments antiviral activity. *eLife* **10**, e71047 (2021).

207. Kessler, D. S., Levy, D. E. & Darnell, J. E. Two interferon-induced nuclear factors bind a single promoter element in interferon-stimulated genes. *Proceedings of the National Academy of Sciences* **85**, 8521–8525 (1988).

208. Symons, J. A., Alcamí, A. & Smith, G. L. Vaccinia virus encodes a soluble type I interferon receptor of novel structure and broad species specificity. *Cell* **81**, 551–560 (1995).

209. Miyamoto, M. *et al.* Regulated expression of a gene encoding a nuclear factor, IRF-1, that specifically binds to IFN-β gene regulatory elements. *Cell* **54**, 903–913 (1988).

210. Suschak, J. J., Wang, S., Fitzgerald, K. A. & Lu, S. A cGAS-Independent STING/IRF7 Pathway Mediates the Immunogenicity of DNA Vaccines. *The Journal of Immunology* **196**, 310–316 (2016).

211. Ablasser, A. & Hur, S. Regulation of cGAS- and RLR-mediated immunity to nucleic acids. *Nat Immunol* **21**, 17–29 (2020).

212. Saito, T., Owen, D. M., Jiang, F., Marcotrigiano, J. & Gale, M. Innate immunity induced by composition-dependent RIG-I recognition of hepatitis C virus RNA. *Nature* **454**, 523–527 (2008).

213. Ishikawa, H., Ma, Z. & Barber, G. N. STING regulates intracellular DNA-mediated, type I interferon-dependent innate immunity. *Nature* **461**, 788–792 (2009).

214. Yount, J. S., Gitlin, L., Moran, T. M. & López, C. B. MDA5 Participates in the Detection of Paramyxovirus Infection and Is Essential for the Early Activation of Dendritic Cells in

Response to Sendai Virus Defective Interfering Particles. *The Journal of Immunology* **180**, 4910–4918 (2008).

215. Liu, S. *et al.* Phosphorylation of innate immune adaptor proteins MAVS, STING, and TRIF induces IRF3 activation. *Science* **347**, (2015).
216. Petrasek, J. *et al.* STING-IRF3 pathway links endoplasmic reticulum stress with hepatocyte apoptosis in early alcoholic liver disease. *Proceedings of the National Academy of Sciences* **110**, 16544–16549 (2013).
217. Chen, L. *et al.* The Augmented R-Loop Is a Unifying Mechanism for Myelodysplastic Syndromes Induced by High-Risk Splicing Factor Mutations. *Molecular Cell* **69**, 412-425.e6 (2018).
218. Härtlova, A. *et al.* DNA Damage Primes the Type I Interferon System via the Cytosolic DNA Sensor STING to Promote Anti-Microbial Innate Immunity. *Immunity* **42**, 332–343 (2015).
219. Maréchal, A. & Zou, L. DNA Damage Sensing by the ATM and ATR Kinases. *Cold Spring Harb Perspect Biol* **5**, a012716 (2013).
220. Froggatt, H. M., Harding, A. T., Chaparian, R. R. & Heaton, N. S. ETV7 limits antiviral gene expression and control of influenza viruses. *Science Signaling* **14**, eabe1194 (2021).
221. Bianchi, V., Pontis, E. & Reichard, P. Changes of deoxyribonucleoside triphosphate pools induced by hydroxyurea and their relation to DNA synthesis. *J Biol Chem* **261**, 16037–16042 (1986).
222. Stork, C. T. *et al.* Co-transcriptional R-loops are the main cause of estrogen-induced DNA damage. *eLife* **5**, e17548 (2016).

223. Crossley, M. P., Bocek, M. & Cimprich, K. A. R-Loops as Cellular Regulators and Genomic Threats. *Molecular Cell* **73**, 398–411 (2019).

224. Mosler, T. *et al.* R-loop proximity proteomics identifies a role of DDX41 in transcription-associated genomic instability. *Nat Commun* **12**, 7314 (2021).

225. Weinreb, J. T., Gupta, V., Sharvit, E., Weil, R. & Bowman, T. V. Ddx41 inhibition of DNA damage signaling permits erythroid progenitor expansion in zebrafish. *Haematologica* **107**, 644–654 (2022).

226. Kotsantis, P. *et al.* Increased global transcription activity as a mechanism of replication stress in cancer. *Nat Commun* **7**, 13087 (2016).

227. Decout, A., Katz, J. D., Venkatraman, S. & Ablasser, A. The cGAS–STING pathway as a therapeutic target in inflammatory diseases. *Nat Rev Immunol* **21**, 548–569 (2021).

228. Dowling, J. W. & Forero, A. Beyond Good and Evil: Molecular Mechanisms of Type I and III IFN Functions. *The Journal of Immunology* **208**, 247–256 (2022).

229. Beyer, D. K. & Forero, A. Mechanisms of Antiviral Immune Evasion of SARS-CoV-2. *Journal of Molecular Biology* **434**, 167265 (2022).

230. Calcagno, D. M. *et al.* The myeloid type I interferon response to myocardial infarction begins in bone marrow and is regulated by Nrf2-activated macrophages. *Sci Immunol* **5**, eaaz1974 (2020).

231. Desjardins, C. A. & Naya, F. J. Antagonistic regulation of cell-cycle and differentiation gene programs in neonatal cardiomyocytes by homologous MEF2 transcription factors. *Journal of Biological Chemistry* **292**, 10613–10629 (2017).

232. Aguilera, A. & Gómez-González, B. DNA–RNA hybrids: the risks of DNA breakage during transcription. *Nat Struct Mol Biol* **24**, 439–443 (2017).

233. Chakraborty, P., Huang, J. T. J. & Hiom, K. DHX9 helicase promotes R-loop formation in cells with impaired RNA splicing. *Nat Commun* **9**, 4346 (2018).

234. Chlon, T. M. *et al.* Germline DDX41 mutations cause ineffective hematopoiesis and myelodysplasia. *Cell Stem Cell* **28**, 1966-1981.e6 (2021).

235. Burleigh, K. *et al.* Human DNA-PK activates a STING-independent DNA sensing pathway. *Science Immunology* **5**, (2020).

236. Forero, A. *et al.* Differential Activation of the Transcription Factor IRF1 Underlies the Distinct Immune Responses Elicited by Type I and Type III Interferons. *Immunity* **51**, 451-464.e6 (2019).

237. Fredericksen, B. L. & Gale, M. West Nile Virus Evades Activation of Interferon Regulatory Factor 3 through RIG-I-Dependent and -Independent Pathways without Antagonizing Host Defense Signaling. *Journal of Virology* **80**, 2913–2923 (2006).

238. Laufman, O., Perrino, J. & Andino, R. Viral Generated Inter-Organelle Contacts Redirect Lipid Flux for Genome Replication. *Cell* **178**, 275-289.e16 (2019).

239. Gray, E. E. *et al.* The AIM2-like Receptors Are Dispensable for the Interferon Response to Intracellular DNA. *Immunity* **45**, 255–266 (2016).

240. Schindelin, J. *et al.* Fiji: an open-source platform for biological-image analysis. *Nat Methods* **9**, 676–682 (2012).

241. Kim, D., Liu, Y., Oberly, S., Freire, R. & Smolka, M. B. ATR-mediated proteome remodeling is a major determinant of homologous recombination capacity in cancer cells. *Nucleic Acids Research* **46**, 8311–8325 (2018).

242. Stirling, D. R. *et al.* CellProfiler 4: improvements in speed, utility and usability. *BMC Bioinformatics* **22**, 433 (2021).

243. Schmid, S., Mordstein, M., Kochs, G., García-Sastre, A. & Tenoever, B. R. Transcription factor redundancy ensures induction of the antiviral state. *J Biol Chem* **285**, 42013–42022 (2010).

244. Nan, Y., Nan, G. & Zhang, Y.-J. Interferon Induction by RNA Viruses and Antagonism by Viral Pathogens. *Viruses* **6**, 4999–5027 (2014).

245. Dixit, E. & Kagan, J. C. Intracellular pathogen detection by RIG-I-like receptors. *Adv Immunol* **117**, 99–125 (2013).

246. Liu, G. & Gack, M. U. Distinct and Orchestrated Functions of RNA Sensors in Innate Immunity. *Immunity* **53**, 26–42 (2020).

247. Trinchieri, G. Type I interferon: friend or foe? *J Exp Med* **207**, 2053–2063 (2010).

248. Rice, G. I. *et al.* Mutations in ADAR1 cause Aicardi-Goutières syndrome associated with a type I interferon signature. *Nature Genetics* **44**, 1243–1248 (2012).

249. Maurano, M. *et al.* Protein kinase R and the integrated stress response drive immunopathology caused by mutations in the RNA deaminase ADAR1. *Immunity* S1074-7613(21)00263–6 (2021) doi:10.1016/j.immuni.2021.07.001.

250. Wang, L., Wen, M. & Cao, X. Nuclear hnRNPA2B1 initiates and amplifies the innate immune response to DNA viruses. *Science* **365**, eaav0758 (2019).

251. West, K. O. *et al. The splicing factor hnRNP M is a critical regulator of innate immune gene expression in macrophages*. http://biorxiv.org/lookup/doi/10.1101/617043 (2019) doi:10.1101/617043.

252. Tremblay, N. *et al.* Spliceosome SNRNP200 Promotes Viral RNA Sensing and IRF3 Activation of Antiviral Response. *PLoS Pathog* **12**, (2016).

253. Barnhart, M. D., Moon, S. L., Emch, A. W., Wilusz, C. J. & Wilusz, J. Changes in cellular mRNA stability, splicing, and polyadenylation through HuR protein sequestration by a cytoplasmic RNA virus. *Cell Rep* **5**, 909–917 (2013).

254. Tsai, P.-L. *et al.* Cellular RNA binding proteins NS1-BP and hnRNP K regulate influenza A virus RNA splicing. *PLoS Pathog* **9**, e1003460 (2013).

255. Boudreault, S., Roy, P., Lemay, G. & Bisaillon, M. Viral modulation of cellular RNA alternative splicing: A new key player in virus–host interactions? *WIREs RNA* e1543 (2019) doi:10.1002/wrna.1543.

256. Herrmann, C. *et al.* Adenovirus-mediated ubiquitination alters protein–RNA binding and aids viral RNA processing. *Nature Microbiology* **5**, 1217–1231 (2020).

257. Dunker, W. *et al.* TDP-43 prevents endogenous RNAs from triggering a lethal RIG-I-dependent interferon response. *Cell Reports* **35**, 108976 (2021).

258. Uhlén, M. *et al.* Proteomics. Tissue-based map of the human proteome. *Science* **347**, 1260419 (2015).

259. Smith, J. R. *et al.* MEF2A suppresses replicative stress responses that trigger DDX41-dependent IFN production. 2022.09.15.508100 Preprint at https://doi.org/10.1101/2022.09.15.508100 (2022).

260. So, L. *et al.* Regulatory T cells suppress CD4+ effector T cell activation by controlling protein synthesis. *J Exp Med* **220**, e20221676 (2023).

261. Symons, J. A., Alcamí, A. & Smith, G. L. Vaccinia virus encodes a soluble type I interferon receptor of novel structure and broad species specificity. *Cell* **81**, 551–560 (1995).

262. Pakos-Zebrucka, K. *et al.* The integrated stress response. *EMBO reports* **17**, 1374–1395 (2016).

263. Froggatt, H. M., Harding, A. T., Chaparian, R. R. & Heaton, N. S. ETV7 limits antiviral gene expression and control of influenza viruses. *Science Signaling* **14**, eabe1194 (2021).

264. Zarnegar, B. J. *et al.* irCLIP platform for efficient characterization of protein–RNA interactions. *Nature Methods* **13**, 489–492 (2016).

265. Ladd, A. N., Charlet-B, N. & Cooper, T. A. The CELF Family of RNA Binding Proteins Is Implicated in Cell-Specific and Developmentally Regulated Alternative Splicing. *Molecular and Cellular Biology* **21**, 1285–1296 (2001).

266. Gazzara, M. R. *et al.* Ancient antagonism between CELF and RBFOX families tunes mRNA splicing outcomes. *Genome Res.* **27**, 1360–1370 (2017).

267. Yanaizu, M., Washizu, C., Nukina, N., Satoh, J. & Kino, Y. CELF2 regulates the species-specific alternative splicing of TREM2. *Sci Rep* **10**, (2020).

268. MacPherson, M. J. *et al.* Nucleocytoplasmic transport of the RNA-binding protein CELF2 regulates neural stem cell fates. *Cell Reports* **35**, (2021).

269. Nikitina, E., Larionova, I., Choinzonov, E. & Kzhyshkowska, J. Monocytes and Macrophages as Viral Targets and Reservoirs. *Int J Mol Sci* **19**, (2018).

270. Mallory, M. J. *et al.* Reciprocal regulation of hnRNP C and CELF2 through translation and transcription tunes splicing activity in T cells. *Nucleic Acids Res* **48**, 5710–5719 (2020).

271. Jung, S. *et al.* A ribosomal RNA fragment with 2′,3′-cyclic phosphate and GTP-binding activity acts as RIG-I ligand. *Nucleic Acids Res* **48**, 10397–10412 (2020).

272. Dvinge, H. & Bradley, R. K. Widespread intron retention diversifies most cancer transcriptomes. *Genome Med* **7**, 45 (2015).

273. Lee, S. C.-W. *et al.* Modulation of splicing catalysis for therapeutic targeting of leukemia with mutations in genes encoding spliceosomal proteins. *Nat Med* **22**, 672–678 (2016).

274. Chan, S. *et al.* Basal-A Triple-Negative Breast Cancer Cells Selectively Rely on RNA Splicing for Survival. *Mol Cancer Ther* **16**, 2849–2861 (2017).

275. Hsu, T. Y.-T. *et al.* The spliceosome is a therapeutic vulnerability in MYC-driven cancer. *Nature* **525**, 384–388 (2015).

276. Han, T. *et al.* Anticancer sulfonamides target splicing by inducing RBM39 degradation via recruitment to DCAF15. *Science* **356**, eaal3755 (2017).

277. Uehara, T. *et al.* Selective degradation of splicing factor CAPERα by anticancer sulfonamides. *Nat Chem Biol* **13**, 675–680 (2017).

278. Wang, J. *et al.* miR-615-3p promotes proliferation and migration and inhibits apoptosis through its potential target CELF2 in gastric cancer. *Biomedicine & Pharmacotherapy* **101**, 406–413 (2018).

279. Piqué, L. *et al.* Epigenetic inactivation of the splicing RNA-binding protein CELF2 in human breast cancer. *Oncogene* **38**, 7106–7112 (2019).

280. Wang, J., Lai, X. & Peng, X. CircLIFR Inhibits Non-small Cell Lung Cancer Progression by Acting as a miR-429 Sponge to Enhance CELF2 Expression. *Biochem Genet* **61**, 725–741 (2023).

281. Schwerk, J. *et al.* RNA-binding protein isoforms ZAP-S and ZAP-L have distinct antiviral and immune resolution functions. *Nat Immunol* **20**, 1610–1620 (2019).

282. Tang, A. D. *et al.* Full-length transcript characterization of SF3B1 mutation in chronic lymphocytic leukemia reveals downregulation of retained introns. *Nature Communications* **11**, 1–12 (2020).

283. Kotsantis, P. *et al.* Increased global transcription activity as a mechanism of replication stress in cancer. *Nat Commun* **7**, 13087 (2016).

284. Bowry, A., Kelly, R. D. W. & Petermann, E. Hypertranscription and replication stress in cancer. *Trends in Cancer* **7**, 863–877 (2021).

285. Ginno, P. A., Lott, P. L., Christensen, H. C., Korf, I. & Chédin, F. R-loop formation is a distinctive characteristic of unmethylated human CpG island promoters. *Mol Cell* **45**, 814–825 (2012).

286. Chen, L. *et al.* R-ChIP Using Inactive RNase H Reveals Dynamic Coupling of R-loops with Transcriptional Pausing at Gene Promoters. *Mol Cell* **68**, 745-757.e5 (2017).

287. Smolka, J. A., Sanz, L. A., Hartono, S. R. & Chédin, F. Recognition of RNA by the S9.6 antibody creates pervasive artifacts when imaging RNA:DNA hybrids. *Journal of Cell Biology* **220**, e202004079 (2021).

288. Miller, H. E. *et al.* Quality-controlled R-loop meta-analysis reveals the characteristics of R-loop consensus regions. *Nucleic Acids Res* **50**, 7260–7286 (2022).

289. Zeng, W., Xu, M., Liu, S., Sun, L. & Chen, Z. J. Key Role of Ubc5 and Lysine-63 Polyubiquitination in Viral Activation of IRF3. *Molecular Cell* **36**, 315–325 (2009).

290. Forero, A. *et al.* Simian virus 40 large T antigen induces IFN-stimulated genes through ATR kinase. *J Immunol* **192**, 5933–5942 (2014).

291. Perez-Marques, F. *et al.* Association of polymorphisms in genes of factors involved in regulation of splicing of cystic fibrosis transmembrane conductance regulator mRNA with acute respiratory distress syndrome in children with pneumonia. *Crit Care* **20**, (2016).

292. Brannan, K. W. *et al.* Robust single-cell discovery of RNA targets of RNA-binding proteins and ribosomes. *Nat Methods* **18**, 507–519 (2021).

293. Petibon, C., Malik Ghulam, M., Catala, M. & Abou Elela, S. Regulation of ribosomal protein genes: An ordered anarchy. *WIREs RNA* **12**, e1632 (2021).

294. Robledo, S. *et al.* The role of human ribosomal proteins in the maturation of rRNA and ribosome production. *RNA* **14**, 1918–1929 (2008).

295. Jones, J. D. G. & Dangl, J. L. The plant immune system. *Nature* **444**, 323–329 (2006).

296. Gaidt, M. M. *et al.* Self-guarding of MORC3 enables virulence factor-triggered immunity. *Nature* **600**, 138–142 (2021).

297. Sloan, E., Orr, A. & Everett, R. D. MORC3, a Component of PML Nuclear Bodies, Has a Role in Restricting Herpes Simplex Virus 1 and Human Cytomegalovirus. *J Virol* **90**, 8621–8633 (2016).

298. Barnhart, M. D., Moon, S. L., Emch, A. W., Wilusz, C. J. & Wilusz, J. Changes in Cellular mRNA Stability, Splicing, and Polyadenylation through HuR Protein Sequestration by a Cytoplasmic RNA Virus. *Cell Reports* **5**, 909–917 (2013).

299. Manet, E. *et al.* Modulation of alternative splicing during early infection of human primary B lymphocytes with Epstein-Barr virus (EBV): a novel function for the viral EBNA-LP protein. *Nucleic Acids Research* (2021) doi:10.1093/nar/gkab787.

VITA

Julian Robert Smith was born in Fort Belvoir, VA in 1990 to Wendy Lynn and Charles Gene Smith. He grew up in La Mirada, CA, just south of Los Angeles, where he attended kindergarten through 12th grade. He attended Garden Hill Elementary School, Los Coyotes Middle School and La Mirada High School. Julian attended Cypress College from 2009-2012 and in 2012 received the American Chemical Society Chemistry Student of the Year award. In 2012 Julian received the (STEM)^2 Research Fellowship and got his first exposure to scientific research at California State University, Fullerton in the Department of Biochemistry. He worked in the laboratory of Dr. Maria C. Linder studying iron metabolism. Julian attended the University of California, Irvine from 2012-2014 and graduated with a BS in Biological Sciences. In 2013 Julian joined the laboratory of Dr. Dritan Agalliu in the Department of Developmental and Cell biology as an undergraduate researcher. Julian received the UCI Summer Undergraduate Research Fellowship in 2013. In 2014 Julian continued working in Dr. Agalliu's laboratory as a research technician and laboratory manager and in 2015 moved with the lab to Columbia University Medical Center in the Department of Neurology. During Julian's time in the Agalliu lab he studied blood-brain barrier breakdown in the context of neuro-autoimmune disease, as well as blood-retina barrier development. In 2017 Julian began graduate school at the University of Washington in the Department of Immunology and rotated in the labs of Dr. Estelle Bettelli, Dr. Andrew Oberst and Dr. Ram Savan. Julian preformed his dissertation work in Dr. Ram Savan's laboratory from 2018-2023 where he studied novel regulators of endogenous nucleic acid ligands. Julian defended his dissertation on July 12th, 2023.